NASA SP-78

THE METEOROID ENVIRONMENT AND ITS EFFECTS ON MATERIALS AND EQUIPMENT

COSBY and LYLE

NATIONAL AERONAUTICS AND SPACE ADMINISTRATION

NASA SP-78

THE METEOROID ENVIRONMENT AND ITS EFFECTS ON MATERIALS AND EQUIPMENT

Summary of a Literature Survey by
William A. Cosby and Robert G. Lyle

Prepared under contract for NASA by
Prevention of Deterioration Center
Division of Chemistry and Chemical Technology
National Academy of Sciences-National Research Council

Scientific and Technical Information Division 1965
NATIONAL AERONAUTICS AND SPACE ADMINISTRATION
Washington, D.C.

FOR SALE BY THE SUPERINTENDENT OF DOCUMENTS, U.S. GOVERNMENT
PRINTING OFFICE, WASHINGTON, D.C., PRICE 50 CENTS

Foreword

A summary is presented of current understanding of the meteoroid environment and its effects on materials and equipment. The summary is based entirely on a literature survey of publications primarily appearing since late 1960 and is sectioned: The Environment, Hypervelocity Impact Phenomena, and Design Considerations. The environment section considers in detail the properties and distribution of interplanetary debris determined from: terrestrial observations of meteors; direct measurement by spacecraft and space probes; zodiacal light studies; and analysis of terrestrially accreted dust. The section on hypervelocity impact phenomena summarizes recent theoretical and experimental studies which have contributed to the level of understanding now existent concerning the mechanisms of penetration, cratering, spalling, and perforation which may attend the impingement of meteoroids on surfaces and structures in space. The design considerations section considers weight reduction techniques, particularly the shield or bumper concept and self-sealing structures, and probability for perforation.

Contents

Introduction

The following state-of-the-art summary, developed from a survey of literature compiled over a period of about four years, concerns the meteoroid environment and its hazards to space travel. Conflicting opinions in theory and experiment are included in the summary as reported in the literature; however, where possible, the reasons for such inconsistencies are elucidated. Intent of the summary is to show the level of development of the theory and the nature of estimates presently involved in defining the environment and associated damage mechanisms. It is believed that awareness of this framework of the summary will enable designers and other interested persons to appreciate more quickly the problems involved and then to select that evaluation or estimation technique which they judge as most appropriate.

Approximately 350 references are cited in the report. Many of these references were collected cumulatively by the Prevention of Deterioration Center for input to information and abstracting services well before thought was given to preparation of a state-of-the-art summary. The preparation of this report was greatly facilitated by availability of this collection which obviated a significant part of the difficult task of searching out and acquiring copies of pertinent papers published in previous years.

The Environment

BACKGROUND

With the advent of interplanetary exploration, the success or failure of a mission rests upon the ability to define the environment of the "void" of space. Of the factors of the environment in which a spacecraft must function —vacuum, corpuscular radiation, electromagnetic radiation, weightlessness, ionized gases, and others—probably least is known definitely of the solid matter which constitutes particulate debris. That such debris exists, however, is obvious to all who have viewed the night sky and observed the phenomenon of shooting stars or the zodiacal light.

The understanding of this environment to date has stemmed from terrestrial observations of the interaction of the debris with the upper atmosphere, studies of the solar corona and zodiacal light, examination of dust size particles (believed to be of extraterrestrial origin) collected at high altitudes or recovered from deep sea or ocean sediments and, more recently, with the realization of spacecraft and high altitude rocket probes, direct measurements. Each of these techniques essentially is limited to studying a particular portion of the total debris population. For example, terrestrial observations of interaction of the debris with the upper atmosphere have been limited for the most part to particles with mass greater than approximately 10^{-8} to 10^{-4} gram while direct measurements have been limited to particles with mass greater than approximately 10^{-13} gram but less than approximately 10^{-7} gram, the exact mass limits depending upon assumptions adopted by the investigator. Table I indicates the sizes of particles to be studied. The dimensions given are to be considered as indicative, rather than exact. The table clearly indicates that both the method of study and the basic nature of the phenomenon depend markedly upon the size of the bodies. The methods of detection listed for each class of meteoroids are limited to those that appear to be most useful in each size range. For example, all meteoroids in space must contribute to the zodiacal light, but it has become evident that only the smaller ones contribute enough scattering to make their study profitable by this technique (ref. 1).

Due to the various observational techniques and assumptions adopted by the investigators, it is difficult to draw up a definitive table or graph of debris mass versus number density. Several such tables and graphs have been published in the literature and have been widely quoted with a confidence which the authors themselves probably did not have when they prepared them (ref. 2).

Such tables and graphs will also appear in this publication but one should be cognizant of the assumptions employed in their derivation to appreciate some causes of the variations in the reported data. Therefore, where possible and applicable, the assumptions made by original investigators will be included in the body of this text in order that the reasons for inconsistencies are accountable. In addition, because of the concern over the damaging potential of the debris to spacecraft, each observational technique, its limitations, and its contribution to the overall understanding of the environment will be discussed as will basic meteor theory.

TABLE I.—*Meteoroid Phenomena, Sizes and Detection Techniques*

[From ref. 1]

Class of phenomena or bodies	Rough dimensions	Possible methods of detection
Micrometeoroids	$< 1\mu$	Artificial satellites and rockets
Micrometeoroids and micrometeorites.	1 to 100 μ	Light scattering in space (zodiacal light) Light scattering in atmosphere Meteoritic dust collection Deep sea sediments Rockets
Faint meteoroids	100 μ to 0.1 cm	Radio Zodiacal light Artificial satellites
Meteors	0.1 to 10 cm	Photographic Radio Visual
Fireballs and bolides	10 to 300 cm	Visual Meteorites Radio
Great fireballs and bolides.	> 300 cm	Meteorites Meteoritic craters and geological structures Visual Radio

In the development of any field, particularly when its growth is rapid, the terminology suffers due to one's inability to anticipate needs. As a result, many terms are used to define the same thing. In order to reduce as much ambiguity and confusion as possible, the following definitions will be applicable to this report:

Meteor: Any extraterrestrial particle originating in the solar system which, on entering the Earth's atmosphere, is detectable by the human eye (with or without the aid of optical equipment) due to emission of visible light while ablating and evaporating, or detectable by radar equipment due to ionization of the surrounding atmosphere.

Meteoroid: Any particle originating in the solar system and found outside the practical limits of Earth's upper atmosphere. Generally used to define the larger sized particles (greater than approximately 10^{-6} gram) but not necessarily so restricted.

Micrometeoroid: Any microscopic particle originating in the solar system and found outside the practical limits of Earth's upper atmosphere. Used to define the smaller sized meteoroids with mass less than approximately 10^{-6} gram.

Meteorite: Any meteor which, due to its large original size, survives its burning passage through Earth's atmosphere, and is recovered on Earth's surface. Generally used to define larger sized particles and to indicate asteroidal origin.

Micrometeorite: Any microscopic extraterrestrial particle originating in the solar system which survives passage through Earth's atmosphere and which is recovered on the surface of Earth. These particles are either of such small size originally that they experience no burning on passage through Earth's atmosphere or they may be the microscopic remnants resulting from the ablation and disintegration of a meteor in Earth's atmosphere. May be cometary or asteroidal in origin.

Dust: Any microscopic particle of extraterrestrial origin but belonging to the solar system. The term embodies both micrometeorites and micrometeoroids. When used in the text of this report, the location of the dust will always be specified.

It is realized that the definitions given are too broad to be accepted by all authorities in the field; however, they essentially embrace the concepts of most. Generally, investigators use the terms defined above in an attempt to indicate origin, location and size of particles. When the terms are used in this text, an effort will be made to eliminate confusion on these points. Other terms will be defined as needed in the body of the text.

ORIGIN

It is generally accepted that interplanetary debris has two sources of origin, the asteroids and the comets, and this subject has been well documented (refs. 3 to 10). It is thought to be helpful, however, for the sake of completeness, to describe briefly the main characteristics of each source. No mention will be made of interstellar contribution to the interplanetary debris environment in this report since most investigators feel positively that any such contribution is at most negligible.

Asteroids.—Asteroids are solid bodies concentrated in interplanetary space between the orbits of Mars and Jupiter which orbit the Sun in the same direction as the planets (i.e., direct orbits). This area is referred to as the asteroidal belt. Most asteroids have orbits with eccentricities between 0 and 0.3 (average approximately 0.15) and inclinations to the ecliptic plane up to 40° (average approximately 9°). Although concentrated in an average orbit

of about 2.8 astronomical units (A.U.), the highly eccentric orbits of some asteroids take them far from this average, one, Hildago, as far as about 9.6 A.U. and one, Icarus, as close as about 0.187 A.U. Orbits of 10 asteroids come within Earth's orbit and the Sun. Hermes came within 400 000 miles of Earth in 1937 and could come within the Earth-Moon distance, but its orbit has yet to be definitely established. One asteroid, Eros, comes within half the distance of Mars from Earth a few times every century.

There are approximately 1600 tabulated asteroids (ref. 11). Of these, the largest, Ceres, has a diameter of approximately 425 miles. The smallest yet discovered is around 1 to 2 miles across. There are estimates of as many as 10^5 asteroids with diameters larger than about 1000 feet. The number of still smaller ones is only speculative but extrapolation indicates an enormous amount. The four largest asteroids are estimated to contain about ¾ of the total mass of the entire population of these bodies.

Whether asteroids are the remains of a proto-planet or partially condensed matter, they are believed to suffer collisions continually among themselves, breaking up into still smaller bits and fragments. The various perturbation forces influencing the orbits of the asteroids, particularly the gravitational fields of Sun, Jupiter, Earth and Mars, may draw the fragments into many orbits and distribute them throughout interplanetary space. Some of these fragments enter Earth's atmosphere and become meteors. The present asteroids with such paths are probably due to fairly recent perturbations by Mars and Jupiter. Whipple and Hawkins (ref. 5) have concluded that all meteorites of the larger size found on the surface of Earth and probably some of the brightest meteors are pieces of asteroidal material. These investigators found that the percentage of interplanetary debris of asteroidal origin decreases rapidly as particle size decreases, with the extrapolated result that the smaller meteors (greater than approximately —2 visual magnitude, see text for definition) and interplanetary dust are almost entirely of cometary origin.

Based on analysis of the recovered meteorites, asteroids are thought to be irregular shaped bodies of hard, dense material. The main-body chemical composition of the meteorites is iron, nickel, and stone. Some are almost entirely iron and others mostly stone, while a large proportion are a combination of all three ingredients. Hence, asteroids are assumed to have densities ranging from approximately 3.5 g/cm^3 (stone) to approximately 7.8 g/cm^3 (iron).

The physical size of meteorites found on the ground range from many tons (no upper limit) to particles only a few microns in diameter. Fortunately, only a few of the extremely large particles strike Earth each century. In every hundred years, it is estimated that Earth is struck approximately three times by meteorites weighing several hundred tons. Although bodies large enough to survive passage through the atmosphere are some of the most deadly debris one could encounter in space, they are fortunately so infrequent that they do not represent a great hazard. It is estimated that about five per day strike

Earth's surface, although occasionally swarms of these particles are encountered. It is estimated that asteroidal particles constitute less than 10 percent of the total influx of interplanetary debris entering the Earth's atmosphere; Whipple (ref. 12) estimates this percentage to be closer to one. It should be recognized that these particles will probably be more frequent in the vicinity of Mars and Jupiter.

The lack of a great quantity of asteroidal dust in interplanetary space as previously mentioned indicates that its rate of production by collisions among asteroids, and between asteroids and other debris in interplanetary space, is relatively unimportant compared with the major source of such material, comets.

Comets.—Observable only as flying fireballs in the heavens, comets have been objects of wonder throughout the history of man. It is not known how they came into being. They have been thought perhaps to represent condensations from interstellar material, or to stem from disintegrations of solar system bodies, or possibly to have been formed at the time of origin of the solar system. It is not even known for certain that all orbit the Sun; in any case however, all that have been observed can be attributed to at least having been members of the solar system at one time. Öort has proposed that there may be an enormous number, approximately 10^{11}, of cometary nuclei which form a vast cloud at a distance of some 50 000 to 100 000 A.U. from the Sun (ref. 6). It is suggested that occasionally the orbit of one of these objects is disturbed, perhaps by a passing star, sweeping it into the inner regions of the solar system where it may possibly be further perturbed by planetary bodies. Being far too slight to be visible to a terrestrial observer, comet nuclei remain invisible unless they approach close to the Sun (within approximately several astronomical units), which causes them to be heated and so rapidly evaporate and evolve matter as to become visible during that brief period of their orbit. A typical nucleus is probably less than 10 kilometers in diameter. Halley's, a truly unique comet which has returned every 76 years for 30 known trips, has an estimated diameter of 15 kilometers.

In contrast to the planets and asteroids, comets are not confined to the ecliptic plane and may travel in orbits of any inclination from 0° to 180°. Some travel in retrograde orbits (opposite to that of the planets), some in direct orbits. A comet originally at a great distance from the Sun will have nearly a parabolic orbit. The periods of comets are apparently of the order of a hundred thousand years, and their aphelions (most distant point from the Sun) are of the order of a hundred thousand times the radius of Earth's orbit. Such orbits may carry the comets nearly out of the solar system or halfway to the nearest star. Most of these so-called long period comets have perihelions (closest point to the Sun) of less than several astronomical units and have been observed at only one apparition.

Watson states that the influence of Jupiter's gravitational field on the orbit of a long-period comet, as the two pass close together in the same direction,

will tend to throw the comet into an orbit of direct motion and to shorten its period (ref. 6). Successive approaches to Jupiter will result in further reductions in period and more complete domination by the solar system. It is possible that most of the present short-period (less than 100 years) comets tabulated, approximately 70 (ref. 5), were captured in this manner. Most of these short-period comets have orbits with eccentricities between 0.4 and 0.9 (average approximately 0.5), inclinations to the ecliptic plane of less than 20° and perihelion distances between 1.0 and 2.0 A.U. (ref. 13).

Only four or five new comets are seen on the average annually, though many undoubtedly escape detection, and their orbits are completely random with respect to the motion of Earth about the Sun. One cannot be certain, however, that the comets are really new since they may be long-period comets whose previous arrivals have not been recorded. Approximately three large comets per century pass close to Jupiter and have their orbits shortened to less than a hundred years. The comets disappear at the same rate—three per century—through the continual evolution of matter on successive approaches to perihelion due to heating by solar radiant energy.

While little is actually known about the nuclei of comets, there have been numerous theories concerning their formation and composition. The most popular theory is that of Whipple (ref. 6) who has proposed that the nucleus or central core of a comet is matter of low average density consisting of a loose collection of frozen gases (e.g., H_2O, NH_3, CH_4 and possibly CO_2 and C_2N_2) held together by their mutual gravitational attraction. Interspersed in this matrix of ices are heavier, less volatile mineral compounds in the form of dust grains or porous, fragile matter loosely cemented together. Such minerals would include compounds of iron, nickel, aluminum, and some silicates. It also has been suggested that the nuclei may contain free radicals produced by the bombardment of low energy solar protons.

As the frozen masses approach near perihelion, the ices evaporate and the gases thus formed produce a large luminous envelope (coma) around the leading front. When within 1 or 2 astronomical units, a tail is often developed, which consists of both gases and nonvolatile products. Whipple has cited evidence that the tails of many comets may contain iron fragments about 6 microns in size (ref. 6). In addition to the evaporation of ices from the nucleus, parts of the remaining material may fracture, separating larger volumes from the original body. These separated fragments initially follow along in the orbit of the parent comet in swarms or showers, but they are eventually distributed throughout interplanetary space by the perturbing force of gravitational attraction of planetary bodies and other lesser forces to be discussed in a later section of this report.

The smallest comets have heads (nucleus and coma) at least 10 000 miles in diameter; the largest ever observed, the comet of 1811, was 1.25 million miles in diameter. The average head is about 80 000 miles in diameter, the size varying with solar distance. Tails extend for enormous distances, fre-

quently several million miles. The longest tail observed, associated with the comet of 1813, was 200 million miles in length which is greater than twice the distance of Earth from the Sun (ref. 4). Tails, diverging as they stream away from the heads, may also become millions of miles across. Spectral investigations show that light from a coma is mostly emitted by short lived molecules such as C_2, CN and CH, whereas the light emitted from the tail arises from more stable molecules such as CO and N_2 (ref. 6).

It is believed by some investigators that the tails are produced by the interaction (ionization) of solar corpuscular and electromagnetic radiation with the constituents separated from the comet and that their direction away from the Sun is maintained by the pressure of solar electromagnetic radiation. Beard (ref. 7) has stated that solar rediation pressure alone appears insufficient to maintain the direction of comet tails and cites evidence that the interplanetary magnetic field is acting on the ionized cometary vapor.

The low average density of these bodies was demonstrated when Brook's comet passed between Jupiter and one of its moons in 1889. The comet exerted no perceptible perturbations to the planet's trajectory nor did it influence the orbit of the Moon. The period of the comet was severely perturbed, however, changing from 29 to 7 years. Since Brook's comet did not affect the moon of Jupiter, there is little reason to expect that the comets have enough mass to hold an atmosphere; thus it may be concluded that the coma and tail are not permanent and are present only near perihelion.

In summation, it appears then that interplanetary debris exists in two distinct forms: hard dense particles of asteroidal origin in relatively sparse quantities, and porous, fragile low-density particles of cometary origin, the latter source contributing almost 100 percent to the total present in interplanetary space. The debris is distributed throughout interplanetary space through the efforts of many influential forces, the most important of which are discussed in the section which follows.

PARTICLE DISPERSIVE FORCES

The most influential force experienced by debris in interplanetary space is that due to gravitational attraction of the larger bodies in the solar system (Sun, Jupiter, Earth, etc.). This force is, of course, experienced by all particles and is capable of perturbing the orbits of the largest. However, there are many other lesser forces acting on the debris which tend to further distribute it throughout interplanetary space, the most important of which is probably solar radiation pressure.

When electromagnetic waves are reflected or absorbed, they undergo a change in momentum which manifests itself as a force on the reflecting or absorbing surface. For example, the radiation pressure due to sunlight (intensity 2 cal/cm^2 min) normally incident on an absorbing object placed just outside the atmosphere of Earth is approximately 4.6×10^{-5} dyn/cm^2 (ref. 6). The object suffers an outward force away from the Sun opposing the

inward solar gravitational force. Since the force of the solar radiation pressure is proportional to projected particle area, and solar gravitational pull is proportional to particle volume, particles less than a certain minimum size are quickly blown out of the solar system (ref. 6). The minimum size of a particle allowable in the solar system due to the effect of solar radiation pressure was given by Robertson for a completely absorbing particle to be:

$$a = 0.6/\rho \tag{1}$$

where a is particle radius in microns and ρ particle density (ref. 7). Particles in the vicinity of Earth which are one micron in diameter and which have a density equal to that of aluminum (2.70 g/cm^3) are the proper size for the solar pressure to just balance the force of the solar gravitational field (ref. 8).

Poynting (refs. 6 and 7) originally noted that solar electromagnetic radiation pressure is not impressed radially even on a particle in a circular orbit. Owing to the particle's orbital motion with respect to the Sun there is a slight relativistic aberration in the direction of the incident radiation so that it impinges in a direction against the particle's motion. The subsequent reduction in the angular momentum of the particles reduces its orbit to a circular one and eventually causes it to spiral into the Sun. (This effect is referred to in the literature as the Poynting-Robertson effect.) One sees then that in the course of time, the Poynting-Robertson effect will separate out the particles created in the asteroidal belt or orbiting along behind comets according to their size, the smaller particles faster than the larger. Of course, the particles never drift all the way into the Sun because as they are diminished by vaporization below the minimum size allowable in the solar system, they are swept out by the solar radiation pressure.

The radial velocity—due to the Poynting-Robertson effect—of a particle in a circular orbit is given by:

$$v_r = \text{Constant}/\rho(a)r \tag{2}$$

where ρ is the particle's inherent density, a the particle's radius, and r the particle's distance from the Sun. A particle 100 microns in radius would spiral into the Sun in about 4000 years from the position of Earth's orbit (ref. 7). For additional discussions on the Poynting-Robertson effect, the reader is referred to references 14 and 15.

In addition to the solar electromagnetic radiation effect, Whipple has shown that solar corpuscular radiation (solar wind) tends to enhance the Poynting-Robertson effect and tends to double the minimum size of particles allowable in the solar system before being blown out by the radiation pressure (refs. 6 and 7). Whipple has also suggested that the interactions of solar corpuscular radiation with the surface of solid objects in interplanetary space resemble cathode sputtering causing the gradual erosion of the surfaces (ref. 16). He deduced that erosion is a greater cause of meteoroid destruction (or generation of smaller particles) than the Poynting-Robertson effect (ref. 8). In his 1962 publication (ref. 12), Whipple reported erosion rates of less than 1.5×10^{-7} cm/yr for an iron type asteroidal particle in a typical orbit that may encounter

Earth; of less than 1.7×10^{-6} cm/yr for stony type asteroidal particles or material of this strength; and 4×10^{-5} cm/yr for fragile "fluffy" cometary particles. Other forces (electrostatic, interstellar wind, etc.) acting on the interplanetary debris have been reported in the literature (refs. 6 and 17).

Wyatt and Whipple (ref. 8) have calculated that in 3×10^9 years, the Poynting-Robertson effect and solar electromagnetic radiation pressure would have swept out of the solar system all particles with diameters less than 8 centimeters. The fact that there are still particles of 8 centimeters and smaller diameters in space indicates that there is a continuous source of these particles. Whipple (ref. 12) has estimated that 30 tons of grit and cobwebby material is injected into the solar system each second by comets alone. Such a quantity is sufficient to account for the large number of particles indicated by the zodiacal light, satellite measurements, and meteor observations. Though the asteroidal belt would also have been swept free of particles the sizes of which are responsible for the large meteors presently being observed in the upper atmosphere and recovered on the ground as meteorites, it is reasonable to consider that collisional breakup and subsequent planetary gravitational perturbations of asteroidal fragments are sufficient to account for the number observed (ref. 18).

We have then an overall picture of numerous particles created in the asteroidal belt and along cometary paths, with forces tending to reduce the average particle size and perturb their orbits. The final result is the distribution of the debris throughout interplanetary space. Much of the debris is perturbed into an orbit destined to collide with Earth. The relatively larger, heavier particles manifest themselves in the form of meteors in Earth's atmosphere and can be observed either visually or with radar equipment. Terrestrial observations of these meteors represent the only means of gaining knowledge on the number, density, and physical characteristics of this portion of the debris environment. It is appropriate that a discussion of the parameters and characteristics of interplanetary debris determined from terrestrial observations of meteors follow; however, such a discussion must be preceded by the basic concepts of the meteor magnitude rating scale and contemporary meteor theory to provide the necessary background used in interpreting the observations.

METEOR MAGNITUDE

Inasmuch as no direct measurements have been made, meteor size is generally categorized by relative brilliance. On the relative visual astronomical (or apparent) scale, relative magnitude, based on response of the human eye, is given by the expression:

$$M_1 - M_2 = 2.5 \log_{10} I_1 - 2.5 \log_{10} I_2 \qquad (3)$$

where M_1 and M_2 are the magnitudes of the bodies being compared and I_1 and I_2 their respective intensities. The zero-magnitude point has been defined by adopting a value of 1.944×10^{-7} foot-candles for I_1 (ref. 19) which corresponds approximately to the illuminance of 10 moderately bright, nonvariable

stars (e.g., Vega and Arcturus). On this scale, the Sun has a magnitude of −26.72, the Moon, −12.7; thus, as the brightness of a body decreases, its magnitude increases. Note that from equation (3), the intensity ratio of two bodies is given by:

$$I_1/I_2 = 10^{-0.4\Delta M} \tag{4}$$

and that two bodies whose intensity ratio is 100 would have an absolute difference of exactly 5 magnitudes (refs. 5, 8, and 20).

In meteor observational practices today, three magnitude classifications based on the astronomical scale are used which indicate the techniques employed in obtaining data: vis., visual, photographic, and radar (or radio) magnitudes. Each observational technique has its own restrictions based on limiting magnitude (visual light or ionization intensity), field of view, or meteor path geometry; hence, a somewhat different portion of the meteor population is sampled by each method. The most precise information to date has been obtained with the photographic technique: radar, though a late starter, is fast becoming a close competitor.

Visual magnitude.—The oldest technique for observing meteors is, of course, with the naked eye. With this technique the visual observer compares and rates the brilliance of a meteor with that of stars in its vicinity. The comparison is largely subjective and is dependent on many factors such as meteor velocity, composition and altitude, but trained observers can usually agree remarkably well, within ± 0.5 (ref. 21), on their assessments of visual meteor luminosities.

Öpik (ref. 22) derived the following relation between the *absolute* visual magnitude of a meteor M_v (defined as the apparent magnitude of a meteor at a distance of 100 kilometers in the direction of the zenith) and, I, the average intensity of visual radiation emitted by the meteor:

$$M_v = 24.3 - 2.5 \log_{10} I \tag{5}$$

where I is in erg/sec. The constant (24.3 erg/sec) corresponds to the Sun's stellar magnitude of −26.72 and to the energy distribution of solar radiation according to the results of the Astrophysical Observations of the Smithsonian Institution. The intensity refers to that portion of radiation detectable by the human eye which is sensitive to wavelengths between roughly 4000 and 7000 angstroms; maximum sensitivity of the eye occurs at about 5600 angstroms corresponding to light in the middle, or yellow-green, part of the spectrum.

Öpik's expression, equation (5), allows an absolute comparison of all observed meteors by establishing a common point of observation (100 kilometers in the direction of the zenith). In practice, experienced observers seem to develop an absolute sense of magnitude, that is, they tend to express all meteor magnitudes in terms of the 100-kilometer zenith distance. All magnitudes referred to hereafter in this report will be absolute values unless clearly stated differently.

Three obvious shortcomings of the visual technique are: (1) no permanent records for later study; (2) the limit imposed on observation time, that is, the

technique is applicable only during clear, moonless nights (visual meteor data are generally corrected for the restricted viewing time); and (3) the limit of detectability. On the absolute magnitude scale this limit for the average naked eye is about +5 or +6 magnitude; popular 50-millimeter binoculars should enable one to see +8 or +9 magnitude meteors but such equipment severely curtails the field of view, one advantage associated with visual observations.

Photographic magnitude.—Photographic magnitude is the magnitude of a meteor deduced from a photographic plate. The photographic intensity of a meteor is compared with the intensities of star images on the same plate and an absolute photographic meteor magnitude M_p may be derived directly without reference to the visual magnitude. Because an untreated photographic emulsion is most responsive to light in the blue-violet part of the spectrum, the photographic magnitude deduced is not identical to the visual magnitude; however, reduction of photographic to visual magnitude is less troublesome than one might expect. For this report, it is sufficient to state that a large amount of simultaneous visual and photographic observations show that the relationship between two magnitudes is:

$$M_p = M_v + C \tag{6}$$

where C is a variable color index. The color index as derived by Jacchia (refs. 23 and 24) relates photographic and visual magnitudes in accordance with the following chart:

M_p	C
+4	−0.90
+2	−0.93
0	−1.31
−2	−1.86
−4	−1.94

The Baker Super-Schmidt camera has no peer in meteor photography as it provides a fairly continuous record of the night sky, the major interruptions being due to periods of intense moonlight as in the case of visual observations. The magnitude limitation for such equipment is approximately +4.1 on the photographic scale, which corresponds to approximately +5 on the visual scale (ref. 24). Since the photographic technique provides a more reliable and consistent measurement, it is now used as the basic standard.

Radar magnitude.—As stated earlier, debris entering the upper atmosphere can be detected by the reflection of a radar beam from the ionized wake the body creates. Whether or not a beam is reflected (echo received) is dependent on the frequency of the incident radar beam and the density of electrons in the ionized area. The "electron line density" q (the ionization produced per meter of the meteor path) of a meteor incident on the atmosphere may be expressed as:

$$q = \frac{\beta}{\mu v} \frac{dm}{dt} \tag{7}$$

where β is the probability that a single evaporated meteor atom will produce a free electron, μ the mass of the meteor atom, v the forward velocity, and dm/dt the rate of ablation (ref. 25).

As in the case of the photographic observations, an absolute radar magnitude relation can be defined in terms of the ionization produced per unit length of the meteor path without reference to visual magnitude. However, for comparative purposes, Kaiser derived the following expression:

$$M_r = 35 - 2.5 \log_{10} q \simeq M_v \tag{8}$$

for the radar magnitude M_r of a meteor which he stated corresponds approximately to the visual magnitude (ref. 26).

A similar expression later reported by Hawkins and Southworth (ref. 27) and McKinley (ref. 2) as:

$$M_r = 40 - 2.5 \log_{10} q \simeq M_v \tag{9}$$

has been adopted for the radar magnitude scale. Such a magnitude corresponds approximately to the visual magnitude of the meteor, although to be precise it must be called a radar magnitude. One may convert to the visual scale by adding a small correction γ for velocity (refs. 24 and 27) in the following manner:

$$M_r = 40 - 2.5 \log_{10} q - \gamma = M_v \tag{10}$$

McKinley's latest data on velocity index γ relates M_r and M_v in accordance with the following chart (ref. 27):

Velocity index (visual = radar + index)

v, km/sec	10	20	30	40	50	60
Index	−1.5	−0.7	−0.3	0.0	+0.2	+0.4

It can be seen that the two magnitude scales coincide at a velocity of 40 km/sec. Equation (10) was based on observations of meteors with visual magnitudes less than +5 and greater than −2.

Fifteen-inch (380-millimeter) telescopes are not likely to be readily available to the radio worker, but if he had one he would be able to see +12 or +13 M_v meteors—provided that he were blessed with the quality of patience in abundance. Owing to the very small field of view of most telescopes of this size, the actual yield is usually measured in terms of hours per meteor rather than meteors per hour. Radar records (Gallagher 1958) indicate that meteors as faint as $M_v = +15$ have been recorded (ref. 2) and instrumental limits have not yet been reached. It will be interesting to see if more sensitive apparatus will detect fainter meteors or if, as Astapovich suggested some time ago, there are no true meteors fainter than about +19 or +20 M_v (ref. 2).

Though the preceding statements indicate that extremely small sized particles can be observed with radar equipment, reported data to date have

been essentially limited to particles with masses greater than approximately 10^{-3} gram. As calibration of the radar-meteor technique becomes more refined, data on the smaller sized particles, at least down to about 10^{-4} gram will be available with a greatly increased reliability over the present estimates.

Radar observations are not limited in sampling period as are the visual and photographic observations; therefore, the population sampled by this technique may be more statistically significant than comparable data for the other methods.

METEOR THEORY

Basic meteor theory as it exists today results from the work of a number of people, including in particular Morris, Sparrow, Hoppe, Öpik and Whipple, and has been documented many times (see, e.g., refs. 1, 2, 28, and 29).

It is supposed that a meteoroid of mass m, irregular dimensions, and internal density ρ enters the upper atmosphere with velocity v. Because of the high velocity, the kinetic energy of the incoming body exceeds the internal energies necessary to pulverize, melt, or vaporize the material. Air particles are trapped momentarily on or near the surface of the meteoroid, imparting to it the energy of collision and decreasing its forward momentum. The air particles are given a forward velocity while the meteoroid suffers a deceleration, dv/dt, so that by the principle of conservation of momentum:

$$m\frac{dv}{dt} = -\Gamma S\rho_a v^2 \tag{11}$$

where ρ_a is the density of the atmosphere, and Γ, v, m, and S the drag coefficient $(C_d/2)$, velocity, mass and effective cross-sectional area of the meteor, respectively.

It is convenient to eliminate one variable from equation (11) by expressing the cross section as a function of the mass m. If, for example, the meteor is a sphere of density ρ, the radius a may be found as a function of density from:

$$a = (3/4\pi)^{1/3} m^{2/3} \rho^{-1/3} \tag{12}$$

The cross sectional area (equal to πr^2) may then be expressed as:

$$S = (9\pi/16)^{1/3} m^{2/3} \rho^{-2/3} \tag{13}$$

In general, the meteoroid will be an irregularly shaped object; therefore, the quantity $(9\pi/16)^{1/3}$ may be replaced by a general dimensionless shape factor, A, which ranges from 1.21 for a sphere to 1.50 for a randomly oriented cube. Equation (11) may then be written as:

$$\frac{dv}{dt} = -\Gamma A \rho^{-2/3} m^{-1/3} \rho_a v^2 \tag{14}$$

establishing the first fundamental equation in meteor theory, the drag equation.

From the principle of the conservation of energy we may equate the energy imparted by the colliding particles to the energy required for ablation (vaporization, melting, or fragmentation) of the meteoroid, since the kinetic energy

lost by deceleration of the meteoroid is negligible. Thus:

$$2\zeta\frac{dm}{dt} = -\Lambda A\,\rho^{-2/3}\,m^{2/3}\,\rho_a v^3 \tag{15}$$

where ζ, the heat of ablation, is the energy required to ablate 1 gram of the meteoroid, and Λ, the heat transfer coefficient, is the efficiency of the energy exchange. Values of Λ in the range 0.6 down to 0.1 or less have been proposed. The second fundamental equation, the mass equation, is obtained by dividing equation (15) by equation (14), which gives:

$$\frac{1}{m}\frac{dm}{dt} = \frac{\Lambda}{2\Gamma\zeta}\,v\,\frac{dv}{dt} \tag{16}$$

The material ablated from the surface of the meteoroid collides with the particles of the atmosphere with the forward velocity v, and hence each meteor atom has a kinetic energy of from 100 to 1000 electron volts. This energy is sufficient to ionize and excite the air particles with consequent emission of light. If the fraction of the kinetic energy converted into light is τ (luminous efficiency), then the luminous intensity I may be expressed as:

$$I = -\frac{1}{2}\frac{dm}{dt}v^2\tau \tag{17}$$

The luminous efficiency term τ is a combination of the luminous efficiency of meteor vapors which are ionized and excited during the conversion of kinetic energy to visible light, the luminous efficiency associated with thermal collisions between atoms in the coma (the jet of vapor atoms which emerge from the meteoroid and mix with the atmosphere), and the component associated with blackbody radiation of the hot meteoroid surface (ref. 8).

Unfortunately, in practice only a fraction of the luminous intensity is perceived by the eye or by the photographic plate and this fraction presumably varies with velocity, height, and composition of meteors. The fact that most of the meteoric light is emitted in bright spectral lines adds to the observational problem. If one is to evaluate the radiative energy perceived of a meteor from equation (17), he must expect to deal with a variable coefficient τ.

The most elaborate theoretical attempt to derive and analyze the behavior of τ in the visual domain as a function of the meteor velocity was originally made by Öpik in 1936–1937 (ref. 2). A plot of Öpik's values of τ for bright meteors against velocity shows that for velocities greater than 12 km/sec it can be very nearly represented by a linear relation as $\tau = \tau_0 v$. This relation is applicable to the brighter photographic meteors only, and even in these cases its validity is regarded skeptically (ref. 2). For fainter meteors as seen by the eye, τ appears to vary more slowly than the first power of v and for faint dustballs, perhaps even to a negative power. For the brighter photographic meteors, one would obtain on acceptance of $\tau = \tau_0 v$:

$$I = -\frac{\tau_0 v^3}{2}\frac{dm}{dt} \tag{18}$$

Integration of equation (18) from a given instant t on the light path of the meteor to the time t_e when the meteor disappears at the end of its flight yields the mass at any time t:

$$m = \frac{2}{\tau_o}\int_t^{t_e} Iv^{-3}\,dt \tag{19}$$

For this purpose the change in velocity to the end of the meteor may be neglected and v^{-3} brought out from under the integral sign. From this equation, the product $m\tau_o$ can be evaluated in terms of observable quantities but neither can be determined alone. It is the various values used for τ_o, or τ, which cause the discrepancies between published values of mass. Note that a complete light curve is necessary to obtain the mass of a meteoroid before it enters Earth's atmosphere.

For the last basic equation of meteor theory, recall that the ionization produced per meter of the meteor path was expressed as:

$$q = \frac{\beta}{\mu v}\frac{dm}{dt} \tag{7}$$

Thus, there are four basic equations in meteor theory, equations (7), (14), (16), and (18), with mass, density, velocity, and time as unknown variables. Two of these, v and t, can be evaluated by observations, but the two most important, m and ρ, cannot. There are five unknown quantities, Γ, A, ζ, τ_o, and β which are approximately constant. From the four basic equations, quantities which lump the unknown constants can be determined from observational results. Such quantities include $2\rho^2/\tau_o(\Gamma A)^3$, $\Lambda/2\Gamma\zeta$, and $\tau_o\beta$ and their correct evaluations represent the crucial problems facing meteor theory at the present. To evaluate $2\rho^2/\tau_o(\Gamma A)^3$, referred to in the literature and later in this report as K, the expression for mass from equation (19) can be substituted into equation (14) to obtain:

$$\frac{\tau_o}{2\rho^2}(\Gamma A)^3 = -(1/\rho_a v^2)^3\,(dv/dt)^3\int_t^{t_e} Iv^{-3}\,dt \tag{20}$$

Note that for a particular magnitude meteor all quantities on the right-hand side of this equation except ρ_a are obtainable from photographic observations and that ρ_a is available from standard atmospheric tables.

The quantity $\sigma = \Lambda/2\Gamma\zeta$ may be found by combining equations (16), (17), and (19) to obtain:

$$\frac{1}{\sigma} = \frac{2\Gamma\zeta}{\Lambda} = \frac{-v}{I}\frac{dv}{dt}\int_t^{t_e} I\,dt \tag{21}$$

To express τ_o/β in terms of measured quantities, eliminate dm/dt between equations (7) and (18) to obtain the relation, $I = qv^4\,\mu\tau_o/2\beta$. Substitution for I in equation (5) yields the approximate magnitude relationship:

$$M_v = 25.35 - 2.5\left(4 \log_{10} v + \log_{10} \frac{\tau_o}{\beta} + \log_{10} \mu + \log_{10} q\right) \quad (22)$$

in cgs, from which τ_o/β may be estimated (ref. 28).

TERRESTRIAL OBSERVATIONS OF METEORS

A vast amount of the present knowledge of interplanetary debris has resulted from terrestrial observations of the interaction of the debris with the upper atmosphere of the Earth and will be summarized in this section. Debris smaller than that observable by radar equipment cannot be detected as it floats through the atmosphere to settle on Earth's surface; however it can be collected and analyzed. The knowledge acquired in this way concerning such debris will be discussed in subsequent sections of this report.

Spatial distribution.—Meteors of all magnitudes may be divided into two general classes, shower and sporadic. Shower meteors occur when Earth intercepts the common orbital path of a swarm of meteoroidal particles. Meteor fluxes may range up to 10^5 times the normal sporadic background during a shower, but they are more commonly less than 10, and typically less than 4 or 5 times the normal background (refs. 6 and 20). Certain meteor showers appear on about the same date each year while some do not reappear for several years, if ever (ref. 30). A list of some of the more definite meteor streams is given in table II. Orbital parameters of table II include: inclination to ecliptic plane, i; eccentricity, e; perihelion distance, q; argument of perihelion, ω; longitude of ascending node, Ω; and geocentric velocity outside Earth's atmosphere, v_∞. The meteors in a given shower all appear to originate from the same point in the sky and are thus named from some stellar feature near that point. In addition, there is a remarkable similarity between the orbits of certain comets and meteor showers and some of these associations are given in table II. It is this association that is responsible for Whipple's statement that approximately 99 percent of the meteoroidal influx is of cometary origin. Some meteor showers have not as yet been associated with a comet, however, and many comets (especially those with nearly parabolic orbits) whose orbits intersect that of Earth do not appear to have an associated shower.

The compilers of table II, Whipple and Hawkins (ref. 1), have noted that some showers are visible for only a few hours and come from a small area of the sky; for example, an area 3 minutes in radius for the Draconids, while others, such as the Northern Taurids, last for 46 days and come from an area with a radius of 46 minutes (ref. 6).

Any meteor that cannot be identified with a stream or shower of meteoroids is classified as sporadic, that is, of the meteor component constituting the normal background. For meteors with a visual magnitude of less than approximately +5 (essentially those detectable with the naked eye), several investigators have determined that the majority are sporadic; Lovell has estimated 80 to 90 percent of meteors of all sizes are sporadic (ref. 30) while

TABLE II.—*Observational Quantities of Orbital Elements of Known Meteor Streams*

[From ref. 1]

Stream	U.T. date at maximum	Extreme limits	Radiant 1950 R.A. Dec.	V∞, km/sec	Hourly rate at maximum			Radiant transit (local time) midnight = 00^h	ω	Ω	i	π	a, A.U.	e	q, A.U.	Parent comet
					Visual	Photo	Radio									
Quadrantids	Jan. 3	Jan. 1 4	230 + 48	42.7	30	1.9	95	08^h 28^m	167°9	282°6	73°8	90°1	3.42	0.715	0.974	
Virginids	Mar. 13	Mar. 5 21	183 + 4	30.8	1	.....	<5	00 49	285.8	353.7	5.2	279.5	2.82	.857	.403	
II		Mar. 13 Apr. 21	157 + 56	15.2	.....	.....	.....	20 49	187.1	27.3	11.0	214.4	2.67	.626	.999	
Lyrids	Apr. 21	Apr. 20 23	270 + 33	48.4	5	.....	11	03 59	213.9	31.8	79.9	245.6	29.6	.969	.918	1861 I
η Aquarids	May 4	May 2 6	336 + 0	64	5	.....	15	07 36	83.0	43.1	160.0	126.1	5.0	.91	.47	Halley ?
Daytime Arietids	June 8	May 29 June 18	44 + 23	39	.....	.....	66	09 51	29	76.8	21	106	1.6	.94	.09	(Second crossing δ Aquarids)
Daytime ζ Perseids	June 9	June 1 16	62 + 23	29	.....	.....	42	10 59	59	77.8	.4	137	1.6	.79	.34	
Daytime β Taurids	June 30	June 24 July 6	86 + 19	32	.....	.....	27	11 12	246	276.4	6	162	2.2	.85	.34	Encke
Southern Aquarids	July 30	July 21 Aug. 15	339 − 17	43.0	.....	.....	.....	02 14	154	302	29.3	97.6	2.60	.976	.062	
Northern δ Aquarids		July 14 Aug. 19	339 − 5	42.3	10	.....	34	02 08	332.6	138.9	20.4	111.4	2.62	.973	.070	
Southern i Aquarids		July 16 Aug. 25	338 − 14	35.8	.....	.....	.....	02 04	127.5	311.0	6.0	78.5	2.88	.920	.230	
Northern i Aquarids		July 16 Aug. 25	331 − 5	31.2	.....	.....	.....	01 36	308.0	150.9	4.7	98.9	1.75	.842	.265	
α Capricornids	Aug. 1	July 17 Aug. 21	309 − 10	25.5	.....	.....	10	00 00	270.5	132.8	4.0	43.3	2.57	.779	.568	1948 n
Perseids	Aug. 12	July 29 Aug. 17	46 + 58	60.4	37	2.5	49	05 43	151.2	138.1	113.7	289.3	20.8	.955	.936	1862 III

TABLE II.—*Continued*

Stream	U.T. date at maximum	Extreme limits	Radiant 1950 R.A. Dec.	V∞, km/sec	Hourly rate at maximum			Radiant transit (local time) midnight = 00h	ω	Ω	i	π	a, A.U.	e	q, A.U.	Parent comet
					Visual	Photo	Radio									
κ Cygnids		Aug. 19 22	289 + 56	26.6	.....	.....	<5	21 25	204.2	144.3	37.0	348.4	4.09	.762	.973	
Draconids	Oct. 10	Oct. 10	264 + 54	23.1	Periodic			16 13	171.8	196.3	30.7	8.1	3.51	.717	.996	Giacobini-Zinner
Orionids	Oct. 22	Oct. 18 26	94 + 16	66.5	13	2.9	18	04 12	86.8	29.8	163.2	116.5	7.70	.930	.539	Halley ?
Southern Taurids	Nov. 1	Sept. 15 Dec. 15	51 + 14	30.2	5	.....	.....	00 42	111.9	45.1	5.4	156.9	2.30	.835	.380	Encke
Northern Taurids	Nov. 1	Oct. 17 Dec. 2	52 + 21	31.3	5	.....	<15	00 46	298.4	221.8	3.2	160.2	2.14	.849	.323	Encke
Andromedids	Nov. 7	Nov. 7	22 + 27	21.3	.....	.....	<5	22 23	242.4	224.4	6.0	107.8	3.34	.776	.748	Biela
Leonids	Nov. 17	Nov. 14 20	152 + 22	72.0	6	.....	<10	06 22	173.7	235.0	162.5	48.7	12.76	.924	.970	Temple
Geminids	Dec. 14	Dec. 7 15	113 + 32	36.5	55	5.6	80	02 01	324.3	261.2	24.0	225.6	1.39	.899	.140	
χ Orionids		Dec. 9 14	87 + 21	30.6	.....	.....	.....	00 25	105.4	79.8	0.8	185.2	2.92	.859	.412	
Monocerotids		Dec. 13 15	103 + 8	44.0	.....	.....	.....	01 21	128.2	81.6	35.2	209.9		1.002	.186	
Ursids	Dec. 22	Dec. 17 24	206 + 80	35.2	15	.....	13	08 24	212.2	264.6	52.5	116.8	5.91	.845	.916	Tuttle

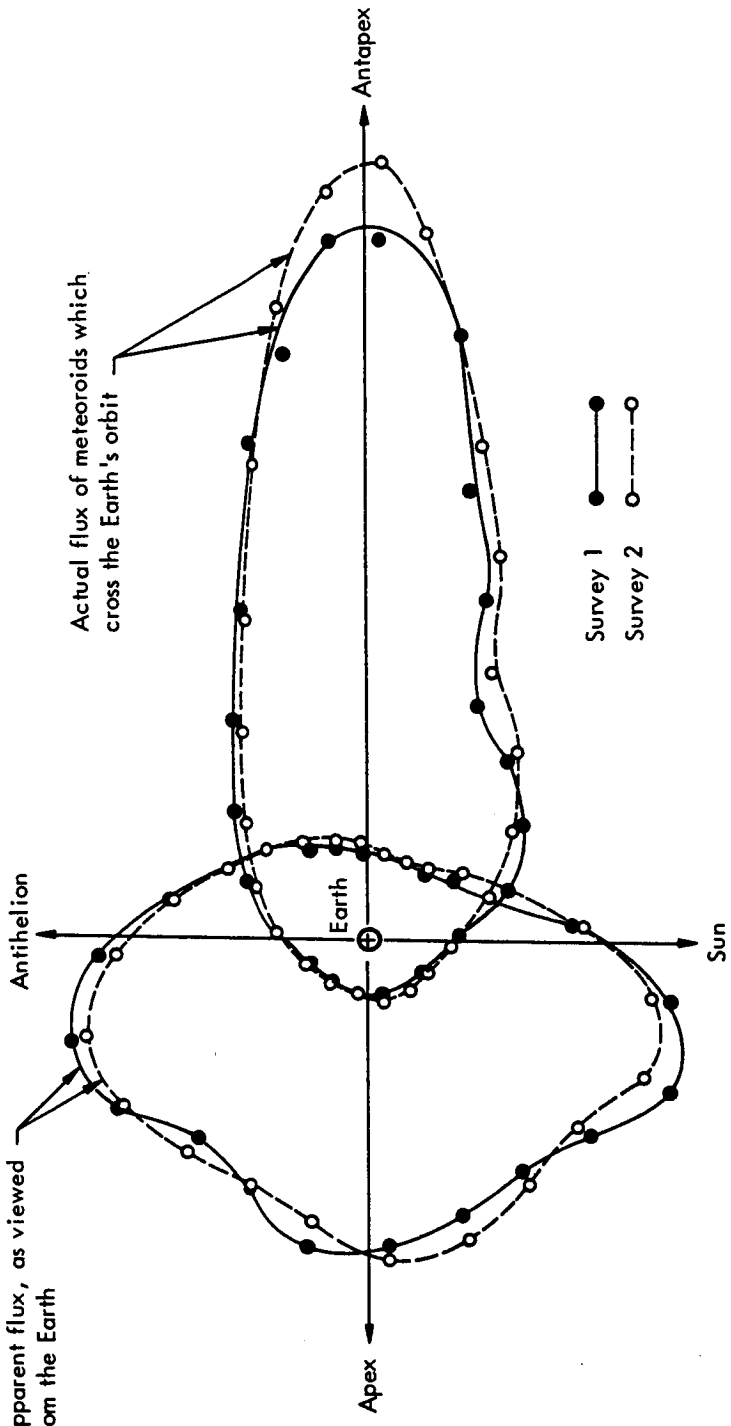

Figure 1.—Polar diagram in the plane of Earth's orbit showing the apparent number of meteor radiants detected per unit angle, per unit time.

Hawkins estimates the amount to be a minimum of 50 percent (ref. 31 and an unpublished paper entitled "Interplanetary Debris"). One might conclude then that the majority of meteoric material striking the Earth is sporadic; however, it is quite feasible that these meteors originally belonged to showers which have been dissipated in time by the continual action of the Poynting-Robertson effect. However, large daily and even hourly fluctuations occur, particularly among the fainter meteors observed with radar equipment, in the influx rates. These fluctuations support the hypothesis that many of the sporadic meteors actually belong to so-called minor streams or showers which are much less concentrated than the major ones (refs. 8 and 30).

Figure 1 (refs. 1, 8, 13, and 32) shows some directional characteristics of meteoric particles determined from radar data. The figure is a polar plot of the observed (apparent) and actual flux of particles in the plane of the ecliptic at Earth's distance from the Sun and indicates the relative number of meteor radiants detected per unit angle per unit time. In this figure, the length of the radius vector is proportional to the number of meteors crossing Earth's orbit at a given polar angle. The plot represents the yearly averages of all particles for two surveys: the solid line is faired through data obtained in 1949–1950, and the dashed line through data obtained in 1950–1951. It is obvious that the apparent flux is more concentrated at the apex of Earth's way; however, this results from the fact that Earth is catching up with a large number of particles and when the data is corrected for the orbital velocity of Earth, the longitudinal profile labeled "actual" is obtained. The actual distribution thus indicates that meteoroid heliocentric movement is predominantly direct, and that most of the particles are overtaking Earth. The ratio of direct to retrograde orbiting meteors from the radar data is approximately 30 to 1 and from visual data approximately 50 to 1 (ref. 1).

Figure 2 (refs. 8 and 13) illustrates the distribution in latitude from the ecliptic plane in the vicinity of Earth. The figure shows that most of the incoming particles have trajectories at small angles with the plane of the ecliptic. More than 40 percent—Davidson and Winslow report approximately 50 percent (ref. 32)—of the meteoric particles have orbits within 15° of the ecliptic plane (ref. 6); more than 90 percent of the particles are included within 40° of this plane. This distribution is not surprising because most of the comets which are seen from Earth also approach from within 40° of the ecliptic plane. Such a correlation supports Whipple's hypothesis that most meteoroids are of cometary origin. The meteors of cometary origin thus far discussed burn up or disintegrate in the atmosphere; some of the resulting debris slowly filters to Earth's surface as dust.

Meteors falling to Earth's surface as meteorites also contribute to the total sporadic background and orbital data on such particles indicate asteroidal origin. Near Earth's orbit, at least, the flux of asteroidal debris is so low that the chance of such a particle colliding with a spacecraft is negligible (ref. 33).

A summary of the sources of interplanetary debris colliding with Earth

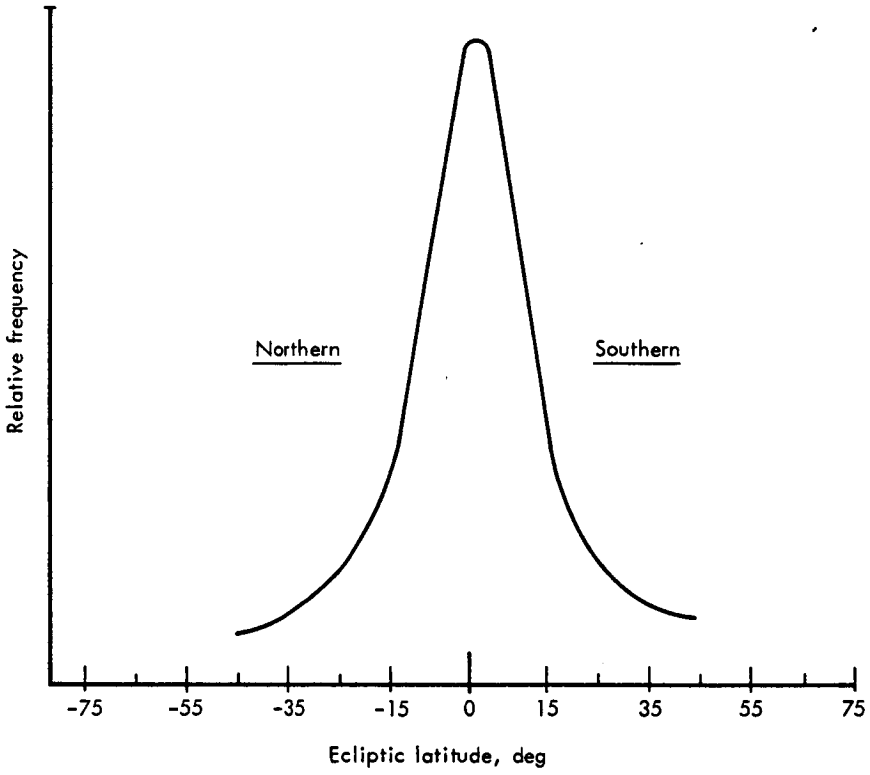

Figure 2.—Distribution of the meteor flux about the plane of the ecliptic at Earth's distance from the Sun.

is depicted in the manner of a flow chart in figure 3 (ref. 4). The figure is a slightly revised version of the original to correlate with the definitions adopted for this report.

Velocity.—The most unambiguous characteristic of meteors is their velocity extremes relative to Earth (refs. 6, 21, 34, 35, and 36). These extremes, for meteoroids originating within the solar system, are approximately 11 and 73 km/sec. Flight along a hyperbolic trajectory would result in velocities in excess of 73 km/sec and consequently indicate interstellar origin. The small number that has been observed at slightly higher velocities are believed to have resulted from gravitational perturbations.

The value 73 km/sec is the maximum magnitude of the vector sum of Earth's orbital velocity (approximately 29.70 km/sec) and the parabolic heliocentric velocity for a particle at Earth's distance from the Sun (approximately 43 km/sec). The lower limit of 11 km/sec is simply the velocity a particle would have if it fell a great distance in space and experienced only the gravitational force of Earth; more simply, it is Earth's escape velocity.

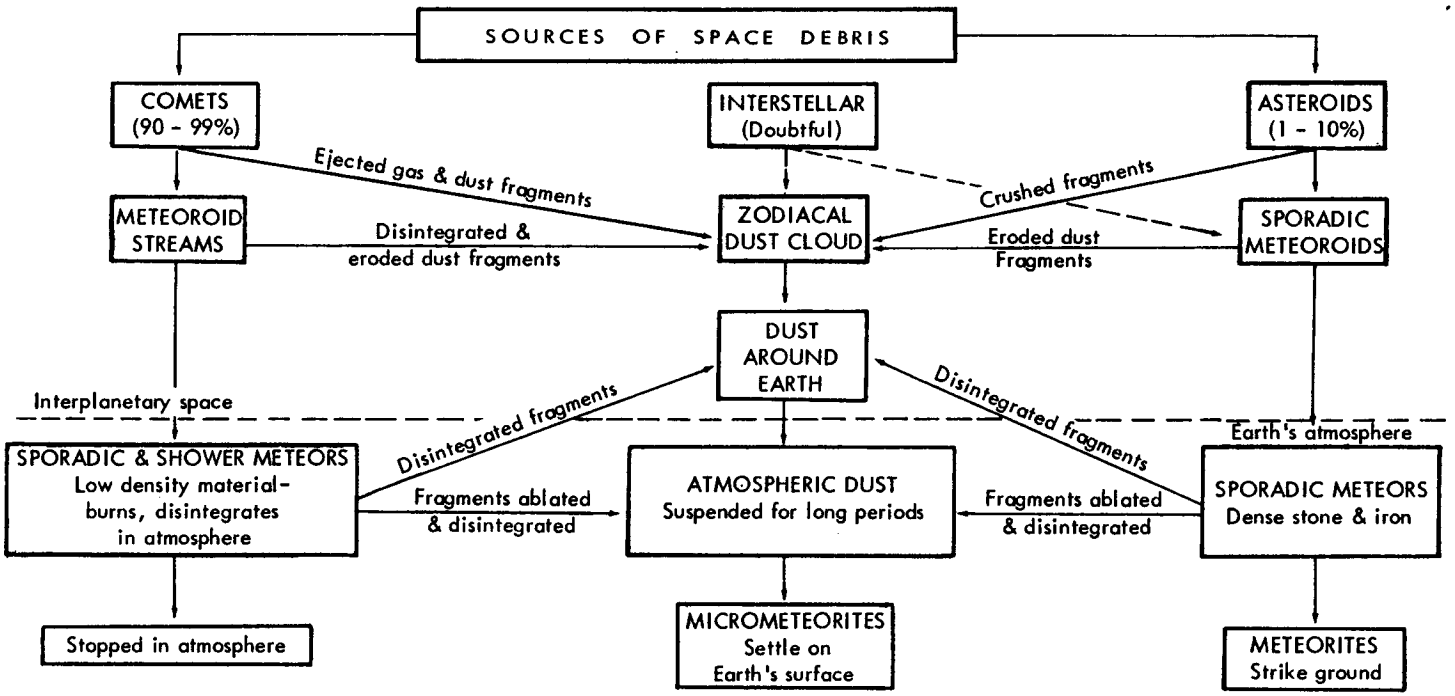

Figure 3.—Sources of interplanetary debris colliding with Earth.

Close to Earth, a meteoroid's geocentric velocity may be expressed by:

$$v^2 = v_2^2 + v_e^2 \frac{a_e^2}{x^2} \qquad (23)$$

where v_2 is the geocentric velocity of the meteoroid far from Earth (11 to 73 km/sec), v_e, the escape velocity (11 km/sec), a_e, the radius of Earth and x, the distance from the center of Earth (ref. 36). Thus, at Earth's surface, the gravitational attraction increases the 11- and 73-km/sec velocities to 15.6 and 73.9 km/sec, respectively. Velocities relative to a space vehicle will, of course, depend on the velocity of the vehicle relative to Earth. An Earth-orbiting vehicle at an altitude of 555 km has a velocity of 7.6 km/sec relative to Earth; hence, meteoroid impacts can occur in the velocity range between approximately 7.8 and 81.5 km/sec.

In the vicinity of Venus, the maximum relative velocity of a meteoroid would be approximately 84 km/sec; 35 km/sec orbital velocity plus 49 km/sec for the parabolic heliocentric velocity for a particle at Venus' distance from the Sun (ref. 30).

The velocity distribution as determined by photographic observation of sporadic and shower meteors with visual magnitudes between approximately −2 and +4.5 is shown in figure 4 (refs. 23 and 28). The histogram was prepared by Hawkins and Southworth from photographic data on 285

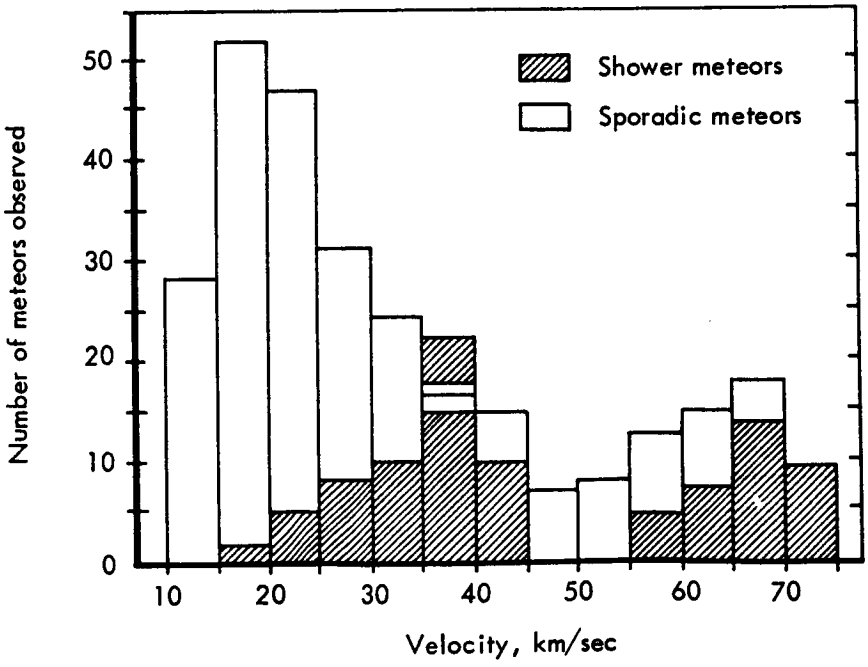

Figure 4.—Meteor velocity distribution from photographic observations.

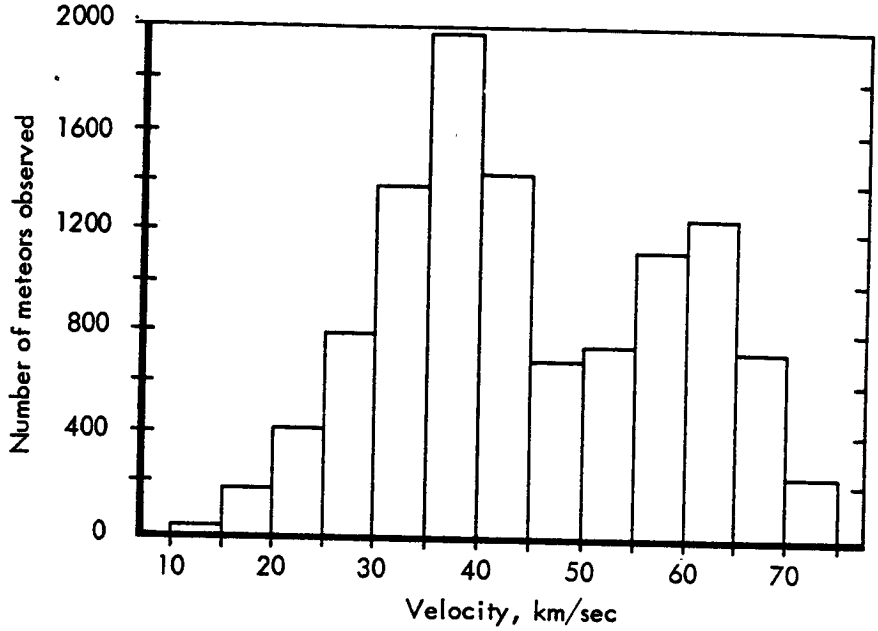

Figure 5.—Meteor velocity distribution from radar observations.

sporadic meteors and 74 shower meteors. In the figure, the shaded area represents shower meteors, and the clear area represents sporadic meteors. The distribution for sporadic meteors is bimodal peaking at velocities of 22 and 67 km/sec. The minimum between 45 and 55 km/sec represents meteors with two relatively unlikely types of orbits. One type is retrograde with small inclinations to the ecliptic plane and semimajor axes between 0.7 and 2.5. Orbits of this type are rare in the photographic records and it is difficult to visualize a process by which meteors could be injected or moved into them by the perturbative forces (ref. 28). The second type meets Earth's orbit nearly perpendicularly, and has a semimajor axis between 2 and infinity. Meteors of this type, which have radiants near the ecliptic plane, are almost linear oscillators and their collision with the Sun or the outer corona is highly probable (ref. 28). The distribution for shower meteors also has a bimodal character; however, the velocities tend to be concentrated in two ranges, between 25 and 45 km/sec and between 55 and 70 km/sec. Hawkins and Southworth calculated mean velocities of 33.6 km/sec for the sporadic meteors and 42.8 km/sec for shower meteors. Their weighted average of the two types was 35.5 km/sec (ref. 30). Whipple has adopted a mean velocity of 22 km/sec from photographic data on cometary meteors with magnitudes of less than approximately +5 (ref. 37).

It is interesting to compare the velocity distribution of meteors obtained from radar observations with that obtained from the photographic data.

Figure 5 (refs. 1 and 2) is a velocity histogram computed from McKinley's meteor radar echo data on approximately 11 000 meteors. The bimodal character of the distribution is again present; however, a comparison of figures 4 and 5 shows a general displacement of the data toward higher velocities. The mean velocity for this radar determined distribution has been estimated by Manning at 40 km/sec (ref. 23).

The variance in the velocity distribution obtained from photographic and radar data has been explained by Whipple (ref. 1) in terms of the limiting magnitude detectable as a function of velocity. For meteors detected at a constant line density of electrons, Whipple relates the limiting visual magnitude to the velocity of the meteor in the manner shown in the following chart:

	Limiting visual magnitudes at velocities, km/sec, of —				
	20	30	40	50	60
Radar equipment	0.0	0.7	1.2	(1.6)	(1.9)
Camera	0.0	−0.3	−0.8	−1.0	−1.2

The actual limiting magnitude, of course, depends on the sensitivity of the equipment, and the chart quotes a relative scale on the assumption that a visual magnitude of zero is detectable by radar at a velocity of 20 km/sec. On the other hand, the photographic intensity of a meteor image decreases as the trailing velocity across the photographic plate increases. The dependence of limiting magnitude on velocity for the camera is based on the assumption that there is no reciprocity failure in the photographic plate. Since meteors become more numerous as magnitude increases this difference in sensitivity adequately accounts for the different velocity distributions found by radar and photographic methods. At velocities greater than 50 km/sec, the number of detected radar meteors decreases, probably because diffusion of the ion column reduces the echo amplitude. The limiting magnitudes of meteors affected by diffusion are indicated by parentheses in the chart.

Hawkins and Lindblad have reported systematic changes in the average velocity of meteors which were dependent upon magnitude, and hence size (ref. 38). These authors reported a decrease in average velocity by 5 km/sec between the magnitude +6 and +9 and indicated that the effect becomes more marked for meteors with magnitudes greater than +9. This supports the view that, in the vicinity of Earth at least, the velocity decreases with particle size. Whipple has estimated an average velocity of 15 km/sec for micrometeoroids with visual magnitude greater than +19 (ref. 16).

The velocity distributions discussed above are the results of observations of cometary meteors only. The velocities of asteroidal meteors, relative to Earth or to a spacecraft, are usually about 20 km/sec, although an occasional one may have a relative velocity as high as 72 km/sec (ref. 33). Whipple and

Hughes (ref. 39) have adopted 16.5 km/sec as a best estimate of the mean atmospheric velocity of such meteors.

In general, fast meteors occur during the early morning hours (about 0600 hours local time) when the observer is on the forward side of Earth (that is, the meteors are in retrograde orbits and thus meet Earth head on), and the slow meteors occur in the evening (about 1800 hours local time) when the observer is on the trailing side of Earth (that is, the meteors are in direct orbits and are catching up to Earth).

The faster meteors first become visible at heights of 120 to 105 kilometers and disappear between 105 and 75 kilometers. The slow meteors first appear 20 to 30 kilometers lower. A typical average meteor as bright as Vega, Capella, or Arcturus (that is, of zero visual magnitude) moving at 40 km/sec appears at a height of 105 kilometers, reaches a maximum brightness at 93 kilometers, and disappears at 88 kilometers. A large bright asteroidal meteor (a fireball) moving at the same speed but 10^4 times as bright (visual magnitude —10) appears probably a shade higher in the atmosphere than the fainter object, reaches maximum brightness at 75 kilometers and disappears at 65 kilometers. These heights and velocities are averages from photographic data secured by the Harvard College Observatory (ref. 40).

Density.—Density has been one of the most difficult parameters to determine since it is not a directly measurable quantity. Even current rocket and satellite measurements have not alleviated the difficulty; piezoelectric or microphone pick-ups used on such vehicles are momentum sensitive and thus do not yield mass, much less density information directly. Consequently, much of the current literature on this parameter is inconclusive, vague and even contradictory. This is particularly true when an attempt is made to determine the correlation between mass densities and spatial number density (ref. 30). The knowledge possessed of meteoroid densities results from estimates based on terrestrial observations of meteors and analyses of recovered meteorites. These investigations indicate that meteoroids differ not only in mass, but that those which have approximately the same mass may differ widely in composition and structure.

Analysis of meteorites observed during their burning descent through the atmosphere and recovered on Earth's surface yields the following rather conclusive density divisions for meteors of asteroidal origin: (1) stones, mainly silicates with some nickel-iron alloy with densities of 3 to 3.5 g/cm^3; (2) irons, mainly nickel-iron alloys with 5 to 20 percent nickel with densities of 7 to 8 g/cm^3; and (3) stony irons (relatively infrequent), mixtures of nickel-iron alloys and silicates with densities of 3.4 to 4.0 g/cm^3 (refs. 6, 30, 33, 41, and 42). For a more complete discussion of the variations in composition of meteorites the reader is referred to references 1, 9, and 43.

Of those meteorites observed falling, stones have predominated over the irons by a factor between 5 and 10 (refs. 6 and 30); however, the actual ratio of one type to the other is a function of mass. For meteors with masses

greater than approximately 10^{10} g, the irons outnumber the stones. The occurrence of meteors with such large masses is truly a rare event, accounting for the over-all predominance of stones (ref. 31 and an unpublished paper entitled "Interplanetary Debris").

Tektites, small glassy bodies found on Earth's surface, are not definitely known to be of meteoroidal origin and, therefore, are not discussed. For treatments of these bodies, the reader is referred to references 8 and 44.

The last density category of meteoroids embraces the so-called dustballs of cometary origin. The problem of determining densities of this class of meteoroids from meteor observations is complicated by the fact that they appear to be porous bodies of loosely bound particles many of which shatter completely on experiencing very slight forces. From the height at which disintegration takes place and from the velocity of the meteor, it is possible to calculate the dynamic pressure exerted on the body. Such calculations indicate that cometary meteors have extremely low crushing strengths by terrestrial standards, comparable to that of cigar ash (ref. 31). At the limit of photographic observations, approximately 10^{-3} gram, most of the meteors are totally disintegrated at or before the onset of ionization and are observed as a closely packed cloud of many independent fragments.

As a result of the fragmentation and disintegration, density estimates for particles outside Earth's atmosphere have been various. Öpik is reported to support a value of 0.01 to 0.1 g/cm^3; Jonah, a value of 0.3 g/cm^3 for particles with masses corresponding to magnitudes of +15 or less and 4 g/cm^3 for particles with masses corresponding to magnitudes greater than +15 (ref. 30); and Verniani, a value of about 0.2 g/cm^3 (ref. 45). Whipple in 1963 adopted a value of 0.44 g/cm^3 for the average density of a zero magnitude meteor of cometary origin (refs. 37 and 46), an increase by nearly an order of magnitude over his 1958 value of 0.05 g/cm^3 (ref. 16).

Whipple's 1963 (ref. 37) density estimate was based on results obtained from the Trailblazer 1 experiment which consisted of ejecting an iron particle of known mass and composition from a rocket into the upper atmosphere at a velocity of approximately 10 km/sec. From photographic observations of velocity and luminosity and by applying equation (19) values of τ_o for the iron particle were calculated. The value of τ_o thus obtained was corrected by Whipple to apply to cometary meteoroids of stony composition and the density computed from K values [$K = (\Gamma A)^{-8}\, 2\rho/\tau_o$] determined observationally from equation (20); a value of 0.92 was assumed for ΓA. In this publication, Whipple reported that data on τ_o obtained by Cook, *et al.*, just prior to his going to press would, if adopted, lead to a mean density of 0.25 g/cm^3 for a zero magnitude meteor of cometary origin.

In his 1958 paper (ref. 16), Whipple held the opinion that the average cometary meteoroid density probably increased with decreasing mass, attaining that of stony or possibly iron asteroidal particles. In his 1963 publication (ref. 37), he states that it is possible that the mean density and particle

strength may either increase or decrease. This conclusion is based on observational data from the Harvard radar program which indicates that fragmentation of meteoroids also occurs frequently among meteors in the visual magnitude range of approximately +8.

In summary, much weight must be given to the values determined by Whipple and Cook since they are based on the most recently and more reliably obtained data. Therefore, it appears that the average density for zero magnitude cometary meteors is between approximately 0.25 and 0.44 g/cm^3. At some larger magnitude, perhaps greater than +8, the mean density increases, approaching that of stony asteroidal meteoroids (approximately 3.5 g/cm^3); for the smallest particles, the density may be greater yet. Note that the density values given for the zero magnitude meteors are average; there is little doubt that density of these particles before entering the atmosphere encompasses a range of more than one order of magnitude (ref. 37).

Meteor magnitudes and influx rates of sporadic meteors.—Visual observations by numerous investigators have established that the number of meteors, dN, impinging on Earth's atmosphere with visual magnitudes between M_v and dM_v is given by the incremental law:

$$dN = ar^{M_v}\, \mathrm{dM}_v \tag{24}$$

where a is constant and$r$ the ratio of increase in the number of meteors between magnitude intervals M_v and $(M_v + 1)$ and $(M_v - 1)$ and M_v (refs. 1, 2, 6, and 24).

The cumulative law, giving the total number of meteors brighter than magnitude M_v is found by integrating equation (24) between the limits of $-\infty$ and M to give:

$$\log_{10} N = \log_{10} a - \log_{10} (\log_e r) + M_v \log_{10} r \tag{25a}$$

or

$$\log_{10} N = N_o + M_v \log_{10} r \text{ (per unit area per unit time)}$$

after Hawkins (ref. 24) where in the latter arrangement the constant N_o is the logarithm of the influx rate of meteors with M_v less than or equal to zero and is the sum $\log_{10} a - \log_{10} (\log_e r)$ and r is the ratio of increase given by the incremental law. Equation (25a) can be written, as will be shown later, with the variable M_v replaced by photographic magnitude, M_p, the electron line density, q, or the meteoroid mass, m. In any case, there are two problems associated with this equation: determination of the ratio r, and the value of N_o. It is apparent that r will be different for sporadic and shower meteors; therefore each type will be considered separately.

For sporadic meteors, the value of r appears to be constant over various ranges of magnitude; however, there is considerable uncertainty in its actual value. Hawkins and Upton (ref. 24), in discussing the various values assigned to r, attribute to Millman and Burland (1957) the statement that published values vary between 2.0 and 4.1. Hawkins and Upton attribute the variation in the reported values to: an actual decrease in the ratio for faint meteors, since r must finally tend to unity the number of meteors in the solar system

is to be finite; and uncertainties in observations and in the correction factors involved.

McKinley (ref. 2) in summarizing the various values of r, states that Öpik in 1958 found an average value of 3.3 for all meteors observed in the Arizona Expedition program. Furthermore, Öpik was able to break this down according to the types of orbits followed by meteors: for retrograde orbits, he obtained a value of 2.80, for direct orbits near the plane of the ecliptic he obtained $r = 3.56$ and 3.66. According to McKinley, the Jodrell Bank (England) workers concluded that $r = 2.4$ based on radar data corrected for strong showers such as the Perseids and Geminids; however, Dr. J. S. Greenhow concludes that a value of 3.8 may be a more realistic figure based on radar estimates down to $M_v = +10$ (ref. 2). Millman adopted a value of 3.7 for r over the range $M_v = -6$ to $+1$ and for fainter meteors, $M_v < +5$, a value of 2.5 (ref. 2). The values of r attributed to Millman are not consistent, however, with the photographic results of Hawkins and Upton (ref. 24), who deduced a value of 3.44 for $M_v = 0$ to $+4.5$ and found no evidence of a decrease for the fainter meteors. Nor is it consistent with the data of the American Meteor Society which gives $r = 2.5$ for M_v greater than -6 and less than zero (ref. 1). McKinley states that r may drop to values as low as 2.5 at $M_v = +5$, but that it is more likely to be somewhere between 2.5 and 3.7 down to $M_v = +10$.

It appears that, if the visual and photographic data are correct, the ratio r changes from approximately 3.44 to 2.5 at some magnitude M_v between $+2$ and -3, indicating that somewhere near $M_v = -3$ a falloff is observed in the percentage of cometary meteors in the influx, so that relatively few contribute to extremely bright fireballs and none to meteorite falls (ref. 1).

McKinley reports that Millman using $r = 3.7$ for $M_v = -6$ to $+1$ and gradually reducing r to 2.5 in the neighborhood of $M_v = +5$ concludes that the daily influx of particles with $M_v \leq +5$ is 200×10^6; as a fiducial point he estimated N_o to be 10^6 (ref. 2). Hawkins and Upton, using $r = 3.44$ as derived from their 1958 photographic data (ref. 24), computed a value of 91×10^6 meteors for the total daily influx of particles with $M_v \leq +5$. Their value, although slightly higher, is in closer agreement with that reported by Watson in 1956 (75×10^6) who used a value of 2.5 for r (refs. 1 and 2).

In 1958 Hawkins and Upton (ref. 24) give the following variations of equation (25a):

$$\log_{10} N = 0.538\, M_p - 4.33 \text{ (per km}^2\text{/hr)} \qquad (25b)$$

$$\log_{10} N \simeq 0.538\, M_v - 5.17 \text{ (per km}^2\text{/hr)} \qquad (25c)$$

Equation (25c) is simply equation (25b) with an approximate correction for the color index. Both equations give the total number of meteors which pass through 1 km^2/hr rather than the total daily flux incident on the entire atmosphere and are applicable over the range $M_p = -2$ to $+4.1$.

Hawkins and Upton (ref. 24) did not give the area over which they computed their value of 91×10^6 for the daily influx of meteors with visual

magnitudes less than or equal to +5; however, McKinley (ref. 2) in correcting equation (25c) for the area of a sphere with a radius of 6370 kilometers (Earth plus an alititude of 100 kilometers) and for the 24 hr in a day by adding 10.10 ($\log_{10} 5.26 \times 10^8 + \log_{10} 24$) to −5.17, obtained a constant of 4.93 and computed a daily influx of 41×10^6 meteors with $M_v \leq +5$. McKinley then revised the constant upward to 5.27 to be consistent with the evaluation of Hawkins and Upton and reported the following expression for the worldwide daily influx of meteors with magnitudes less than M_v:

$$\log_{10} N \simeq 5.27 + 0.537\, M_v \text{ (daily influx)} \qquad (25d)$$

which he assumes to be applicable over the range of photographic magnitudes observed by Hawkins and Upton.

McKinley expresses Millman's visual observations in a similar manner, covering the range $M_v = -10$ to $+10$ by three equations, each limited to an appropriate range of M_v to provide a better fit to the data. These equations for worldwide daily influx are:

$$\log_{10} N \simeq 6.0 + 0.57\, M_v \qquad -10 \leq M_v \leq 0 \qquad (25e)$$

$$\log_{10} N \simeq 6.0 + 0.50\, M_v \qquad 0 \leq M_v \leq 3 \qquad (25f)$$

$$\log_{10} N \simeq 6.3 + 0.40\, M_v \qquad 3 \leq M_v \leq 10 \qquad (25g)$$

Watson's 1956 data is expressed in a similar manner as:

$$\log_{10} N \simeq 5.88 + 0.40\, M_v \qquad -3 \leq M_v \leq 10 \qquad (25h)$$

Figure 6 (ref. 2) shows in graphical form the three sets of observational

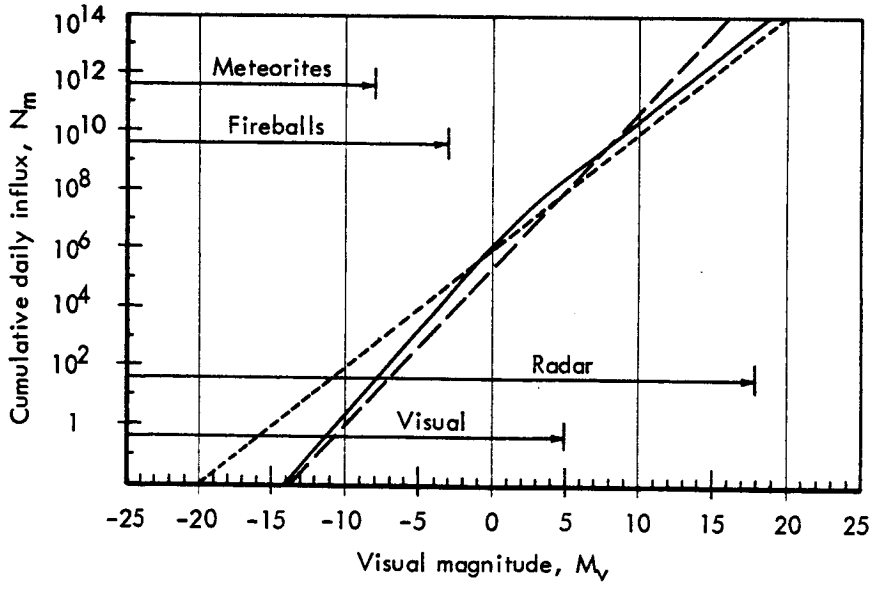

Figure 6.—Cumulative number of meteors incident upon Earth daily vs. visual magnitude. Solid curve, after Millman; dashed curve, after Hawkins and Upton; dotted curve, after Watson.

data summarized by equation (25d) through (25h) inclusive. There is no significant disagreement over the normal visual range; however, any extrapolation outside the range of $-10 \leq M_v \leq 10$ should be regarded as highly speculative. In the vicinity of $M_v = -10$, where equation (25e) implies that the daily influx total may be 1 or 2 meteors, the range of meteorite-dropping objects is entered. At the other extreme, possibly near +18 visual magnitude, the sizes of the particles become so small that they are slowed by the atmosphere without creating visual light or ionization (ref. 2).

McKinley shows that if the radar-visual magnitude relation given by equation (9) is adopted and its value for M substituted into equation (25c), the relation:

$$\log_{10} N \simeq 16 - 1.34 \log_{10} q \text{ (per km}^2\text{/hr)} \tag{25i}$$

is obtained for the number of radar meteors of visual magnitude M_v and brighter arriving per km^2/hr. Similar equations could be derived from equations (25d) through (25h) inclusive. McKinley states that equation (25i) may be considered fairly satisfactory down to about $M_v = +5$ and that recent evidence suggests that the relation may be good even to $M_v = +10$. Note that equation (25i) does not consider the correction for velocity and therefore would be reliable for meteors with velocities of approximately 40 km/sec. For significantly different velocities, velocity corrections should be applied as indicated by equation (10).

Masses and influx rates of sporadic meteors.—Most authorities are agreed that, throughout the visual range at least, the luminosity of a meteor is directly proportional to its mass. Thus, from equation (5):

$$m_{M_v} = k\, 10^{-0.4 M_v} \tag{26}$$

where k is the proportionality constant. Various modifications of this equation appear in the literature illustrating the uncertainties in computing mass. However, for the purpose of the present discussion, equation (26) is considered to sufficiently describe the relation. One can use equation (26) and the general observational relation $\log_{10} N = N_o + M_v \log_{10} r$ to obtain by elimination of M_v between the two expressions:

$$N \propto m^{-2.5 \log_{10} r} \propto m^{1-s} \tag{27}$$

where N is as before the cumulative influx of meteors and s (equal to $1 + 2.5 \log r$) indicates the rate of increase in number of meteors with decreasing mass (ref. 47). The exponent s should be deducible indirectly from radar observations (refs. 2 and 48) and r directly computable from these.

Once the ratio of increase in the number of meteors per magnitude step, r, is established, the adoption of an average mass for a meteor of any magnitude (zero is generally used) results in a cumulative influx-mass law for at least that range of magnitudes over which r is constant. In 1941, Watson, as previously stated, determined r to be 2.5 from visual data, establishing an influx law inversely relating number to mass. By assuming a mass of 0.25 gram for a zero visual magnitude meteor (unspecified velocity) he derived the

following expression for the cumulative influx of particles N to Earth as a function of mass:

$$\log_{10} N = -14.38 - \log_{10} m \text{ (per m}^2\text{/sec)} \quad (28)$$

Such an influx mass law implies that the total mass contributed by each magnitude step is constant. In 1958, Whipple (ref. 16) applying the same magnitude-mass relation tabulated cumulative number of meteoroids incident on Earth for each magnitude step. In this same reference, he indicated a value of 25 grams for a zero visual magnitude meteor with a velocity of 30 km/sec. Maiden (ref. 20) indicated that the tabulated data can be fitted by:

$$\log_{10} N = -11.89 - \log_{10} m \text{ (per m}^2\text{/sec)} \quad (29)$$

In their 1958 publication, Hawkins and Upton (ref. 24), using data obtained by the more reliable photographic technique, determined that $r = 3.44$ throughout the range of visual magnitude from approximately 0 to +4. This value for r resulted in an influx law inversely dependent on mass to the 1.34 power. Based on their best available estimates of τ, the luminous efficiency, these authors adopted a value of 30 grams for the mass of a zero visual magnitude meteor with a velocity of 30 km/sec and derived the cumulative influx equation:

$$\log_{10} N = -12.29 - 1.34 \log_{10} m \text{ (per m}^2\text{/sec)} \quad (30)$$

In 1963, Hawkins (ref. 31) adopted a new value of 4.4 grams for the mass of a zero visual magnitude meteor with a velocity of 30 km/sec, based on more recently obtained luminous efficiency information, and revised equation (30) to yield:

$$\log_{10} N = -13.09 - 1.34 \log_{10} m \text{ (per m}^2\text{/sec)} \quad (31)$$

In 1963, Whipple (ref. 37) adopted the 1958 influx law of Hawkins and Upton, equation (30), but corrected it for a mass of 1.0 gram, corresponding to his newly adopted value for the mass of a zero visual magnitude meteor with a velocity of 30 km/sec, and developed:

$$\log_{10} N = -14.48 + 2.68 \log_{10} (0.44/\rho) - 1.34 \log_{10} m \text{ (per m}^2\text{/sec)} \quad (32)$$

This equation represents the cumulative number of meteoroids which would strike a surface randomly oriented in space near Earth, rather than the cumulative influx to Earth, and therefore, contains a correction factor of $-\log_{10}2$ to reduce the influx by ½ to account for Earth shielding. The shielding factor is necessary since the surface of a small body (on the order of a 3 meter sphere) near Earth would be exposed on only one side; were the Earth removed, the area would receive approximately twice the meteoroid flux. It appears that equation (29) also contains the correction factor. When using the equations given, the reader should determine whether or not the shielding factor is applicable.

The zero visual magnitude mass adopted by Whipple (1.0 gram) was derived using drag equation (14), and his previously computed density value for the average cometary meteor (0.44 g/cm^3) determined from Trailblazer 1 results. With all quantities in the drag equation, except $m^{1/3}\ \rho^{2/3}$, determin-

able for a zero magnitude meteor from photographic records, the establishment of a value for ρ made m a readily computable value. The mass so determined is not, however, independent of density. For this reason, Whipple includes the term $2.68 \log_{10} (0.44/\rho)$ in equation (32) to allow for an arbitrary variation in mean density so that the reader may choose his own value and easily observe the consequences in numerical applications (ref. 37). In the present discussion of density, two values were quoted by Whipple for the average meteoroid density, 0.44 and 0.25 g/cm^3. If the former value is accepted, the density term in equation (32) simply drops out. If the latter value were accepted, a mass of 1.7 gram would derive from the mass-density expression in equation (14) for a zero visual magnitude meteor. The effect of this on the influx would be accounted for by the density term in equation (32).

Whipple (ref. 37) states that equation (32) leads to a total daily (misprinted in publication as annual) influx of 1.41×10^8 meteors to visual magnitude $+5$. For the same influx at $+5$ M_v, equation (29), based on the older Watson law, becomes:

$$\log_{10} N = -13.80 + 2 \log_{10} (0.44/\rho) - \log_{10} m \text{ (per } m^2/\text{sec)} \qquad (33)$$

Whipple concludes that this is the minimum acceptable influx for meteors of fainter magnitudes.

Equations (31) and (32) represent the current best estimates of meteoric flux as a function of average mass and it is encouraging that for a given mass the influxes from the two equations are in agreement within an order of magnitude. There are, or course, diurnal and seasonal variations in the meteor flux which are of the same order of magnitude as the uncertainty of the equations. Both equations were derived based on photographic observations of meteors with visual magnitudes $0 \leqq M_v \leqq +4$ corresponding approximately to masses between 4.4 and 10^{-2} gram (within a factor of less than 5), and any extension of the equations beyond these masses represents extrapolations.

There is considerable uncertainty about the influx rates and masses of meteors of asteroidal origin, where the scarcity of events adds to the difficulty of accumulating reliable statistics. Hawkins (ref. 31) expresses the cumulative number of stones with masses greater than or equal to m that fall on one square meter per second of Earth's surface as:

$$\log_{10} N = -14.23 - \log_{10} m \text{ (per } m^2/\text{sec)} \qquad (34)$$

and that for irons as:

$$\log_{10} N = -17.01 - 0.7 \log_{10} m \text{ (per } m^2/\text{sec)} \qquad (35)$$

Variations in numerical results obtained from the equations of this section are obvious when one compares them graphically. To illustrate this, figure 7 plots log cumulative influx or impacts to a body in space near Earth vs. log mass as derived from equations (28), (29), (32), and (33) (ref. 37).

To determine the influx to Earth, the data from figure 7 must be adjusted by removing the term accounting for Earth shielding. For comparison, the

results of investigations of micrometeoroids by Soberman and Hemenway (1961) from high altitude rocket collections and by Alexander, *et al.* (1962) from acoustic impacts on space vehicles and rockets are included in the figure; these results are subsequently discussed in more detail in this section of the present report. The merging of the curves from equation (32) and the data of Alexander, *et al.* between the masses of 10^{-6} and 10^{-7} gram is encouraging since extrapolation of Whipple's equation may be quite unsafe below a mass of 10^{-5} gram and that of Alexander, *et al.* quite unsafe much above a mass of 10^{-8} gram (ref. 37).

Figure 8, plots log cumulative influx to Earth vs. log mass, as derived from equations (31), (33) and (35) and is Hawkins' representation of the influx to Earth from the entire debris population (ref. 31). The cometary micrometeoroid and meteor section of the plot represents an extrapolation of equation (31) to masses of approximately 300 and 10^{-13} gram. The extrapolation of

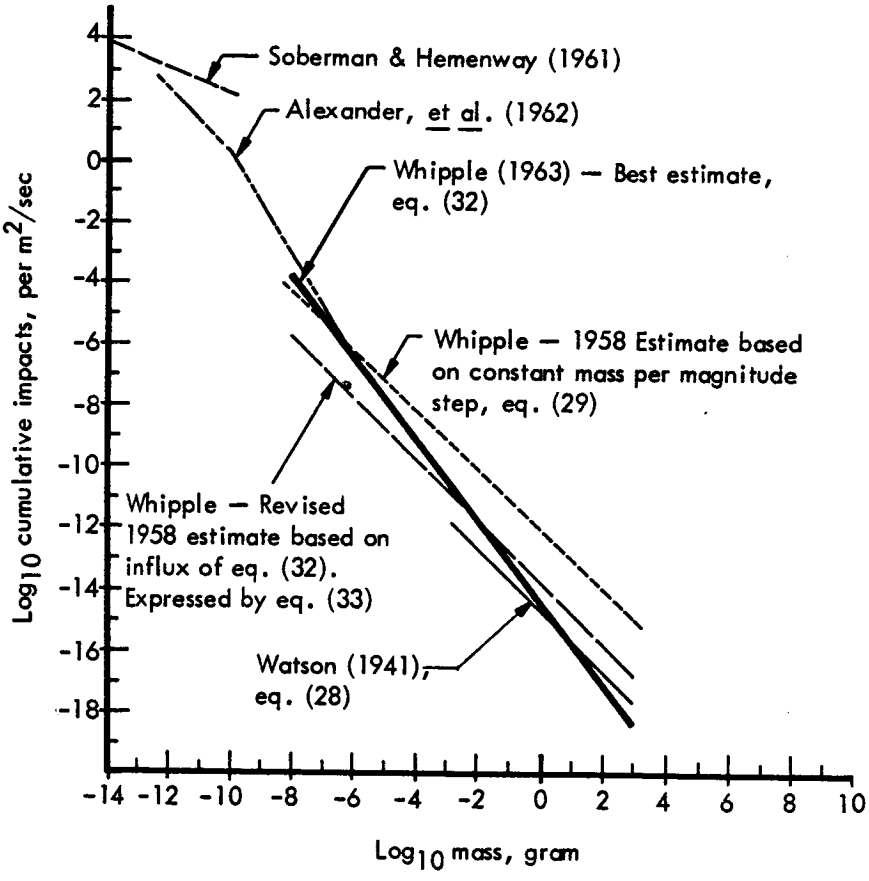

Figure 7.—Cumulative impact rates near Earth—after Whipple.

the curve extends well into the micrometeoroid range, far beyond the mass to which Whipple extended his curve. Were equations (31) and (32) plotted together, Hawkins' curve would be displaced above Whipple's by approximately an order of magnitude; thus, one sees that the two curves somewhat bracket the data of Alexander, *et al.*, with Hawkins' curve possibly giving a slightly better fit. Preliminary radar data of the influx of particles with masses greater than 4×10^{-4} gram are also included on figure 8 and indicate that the extrapolation of equation (31) is probably valid but low by

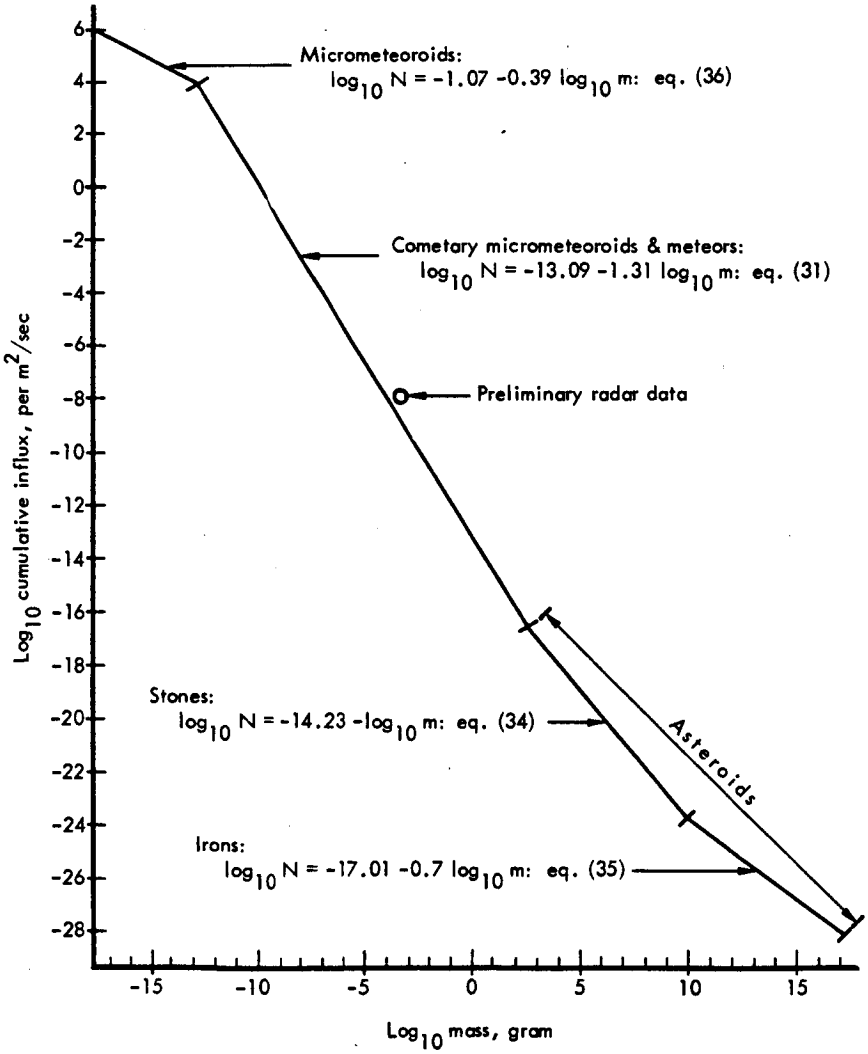

Figure 8.—Cumulative influx rates to Earth—after Hawkins.

perhaps an order of magnitude at this influx (ref. 31). If the radar data proves to be correct, the estimates of both Hawkins and Whipple will have to be revised upward for particles with masses in the range 10^{-3} to 10^{-7} gram. Whipple allows for the possibility that there may be an unobserved large flux of meteoric material in this mass range (ref. 37).

For particles with masses below approximately 10^{-13} gram the curve of figure 8 has an abrupt change of slope in agreement with the results of Soberman and Hemenway (1961). This region (micrometeoroids) of figure 8, was represented by Hawkins (ref. 31) by the expression:

$$\log_{10} N = -1.07 - 0.39 \log_{10} m \text{ (per m}^2\text{/sec)} \qquad (36)$$

which was derived from the data on particle sizes reported by Soberman and Hemenway. In this derivation, Hawkins assumed the particles collected by Soberman and Hemenway to have a mean density of 3.0 g/cm^3. The lower portions (stones and irons) of the influx-mass curve of figure 8 are based on equations (34) and (35). At a mass of 10^5 gram, Hawkins reports that the stones outnumber the irons by a ratio of 20 to 1, while at a mass of 10^{13} gram, the irons outnumber the stones by 10 to 1. Since the stones and irons occur in equal numbers at a mass of about 10^9 gram, this point was used by Hawkins to divide the two regimes of asteroidal meteors. The curve also shows that the flux of cometary meteors equals the flux of asteroidal meteors at a mass of approximately 300 gram. Although a few stone and iron fragments with masses less than 300 gram are undoubtedly present in the meteor population, the bulk of the material is of cometary origin.

Masses and influx rates of shower meteors.—There is evidence that the ratio of increase in the number of meteors per magnitude step r is considerably different for showers, precluding the use of 3.44. This subject has been investigated by, among others, the workers of Jodrell Bank, England, who have computed values of s and r from observed height distributions for three well known showers and for one relatively new daytime shower, the Arietids, which was discovered at Jodrell Bank in 1947. These values are given in table III, (ref. 2).

TABLE III.—*Mass Distribution for Shower Meteors from Radio Observations*

Shower	$0 \leq M_r \leq 2$		$M_r \simeq 3$		$5 \leq M_r \leq 7$		$M_r \simeq 7$	
	s	r	s	r	s	r	s	r
Quadrantids	1.8	2.1	.....	.....	1.78	2.1	.....	.....
Perseids	2.0	2.5	2.0	.....	1.59	1.7	1.38	1.4
Geminids	2.3	3.3	2.24	3.1	1.62	1.8	1.45	1.5
Arietids	1.8	2.1	.....	.....	2.7	4.8	.....	.....

The flux from streams is limited to a few days of maximum activity on certain calendar dates, but during these periods an extra component N_s must be added to the sporadic flux (ref. 31).

Hawkins defines the stream activity in terms of sporadic rates N such that $N_s = \eta N$. The most important of these streams are listed in table IV, (ref. 31) along with values for η.

TABLE IV.—*Shower Flux*

Stream	Dates	η
Quadrantids	Jan. 2–3	5.0
Lyrids	Apr. 20–21	.5
Daytime Arietids	June 5–11	5.0
Daytime Perseids	June 5–11	4.0
Aquarids	July 22–Aug. 7	2.0
Perseids	Aug. 9–14	5.0
Orionids	Oct. 20–24	2.0
Taurids	Oct. 10–Nov. 25	.5
Geminids	Dec. 10–16	5.5

DIRECT MEASUREMENTS WITH SPACECRAFT AND SPACE PROBES

Ground based meteor observations, as stated previously, have been restricted essentially to meteors with masses greater than approximately 10^{-4} gram, corresponding to particles with radii greater than approximately 10^{-2} centimeter. Therefore, any particles with masses less than this are not detected on entry into the atmosphere by terrestrial observational techniques. However, the advent of spacecraft and rockets and their inherent capability of placing detectors in space have made possible direct measurements of the physical and dynamic properties of such particles. This debris, referred to in the literature as dust, micrometeoroids and micrometeorites, has masses less than approximately 10^{-6} gram, corresponding to particles with radii less than approximately $10^{-2.5}$ centimeter. Detectors have been developed which are capable of measuring individual dust particles with masses as small as 10^{-18} gram.

Direct measurements of dust particles in space began with sounding rockets in 1949 (ref. 49) and culminated, perhaps, with the rocket experiments of the Oklahoma State University in 1959 (ref. 21). Since the successful launching of Explorer I (1958 Alpha), results have been obtained from experiments on numerous United States and Soviet Union satellites and space probes. Various types of sensors, acoustic or microphone, light sensitive, penetration, fracture, etc., have been used to measure the following particle parameters: momentum, kinetic energy, penetration and fracture properties. Direct measurements obtained with these sensors can be expressed in terms of particle mass, subject only to minor uncertainties. These uncertainties result from values adopted for: (1) average particle velocity (relative to the satellite); (2) effective coefficient of restitution for hypervelocity microparticle impacts; and (3) correction factors to account for shielding by Earth, solid viewing angle of the sensor, and the orientation of the solid viewing angle relative to the apex of Earth's motion.

The acoustic type of dust particle sensor has provided the greatest quantity of information about near Earth dust particles. Such sensors have flown on more vehicles and over a greater range of geocentric distances than any of the other types. In addition, they are more nearly calibrated than the light sensitive or penetration types. The acoustic sensor system basically consists of a piezoelectric crystal microphone attached to a metallic sounding board. The electrical signal that is generated when an impacting particle delivers a mechanical impulse to the sounding board is amplified and pulse-height analyzed to obtain information about the particle. Analog calibrations, performed in the laboratory by dropping carefully selected glass spheres with velocities less than 10 km/sec onto the sounding boards, have shown that the microphone system is sensitive to the momentum of an impacting particle. Hypervelocity laboratory studies with microparticles with velocities greater than 10 km/sec tend to confirm the momentum sensitivity.

The most proficient analysis and summation of direct measurements to date have been given by Alexander, *et al.* (ref. 50). See also (refs. 49 and 51 to 57). These authors (ref. 50) separated the results into those obtained by: (1) microphone systems; (2) photomultiplier (light sensitive) and rocket collection systems; and (3) penetration and fracture experiments. Their summary included essentially all United States and Soviet Union data available at the time of their publication (1962). No results from Explorer XVI, which employed acoustic, fracture and penetration type sensors, were then available and few have been published subsequently. Results from Explorer XVI that have been published (refs. 58 to 60) are included in the following summary, most of which is that reported by Alexander, *et al.* (ref. 50).

The name, designation, launch date, perigee and apogee of many of the United States satellites and space probes considered in the summary are listed in table V.

Direct measurements from microphone sensors.—In their analysis of available microphone data, Alexander, *et al.* (ref. 50) assumed that the sensor systems were momentum sensitive and that the ratio of the mechanical impulse to the impact-momentum of a particle was unity. They suggest that a small correction factor, estimated to be 2 or 3, could be introduced later when hypervelocity laboratory studies are completed.

The United States spacecraft from which direct measurements with microphone systems were obtained are listed, together with the relevant data, in table VI. Except for the sensors on Explorer VIII, an average particle speed of 30 km/sec was used; for the sensors on Explorer VIII, a particle velocity of 25 km/sec was assumed. An attempt was made by Alexander, *et al.* (ref. 50) to apply correction factors for Earth shielding and to convert all data to omnidirectional influx rates.

The microphone detection system on Explorer VIII (1960 – Xi) utilized two metallic sounding boards attached to a conical section of the spin-stabilized satellite. The solid viewing angle of the system was 2 π steradians and re-

TABLE V.—*Launch Data of Satellites and Space Probes*

Vehicle	Designation	Launch date	Perigee, km	Apogee, km
Explorer I	1958 Alpha 1	1 Feb. 1958	375	2,550
Explorer VI	1960 Delta	7 Aug. 1959	186	39,000
Explorer VII	1959 Iota	13 Oct. 1959	555	1,090
Explorer VIII	1960 Xi	3 Nov. 1960	425	2,300
Explorer XVI	1962 Beta Chi 1	16 Dec. 1962	750	1,180
Vanguard III	1959 Eta	18 Sept. 1959	509	3,750
Midas II	1960 Zeta 1	24 May 1960	500-km circular equatorial orbit	
Samos II	1961 Alpha 1		500-km circular polar orbit	

SLV–1—A Vanguard that failed to achieve orbit.
Pioneer I—Space probe, maximum altitude, 19 Earth radii.
Ranger I—Lunar exploratory vehicle.

mained almost centered on the antapex of Earth's motion during the lifetime of the spacecraft. Microphones with three limiting mass sensitivity ranges were employed in the detection system. The various sensor sensitivities were of particular importance in that they allowed not only a definition of the influx rates for the three ranges, but also establishment of a segment of the average mass distribution curve.

Alexander, *et al.* (ref. 50) applied a correction factor of 2 to convert the observed influx rates to omnidirectional values before the data were plotted as the cumulative mass distribution curve shown in figure 9, (ref. 50). The data point established by the sensor with the lowest sensitivity, though not very significant, lies on the straight line segment established by the two data points that are. The equation of a straight line that very nearly fits the data points shown in figure 9 is:

$$\log_{10} N = -17.0 - 1.70 \log_{10} m \text{ (particles/m}^2\text{/sec)} \qquad (37)$$

in which N is the omnidirectional cumulative influx rate in particles/m^2/sec and m is the particle mass in grams (ref. 50).

It should be noted that large variations in the measured influx rates, at least plus or minus an order of magnitude from the mean, were observed within intervals of only a few hours for dust particles with masses of about 10^{-9} gram.

More than 6000 impacts were recorded during the 80 day lifetime of Vanguard III (1959 Eta). Of this number, approximately 2800 occurred in a 70 hour interval over 16 to 18 November coincident in time with the Leonid meteor shower. Alexander, *et al.* (ref. 50) computed an average influx rate from the Vanguard III data on the basis of approximately 3500 impacts and employed a factor of 1.5 to correct for shielding by Earth.

TABLE VI.—*Direct Measurements From Microphone Systems on United States Satellites and Space Probes*

Spacecraft	Momentum sensitivity, dyn seconds	Mass sensitivity, grams	Effective area, meter^2	Exposure time, seconds	Exposure, m^2 sec	Number of particles	Cumulative influx rate, particles/m^2/sec	
							Observed	Corrected
Explorer VIII	2.5×10^{-3} to 2.5×10^{-2}	1.0×10^{-9} to 1.0×10^{-8}	7.0×10^{-2}	3.5×10^{6}	2.4×10^{5}	~3650	1.5×10^{-2}	3.0×10^{-2}
	2.5×10^{-2} to 2.5×10^{-1}	1.0×10^{-8} to 1.0×10^{-7}				~75	3.1×10^{-4}	6.2×10^{-4}
	$>2.5 \times 10^{-1}$	$>1.0 \times 10^{-7}$				1 or 2	~5.0×10^{-6}	~1.0×10^{-5}
Vanguard III	$>1.0 \times 10^{-2}$	$>3.3 \times 10^{-9}$	4.0×10^{-1}	6.9×10^{6}	2.8×10^{6}	~3500	1.3×10^{-3}	2.0×10^{-3}
Explorer I	$>2.5 \times 10^{-3}$	$>8.3 \times 10^{-10}$	2.3×10^{-1}	7.9×10^{4}	1.8×10^{4}	145	8.4×10^{-3}	1.7×10^{-2}
Pioneer I	$>1.5 \times 10^{-4}$	$>5.0 \times 10^{-11}$	3.9×10^{-2}	1.1×10^{5}	4.2×10^{3}	17	4.0×10^{-3}	4.0×10^{-3}
Ranger I	$>3.0 \times 10^{-5}$	$>1.0 \times 10^{-11}$	8.0×10^{-4}	1.1×10^{4}	8.8	64	7.3	4.0×10
Midas II	$>3 \times 10^{-4}$	$>1 \times 10^{-10}$	6.9×10^{-2}	4.0×10^{3}	2.7×10^{2}	67	2.5×10^{-1}	5.0×10^{-1}
Samos II	$\gtrsim 9 \times 10^{-3}$	$\gtrsim 1 \times 10^{-10}$	6.9×10^{-2}	?	?	?	3.4×10^{-1}	6.8×10^{-1}
SLV–1	$\gtrsim 3 \times 10^{-4}$	$\gtrsim 3 \times 10^{-9}$	8.0×10^{-1}	9.5×10^{2}	7.6×10^{2}	10	1.3×10^{-2}	2.6×10^{-2}

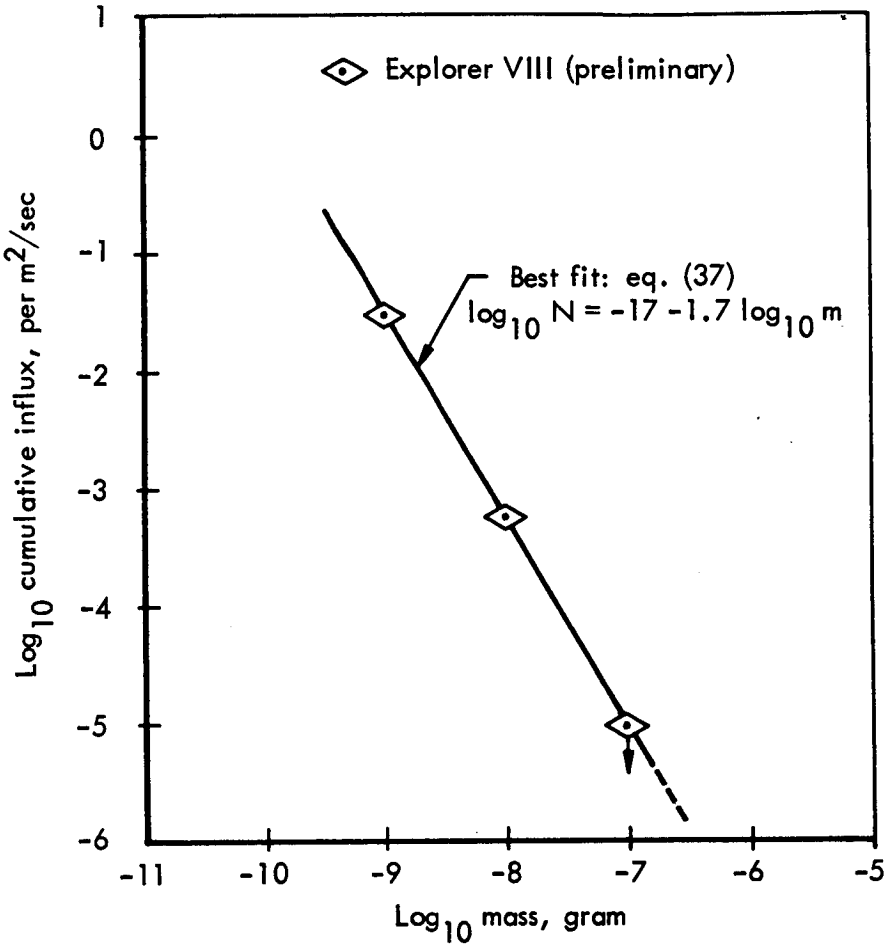

Figure 9.—Cumulative influx rates established by Explorer VIII.

The data given for Explorer I (1958 Alpha) and Pioneer I are those reported by Dubin (refs. 61 and 62). The total number of impacts, 145, reported for Explorer I was used by Alexander, *et al.* in computing an average omnidirectional influx rate even though more than half of the impacts probably were the result of an interplanetary dust particle event (ref. 63). Use of the 145 impacts was justified since the high influx rates during the dust particle event were somewhat counteracted by an interval of extremely low rates. A factor of 2 was applied by Alexander, *et al.* (ref. 50) to correct for Earth shielding and in compensating for the lack of complete omnidirectionality of the detector. The microphone system on Pioneer I registered 25 impacts, of which 17 were considered to result from dust particles. No correction for shield-

ing by the Earth was made because Pioneer I spent most of its time at large geocentric distances (2 to 19 Earth radii).

A preliminary readout of the data from the microphone and coated photomultiplier systems on Ranger I, a lunar exploratory vehicle, was reported by Alexander and Berg (ref. 64). In this system, the two sensors were capable of operating independently as well as in coincidence. Only the data from the microphone system are given in table VI.

Results from the microphone system of Midas II (1960 Zeta) and preliminary results from a similar system on Samos II (1961 Alpha 1) were reported by Soberman and Della Lucca (ref. 65). The data were obtained, as in the case of Explorer I, in real time as the satellite passed over telemetry stations.

The data from a microphone system on SLV–1, a Vanguard satellite that failed to achieve orbit, were reported by LaGow, Schaefer and Schaffert. The bursts of counts reported by these authors were most likely produced when the expended third-stage motor sputtered and bumped the payload (ref. 50). Therefore, only 10 of the 17 impacts reported by LaGow, *et al.* were used by Alexander, *et al.* in computing an omnidirectional influx rate.

Some of the earliest direct measurements of quantitative value were obtained with microphone detection systems on a series of seven successful high altitude rockets instrumented and flown by Oklahoma State University (O.S.U.) (refs. 21, 66, and 67). Data from these rockets used in the analysis of Alexander *et al.* are summarized in table VII (ref. 50). Average particle speeds were estimated since the distribution of orbits of dust particles was not known. Most of the sensors on these rockets were exposed to the high velocity component of dust particle influx.

The direct measurements obtained with microphone systems on rockets, satellites and spacecraft of the Soviet Union have been reported by Nazarova (refs. 68 to 71). (See also references 72 and 73.) These results are summarized in table VIII (ref. 50). Some of the quantities listed in table VIII were computed by Alexander, *et al.* (ref. 50) from the information given by Nazarova. Sensitivities for the microphone systems on the Soviet spacecraft were expressed by Nazarova in terms of particle mass; systems were energy sensitive, and an average particle speed of 40 km/sec was assumed for the spacecraft in converting to particle mass. The average particle speed of 40 km/sec was used in an earlier analysis by McCracken (ref. 21), but this value is now regarded as being too high. Thus, Alexander, *et al.* (ref. 50) adopted a value of 30 km/sec, pending information on the velocity distribution of the dust particles. The mass sensitivities for the microphone systems on the Soviet spacecraft were, therefore, reduced by Alexander, *et al.* (ref. 50) by the square of the ratio of 40 to 30 in order to compensate for the difference in assigned particle speeds. An average particle velocity of 15 km/sec was assumed by Nazarova in computing the mass sensitivities of the microphone systems on the geophysical rockets; therefore, the mass sensitivities given by

TABLE VII.—*Direct Measurements from Microphone Systems on O.S.U. Rockets*

Rocket	Momentum sensitivity, dyn sec	Particle velocity, km/sec	Mass sensitivity, grams	Number of impacts	Exposure h>100 km, m^2 sec	Cumulative influx rate particles/m^2/sec
Aerobee no. 80	$>6.0 \times 10^{-4}$	70	$>8.6 \times 10^{-11}$	49	5.0	9.8
	$>3.0 \times 10^{-3}$	70	$>4.3 \times 10^{-10}$	10	5.0	2.0
	$>1.0 \times 10^{-3}$	40	$>2.5 \times 10^{-10}$	3	50	6.0×10^{-2}
	$>3.0 \times 10^{-3}$	40	$>7.5 \times 10^{-10}$	1	50	2.0×10^{-2}
Aerobee no. 88	$>1.3 \times 10^{-4}$	20	$>6.5 \times 10^{-11}$	6	3.0	2.0
	$>2.0 \times 10^{-3}$	20	$>1.0 \times 10^{-9}$	1	3.0	3.3×10^{-1}
	$>4.7 \times 10^{-4}$	35	$>1.3 \times 10^{-10}$	17	30	5.7×10^{-1}
	$>1.0 \times 10^{-3}$	35	$>2.9 \times 10^{-10}$	7	30	2.3×10^{-1}
Nike-Cajun AF–2	$>6.0 \times 10^{-4}$	40	$>1.5 \times 10^{-10}$	45	31	1.5
	$>1.2 \times 10^{-3}$		$>3.0 \times 10^{-10}$	15		4.8×10^{-1}
	$>4.0 \times 10^{-3}$		$>1.0 \times 10^{-9}$	3		9.7×10^{-2}
Nike-Cajun AA6.203	$>3.0 \times 10^{-4}$	35	$>8.6 \times 10^{-11}$	55	37	1.5
	$>3.0 \times 10^{-3}$		$>8.6 \times 10^{-10}$	3		8.1×10^{-2}
Nike-Cajun AA6.204	$>7.0 \times 10^{-4}$	40	$>1.8 \times 10^{-10}$	32	33	9.7×10^{-1}
	$>3.0 \times 10^{-3}$		$>7.5 \times 10^{-10}$	1		3.0×10^{-2}
Nike-Cajun AA6.206	$>1.5 \times 10^{-4}$	35	$>4.3 \times 10^{-11}$	12	24	5.0×10^{-1}
	$>1.0 \times 10^{-3}$		$>2.9 \times 10^{-10}$	1		4.2×10^{-2}
	$>7.0 \times 10^{-4}$		$>2.0 \times 10^{-10}$	6		2.5×10^{-1}
Spaerobee 10.01	$>5.0 \times 10^{-4}$	60	$>8.3 \times 10^{-11}$	20	8.1	2.5

TABLE VIII.—*Direct Measurements From Microphone Systems on Soviet Union Rockets, Satellites, and Space Probes*

Vehicle	Mass sensitivity, grams		Effective area, m^2	Exposure time, sec	Exposure, m^2 sec	Number of particles	Influx rate, particles/m^2/sec	
	$v = 40$ km/sec	$v = 30$ km/sec					(Nazarova)	Cumulative
Sputnik III	8.0×10^{-9} to 2.7×10^{-8} 2.7×10^{-8} to 1.5×10^{-7} 1.5×10^{-7} to 5.6×10^{-6} $>5.6 \times 10^{-6}$	1.4×10^{-8} to 4.8×10^{-8} 4.8×10^{-8} to 2.7×10^{-7} 2.7×10^{-7} to 1.0×10^{-5} $>1.0 \times 10^{-5}$	0.34	$\sim 8 \times 10^5$	3×10^5	?		$< 1 \times 10^{-4}$
Lunik I	2.5×10^{-9} to 1.5×10^{-8} 1.5×10^{-8} to 2.0×10^{-7} $>2.0 \times 10^{-7}$	4.4×10^{-9} to 2.7×10^{-8} 2.7×10^{-8} to 3.6×10^{-7} $>3.6 \times 10^{-7}$	0.2	3.6×10^4	7.2×10^3	<16 < 4 < 1	$< 2 \times 10^{-3}$ $< 5 \times 10^{-4}$ $< 1 \times 10^{-4}$	$<2.9 \times 10^{-3}$ $<7.0 \times 10^{-4}$ $<1.4 \times 10^{-4}$
Lunik II	2.0×10^{-9} to 6.0×10^{-9} 6.0×10^{-9} to 1.5×10^{-8} $>1.5 \times 10^{-8}$	3.6×10^{-9} to 1.1×10^{-8} 1.1×10^{-8} to 2.7×10^{-8} $>2.7 \times 10^{-8}$	0.2	1.1×10^5	2.2×10^4	0 0 2	$< 5 \times 10^{-5}$ $< 5 \times 10^{-5}$ 9×10^{-5}	 9.1×10^{-5}
Interplanetary Station	1.0×10^{-9} to 3.0×10^{-9} 3.0×10^{-9} to 8.0×10^{-9} $>8.0 \times 10^{-9}$	1.8×10^{-9} to 5.3×10^{-9} 5.3×10^{-9} to 1.4×10^{-8} $>1.4 \times 10^{-8}$	0.1	2.3×10^4	2.3×10^3	1 5 1	4×10^{-4} 2×10^{-3} 4×10^{-4}	3.0×10^{-3} 2.6×10^{-4} 4.3×10^{-4}
Geophysical Rocket I		$\gtrsim 2.5 \times 10^{-9}$	4	1.3×10^2	5.4×10^2	?	6×10^{-2}	6×10^{-2}
Geophysical Rocket II		$\gtrsim 2.5 \times 10^{-9}$	4	1.5×10^2	5.9×10^2	?	5×10^{-2}	5×10^{-2}
Geophysical Rocket III		$\gtrsim 2.5 \times 10^{-9}$	4	8.5×10	3.4×10^2	?	7.5×10^{-1}	7.5×10^{-1}

Nazarova were increased by Alexander, *et al.* (ref. 50) by a factor of 4 when these authors converted to 30 km/sec.

The influx rates measured by Sputnik III (1958 Delta 2) underwent tremendous changes during the first three days of operation of the equipment (ref. 50). The influx rates, as reported by Nazarova, were 4 to 11 particles/m^2/sec on 15 May (day of launch), 5×10^{-4} on 16 and 17 May and less than 10^{-4} during the interval 18 to 26 May. Nazarova attributed the high influx rates during the first few days to a meteoroid shower, but Alexander, *et al.* question this conclusion. In any case, only the influx rate given for the last 9 days of operation was used by Alexander, *et al.* Since it was not clear whether Nazarova corrected the influx rate of Sputnik III for Earth shielding, the value given in table VIII is that reported by Nazarova.

The method of encoding information into the telemetered signal on Lunik I was such that only very crude upper limits to the influx rates could be specified and, therefore, only that influx rate measured by the scale of highest sensitivity was used by Alexander, *et al.* (ref. 50) in computing influx values. Lunik I, Lunik II and the Interplanetary Station (1959 Theta) operated at large geocentric distances, obviating corrections for shielding by Earth. No attempt was made by Alexander, *et al.* to correct the influx rates of the three geophysical rockets to omnidirectional values since the orientations of the rockets and solid viewing angles of the sensors were not reported.

Several hundred impacts have been registered by the acoustical detection equipment of Explorer XVI (ref. 74); however, the data have not, at the time of this writing, been reduced and published.

Direct measurements from photomultiplier sensors and rocket collection systems.—Photomultiplier detectors have been flown on three rockets, Aerobee NRL–25, Jupiter AM–28 and Aerobee NASA–4.12 (ref. 63) and two satellites, Explorer VIII and Ranger I (ref. 64). The Skylark rocket experiment of Lovering also employed a light flash detector very similar to the one on Aerobee NRL–25, but no events were observed by the sensor of this craft: there is a possibility that the experiment did not survive launch (ref. 50).

Photomultiplier sensors measure the intensity and duration of the visible light emitted during each impact of a microparticle with a velocity greater than 5 km/sec, and these characteristics provide a means for determining the kinetic energy of the impacting particles. Light emitted from impacts of micron-size particles with velocities between 4 and 11 km/sec has been observed in the laboratory (ref. 75), and results indicate that the light flash sensors of Aerobee NRL–25, Jupiter AM–28, Explorer VIII and Ranger I detected particles with masses greater than 10^{-3} gram. The configuration of the sensors used on these vehicles was different, but the principle of light flash detection was the same. The basic detector unit was a photomultiplier tube; the surfaces exposed to impacts were Lucite and glass. A few thousand angstroms of aluminum were evaporated on the impact surfaces to shield the

photocathodes from background light. When a dust particle penetrated the aluminum, light from the impact flash could reach the photocathodes. The rocket experiments exposed a larger impact area than the satellite instrumentation to compensate for the shorter exposure time of their flights. An intensive effort was made to make the sensors insensitive to Cerenkov radiation and to energetic particles.

Results of these light flash detector measurements are given in table IX, (ref. 50). The cone of vision of detectors, exposure and total number of impacts are given for each vehicle. The initially reported impact rates were computed, then normalized to 4 π steradians and corrected for Earth shielding. Aerobee NRL–25 was launched at 0200 hours local time. Thus, the light flash detector was exposed to the high speed component of the dust particle influx. The Jupiter AM–28 rocket was launched at 1900 hours local time, so the detector was exposed to the low speed component of the influx. A value of 45 km/sec was originally used as the average speed of the dust particles to which the sensors of Aerobee NRL–25 were exposed while a value of 12 km/sec was used for the sensors of Jupiter AM–28. For purposes of comparison, Alexander, *et al.* (ref. 50) corrected the results to a velocity of 30 km/sec. Since detector sensitivity is a function of the square of the particle velocity, the reported influx rate of 390 particles/m^2/sec from Aerobee NRL–25 was reduced to 173 to obtain the omnidirectional influx at an average speed of 30 km/sec (a linear relationship was assumed between influx rates and mass sensitivity). A similar computation was made for the Jupiter AM–28 data to obtain the omnidirectional influx rate of 25 particles/m^2/sec.

TABLE IX.—*Direct Measurements from Photomultiplier Systems on United States Rockets and Satellites*

Vehicle	Half-angle of detector cone of vision, deg	Exposure, m^2 sec	Number of particles	Influx rate, particle/m^2/sec	Omni-directional influx rate
Aerobee NRL–25	80	0.63	101	160	390
Aerobee NASA–4.12	80	2.4	3	1.2	.....
Jupiter AM–28	80	2.2	4	1.63	4
Explorer VIII (preliminary)	60	4.3	110	25	200
Ranger I (preliminary)	75	8.5	179	21	114

The measurements from Explorer VIII and Ranger I were originally corrected for Earth shielding and normalized to 4π steradians. The data were restricted to satellite night-time measurements to eliminate extraneous counts caused by sunlight. The average omnidirectional influx rates obtained for Explorer VIII and Ranger I by Alexander, *et al.* are 200 and 114 particles/m^2/sec, respectively, for particles with masses of 10^{-13} gram and greater.

Another estimate of the influx rates for dust particles somewhat smaller than those covered by direct measurements obtained with microphone systems was reported by Soberman, Hemenway, *et al.* (ref. 76). These investigators employed a recoverable high altitude rocket, "Venus Flytrap", in obtaining a collection of particles at altitudes between approximately 80 and 150 km. The cumulative influx rate plotted as a function of particle diameter has a negative slope of 1.3 and is applicable to particles with diameters as small as 0.2 μ. By assuming a mass density of 3 g/cm^3, influx rates estimated from this collection may be compared to those obtained from direct measurements of satellites and rockets. For particles with diameters equal to, or greater than 3 μ, Soberman and Hemenway computed an influx of 300 particles/m^2/sec, considerably greater than direct measurements would indicate. No shielding corrections were introduced, since the collectors faced in the general direction of the apex of the Earth's motion.

Three observed results of the collection experiment are: (1) a preponderance of submicron particles; (2) low velocity of fall of the particles; and (3) an unexpectedly large number of particles. These results are consistent with one or both of the following hypotheses: the breakup of larger low-density "fluffy" particles, and the existence of a dust layer of a geocentric distribution of micrometeoritic particles about Earth (ref. 76).

Cumulative mass distribution curve from microphone and photomultiplier systems and the rocket collection experiment.—The direct measurements reported for the microphone, photomultiplier, and rocket collection are plotted as a cumulative mass distribution curve in figure 10 (ref. 50). Two characteristics of the data used in establishing the curve are emphasized: (1) the influx rates are expressed as omnidirectional values; and (2) the curve is the result of a series of experiments in the vicinity of Earth. How well the curve applies to other regions of space is not presently known. A study of the data points in figure 10 demonstrates the degree of consistency with which the average influx rates derived from all microphone measurements fit the curve established by results from Explorer VIII.

The photomultiplier results allow an extension of the distribution curve obtained with microphone systems to particles with masses of approximately 10^{-13} gram. The higher influx rates from the rocket collection experiment (ref. 76) are also indicated on the figure and the discrepancy between them and the photomultiplier detector results are obvious. Alexander, *et al.* (ref. 50) contend that in the 80-to-150-kilometer altitude range an abundance of decelerated microparticles were probably in the collection.

The cumulative mass distribution curve is not a constant mass to magnitude curve, and the slope appears to change rapidly with decreasing particle size above approximately 10^{-10} or 10^{-11} gram. On a cumulative mass distribution plot, the slope of the curve should approach zero as radiation pressure limits are reached. The results for particles with masses between 10^{-18} and 10^{-10} gram represent initial measurements which are inherently more uncer-

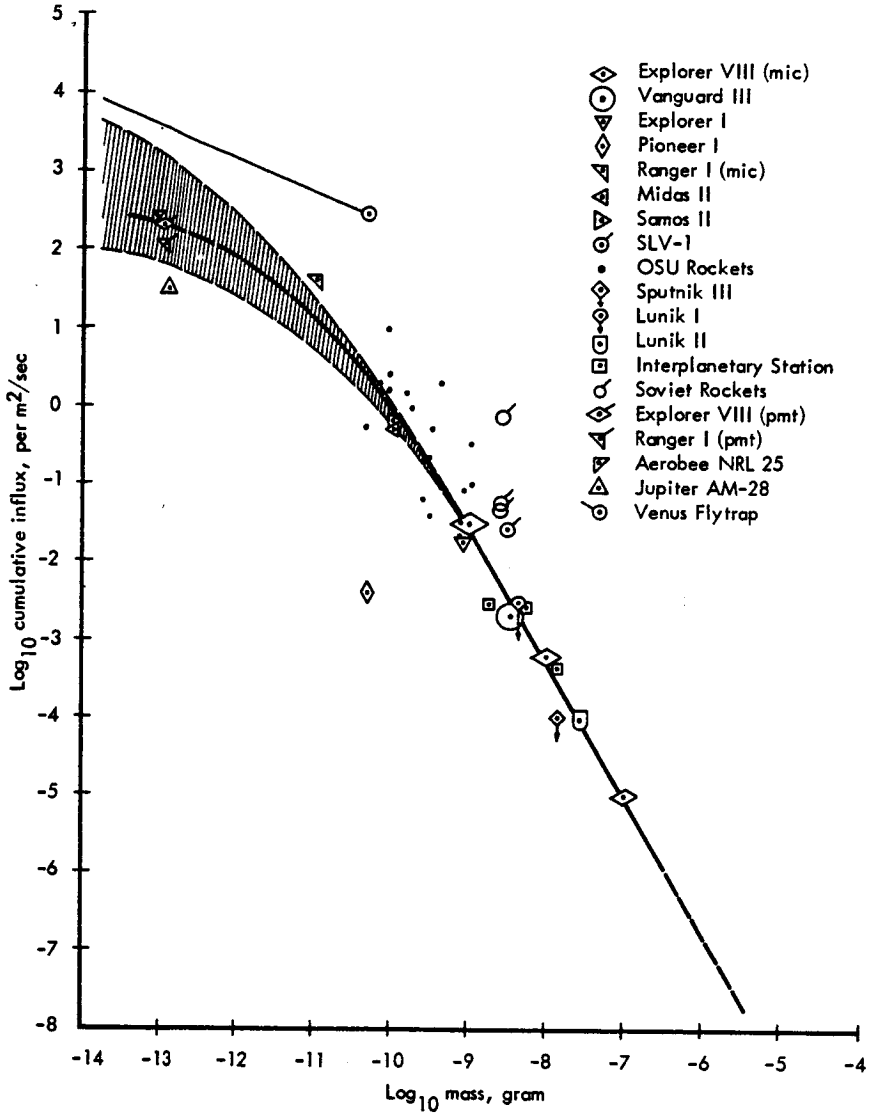

Figure 10.—Average cumulative influx rates established by direct measurements with microphone and photomultiplier systems.

tain than the microphone data. As the number and sophistication of measurements increase for this range of particle sizes, the mechanisms controlling the distributions of these micron-size dust particles will be better understood.

Direct measurements from penetration and fracture sensors.—Various experiments with penetration and fracture type of dust particle sensors have been flown on United States satellites. To date, the number of events detected

by these sensors is so sparse that a measured average influx rate cannot be plotted (ref. 50). However, as shown in figure 11 (ref. 50), a comparison can be made between the results of these experiments and the average mass distribution curve established from available measurements with microphone systems. Figure 11 is as it appears in reference 50 except for data points 14

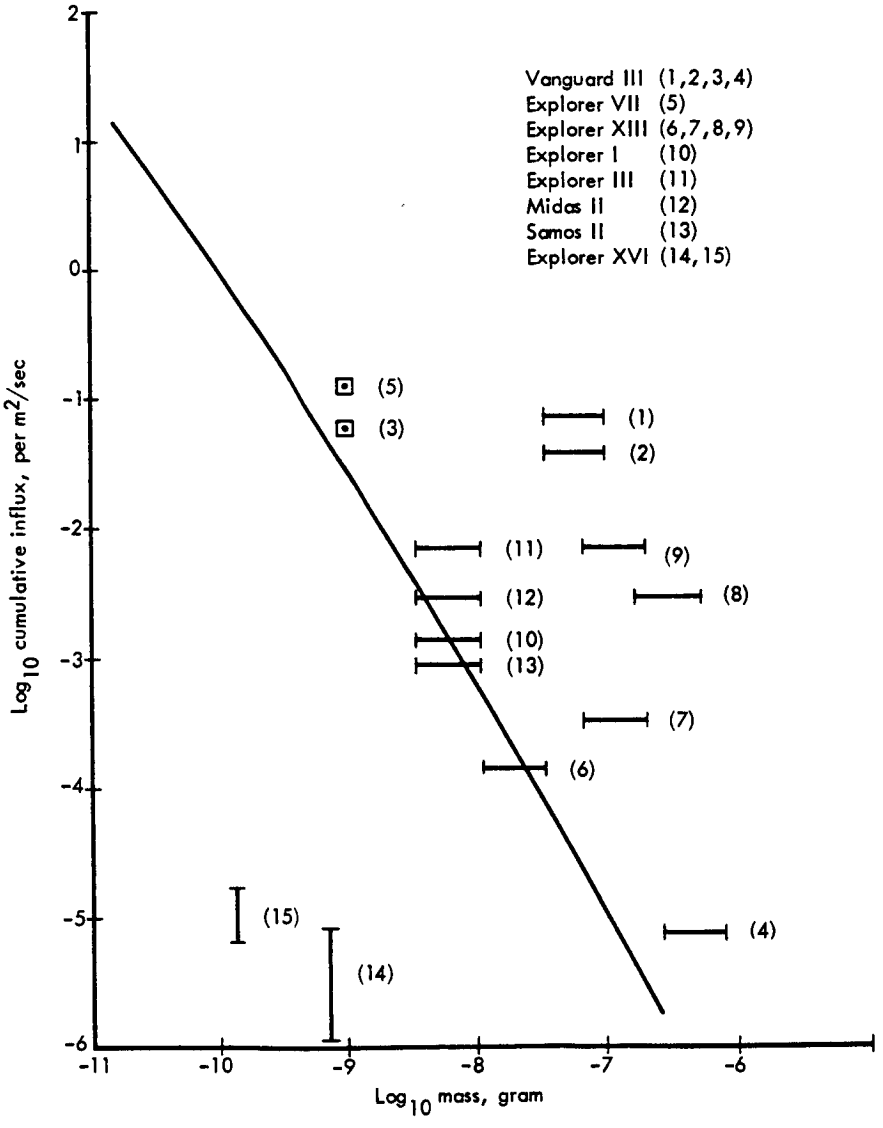

Figure 11.—Average cumulative influx rates established by fracture and penetration sensor systems.

and 15 which represent Explorer XVI results (ref. 58) which were not available when Alexander, *et al.* (ref. 50) published.

The pertinent information concerning the penetration and fracture experiments are presented in table X (ref. 50). Table X is as it appears in reference 50 except for the added data from Explorer XVI as reported by Dáiutolo (ref. 58). The exposure column (area-time product) of table X includes corrections for Earth shielding, except for the measurements of Midas II and Samos II. The influx rates for Explorer III and Samos II were computed from the number of impacts and the corresponding exposures. Only one event was observed on Explorer VII (refs. 77 and 78) and none in the remaining experiments: an average influx rate for these experiments was predicted by Alexander, *et al.* (ref. 50) by computing the influx rate necessary for a 0.99 probability of at least one impact. This was done by assuming an omnidirectional distribution of particles in connection with the following expression based on Poisson statistics:

$$P_1 = 1 - e^{QN} \tag{38}$$

where Q is exposure in m^2 sec, N the average influx rate in particles/m^2-sec, and P_1 the 0.99 probability for at least one impact. The results derived from these calculations are compared in figure 11 with the average mass distribution curve established by measurements with microphone systems.

Penetration type sensors are best illustrated by those developed by LaGow and Secretan for Vanguard III. One type of sensor consisted of a strip of chromium, 300 μ wide and 1 to 3 μ deep, evaporated on Pyrex glass. The resistance of the strip was monitored, and a complete break of the chromium was required to register an impact. The threshold sensitivity in terms of particle mass was determined by computing the diameter of the crater necessary to produce an open circuit. A second type of penetration sensor consisted of two hermetically sealed and pressurized zones. The exposed surface of the zones consisted of the 26 mil thick magnesium skin of the satellite. A differential pressure transducer constantly monitored the pressure between the two zones, so that a puncture of either or both zones could be detected. A third type of penetration sensor consisted of a cadmium sulfide cell covered by a ¼ mil thick Mylar film which was made opaque by aluminum evaporated on both sides. As punctures occurred, the admitted sunlight changed the resistance of the cadmium sulfide cell allowing the effective hole size to be measured. More than one puncture could be observed with this sensor. This type of sensor was also flown on Explorer VII.

Fracture type sensors consist of continuous wire wrapped around an insulating support material and record impacts when colliding dust particles fracture the wire causing an open circuit. This type of sensor was flown aboard Explorer I, III, and VIII, Midas II and Samos II. A similar type of sensor flown on Explorer XIII (refs. 5 and 32) was comprised of a plate of stainless steel mounted in front of a foil gage consisting of a continuous path of gold deposited on silicone rubber. Two thicknesses of stainless steel, 75 and 150

TABLE X.—*Direct Measurements From Penetration and Fracture Sensors on United States Satellites*

Satellite	Type of dust particle sensor	Critical dimension for penetration or fracture	Range of threshold particle mass, gram	Exposure, corrected, m^2 sec	Number of particles	Predicted influx rate $P_1 = 0.99$, particles/m^2/sec	Data point shows in figure 11
Vanguard III	Pyrex-chromium strip	300 μ	4.0×10^{-8} to 1.2×10^{-7}	7.0×10^{1}	0	6.2×10^{-2}	1
	Pyrex-chromium strip	300 μ	4.0×10^{-8} to 1.2×10^{-7}	1.4×10^{2}	0	3.3×10^{-2}	2
	Mylar-CdS cell	¼ mil	1.2×10^{-9}	8.7×10^{1}	0	5.3×10^{-2}	3
	Magnesium zones	26 mil	3.0×10^{-7} to 9.0×10^{-7}	7.2×10^{5}	0	6.4×10^{-6}	4
Explorer VII	Mylar-CdS cell	¼ mil	1.2×10^{-9}	3.9×10^{1}	1	1.2×10^{-1}	5
Explorer XIII	Stainless steel	75 μ	1.1×10^{-8} to 3.3×10^{-8}	3.4×10^{4}	0	1.4×10^{-4}	6
	Stainless steel	150 μ	8.8×10^{-8} to 2.6×10^{-7}	8.5×10^{3}	0	5.6×10^{-4}	7
	Wire grids	75 μ	2.8×10^{-7} to 6.0×10^{-7}	1.7×10^{3}	0	2.7×10^{-3}	8
	Wire grids	50 μ	6.7×10^{-8} to 1.8×10^{-7}	7.7×10^{2}	0	6.0×10^{-3}	9
Explorer I	Wire grids	17 μ	4.2×10^{-9} to 1.2×10^{-8}	3.6×10^{3}	0	1.3×10^{-3}	10
Explorer III	Wire grids	17 μ	4.2×10^{-9} to 1.2×10^{-8}	2.4×10^{2}	2	6.4×10^{-3}	11
Midas II	Wire grids	20 μ	4.2×10^{-9} to 1.5×10^{-8}	2.0×10^{3}	0	2.3×10^{-3}	12
Samos II	Wire grids	20 μ	4.2×10^{-9} to 1.5×10^{-8}	1.1×10^{4}	8	8.0×10^{-4}	13
Explorer XVI[a]			$\sim 10^{-9}$			$\sim 10^{-5}$ to 10^{-6}	14
			$\sim 10^{-10}$			$\sim 10^{-5}$	15

[a] Reference 58.

microns, were used: the foil gage was separated from the metallic plate by a Mylar insulator. Impacts were recorded when particles penetrating the metal fractured the gold foil, causing an open circuit.

Using ¼ mil thick Mylar film and micron-size particles with velocities as high as 11 km/sec, Friichtenicht (ref. 50) found that the diameter of the hole produced is 1.5 ± 0.5 times the diameter of the impacting particle for velocities greater than 3.5 km/sec. Secretan and Berg (ref. 50), using the same accelerator, found no marked deviation from these results. These results formed the basis for the calibration used by Alexander, *et al.* (ref. 50) in interpretation of the Mylar film-cadmium sulfide sensor results of Explorer VII. The results of an extensive series of penetration experiments performed by Summers, *et al.* (ref. 79) were used by Alexander, *et al.* to compute, for the magnesium and stainless steel sensors, the threshold sensitivity in terms of particle mass.

Explorer XVI employed four fracture and penetration experiments: (1) beryllium-copper cells, 0.0025 and 0.0051 centimeter thick; (2) stainless steel grids, 0.0025, 0.0076 and 0.0156 centimeter thick; (3) Mylar-cadmium sulfide pressure cells, 0.0056 centimeter thick Mylar; and (4) copper wire cards, 0.0051 and 0.0076 centimeter thick. Based on the first four months of flight time, 22 penetrations were recorded by the 0.0025 centimeter thick beryllium-copper cells, nine by the 0.0051 centimeter thick beryllium-copper cells, three by the 0.0025 centimeter thick stainless steel grids and several by the Mylar-cadmium sulfide cells. An impact rate of approximately 10^{-5} particles/m^2/sec was reported by Dáiutolo (ref. 58) for particles with masses greater than approximately 10^{-10} gram; Dáiutolo also reported an influx rate between 10^{-5} and 10^{-6} particles/m^2/sec for particles with masses greater than 10^{-9} gram. These values are included in table X.

The uncertainties indicated in figure 11 represent a consideration of the major variations known at the present time concerning the parameters (particle velocity and density) involved in hypervelocity impacts. The data show that some of the experiments did not have sufficient exposure to yield quantitative information (ref. 50). Within the uncertainties exhibited, the measurements support the average mass distribution curve based on results obtained with microphone sensors, especially within the mass range of 10^{-8} to 10^{-6} gram. The curve shown in figure 11 predicts well the wire grid fractures that occurred on Explorer III, data point *11;* Samos II, data point *13;* and the survival (without puncture) of the penetration experiments of Vanguard III, data points *3* and *4;* and Explorer XIII, data points *6* and *7.*

The analysis of all direct measurements for the most part shows no significant departures from the average mass distribution curve based on the microphone sensor data from Explorer VIII, particularly in the mass range 10^{-7} and 10^{-10} gram, indicating the self-consistency of such measurements. It should be noted that the portion of the distribution curve for particles with masses less than about 10^{-10} gram is more uncertain than the segment of the

curve for larger masses. Dust particles with masses less than about 10^{-10} gram can experience severe perturbations due to radiation pressure; thus, the shape of the distribution curve depends critically on location, distribution of orbits and density of the particles (ref. 49).

As previously stated, the fluctuations in influx rates and the grouping of radiants of faint meteors observed with radar equipment suggest that such particles are members of "sporadic showers" rather than dispersed members of major streams. The direct measurements also indicate that large fluctuations in influx rate seem to be the rule (ref. 49). It appears, on the basis of both direct measurements and faint radar meteor data, that the dust particles are not nearly so uniformly distributed as are the larger sporadic meteoroids.

What appears to have been interplanetary dust showers have been observed by Explorer I, Sputnik III, Vanguard III and Explorer VIII (refs. 49, 81 and 82). The event detected by Explorer I on 2 and 3 February 1958 had no relation to a known meteor shower. The large increase in influx rate observed by Vanguard III on 16 to 18 November 1959 was coincident in time with the Leonid meteor shower and suggests that large numbers of small dust particles are being generated in the major meteor stream. Figure 12 (ref. 81) gives the influx rates recorded during the interplanetary dust particle event. For comparison, the influx rates measured from 10 to 15 and 19 to 20 November

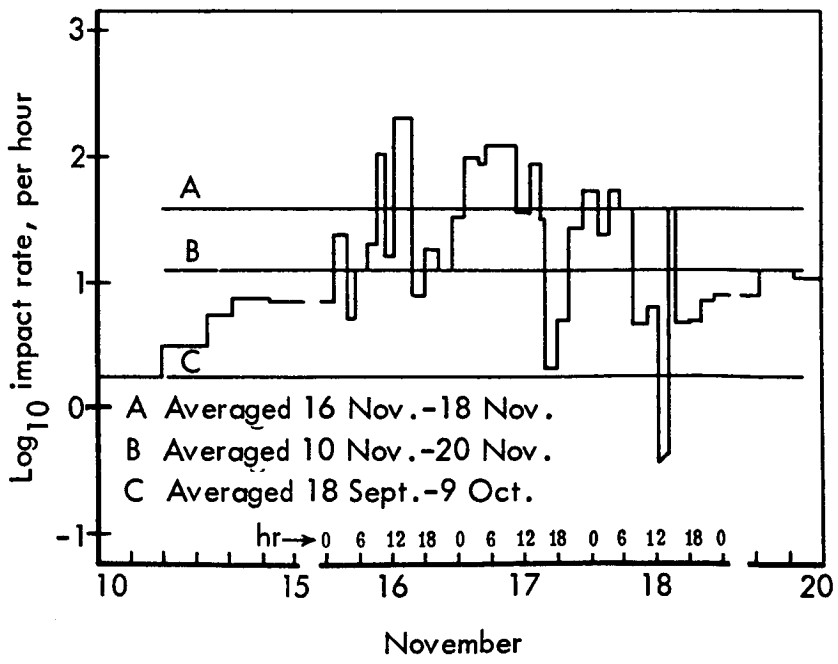

Figure 12.—Variations of impact rates recorded by Vanguard III.

1959 are included. The average rates for the three periods are indicated by the horizontal lines marked *A*, *B*, and *C*.

INTERPLANETARY DUST—THE SOLAR F-CORONA, ZODIACAL LIGHT, AND TERRESTRIAL COLLECTIONS

Two astronomical phenomena which demonstrate the existence of dust in interplanetary space and from which properties of the particles can be estimated are the solar corona and zodiacal light.

The corona, readily observable during a total solar eclipse as a pale aureole around the lunar disc, extends for several diameters from the Sun and gradually merges into the zodiacal light. For nearly 30 years, the corona has been known to consist of three parts: (1) the L–corona, due to scattering of sunlight by highly ionized atoms; (2) the K–corona, due to scattering of sunlight by free electrons; and (3) the F–corona, due to scattering of sunlight at small angles by interplanetary dust particles distributed along the ecliptic plane. The L– and K–corona intensities decrease more rapidly with distance from the Sun than the F–corona so that beyond several solar radii the scattering is primarily caused by dust particles. The dust particles responsible for the F–corona must begin at some distance away from the Sun at which complete vaporization would not occur, perhaps at a distance of approximately 0.1 A.U. (ref. 7).

The intensity and distribution of the scattered light is dependent on: (1) size distribution and number density of the particles along the ecliptic plane; (2) particle shape; and (3) optical reflecting, refracting and diffracting properties of the particles. There is a general lack of agreement concerning the range of particle size that contributes most to the scattered light in interplanetary space; the particle radii used in analyses vary from a fraction of a centimeter down to that allowable under the influence of radiation pressure. Similarly, there is a lack of agreement on limiting particle size due to radiation pressure because of the uncertainties in particle densities; values used in analyses vary from approximately 0.25 to 1.0μ. There are, in fact, so many parameters involved that various plausible combinations of them can be made to fit observational results. Because of this there are large discrepancies between the interpretations of similar data by different investigators (ref. 47). Theory and observations have been combined, however, to form a number of approximations which are useful in correlating data obtained by other methods of observation.

Results from photometric studies of the corona and zodiacal light are generally expressed in terms of the number density of particles of a given radius at a certain distance from the Sun. The incremental size distribution assumed in analyzing the observations of light scattering by dust particles may be determined from:

$$n(a,r)\,do = (C_a/a^\gamma)\ (R/r)^a\,da \quad \text{(particles/unit volume} \qquad (39)$$

where a is the particle radius, R the distance between the observer and the Sun, r the distance between the scattering particle and the Sun, $n(a,r)$ the number density of particles with radii between a and $a + da$ situated at a distance r from the Sun, and C_a, p, and α are constants to be evaluated in the solution (ref. 55).

Incremental size distributions obtained from corona studies by Van de Hulst (1947) and Allen (1946) and from zodiacal light studies by Elsässer (1954) and Blackwell and Ingham (1961) are shown in figure 13 (ref. 55). The figure is a log–log plot of $n(a,r)$ in particles/cm^3 vs. a, particle radius. Discrepancies in the data result from the various values used by these authors for p, α, and C_a in equation (39).

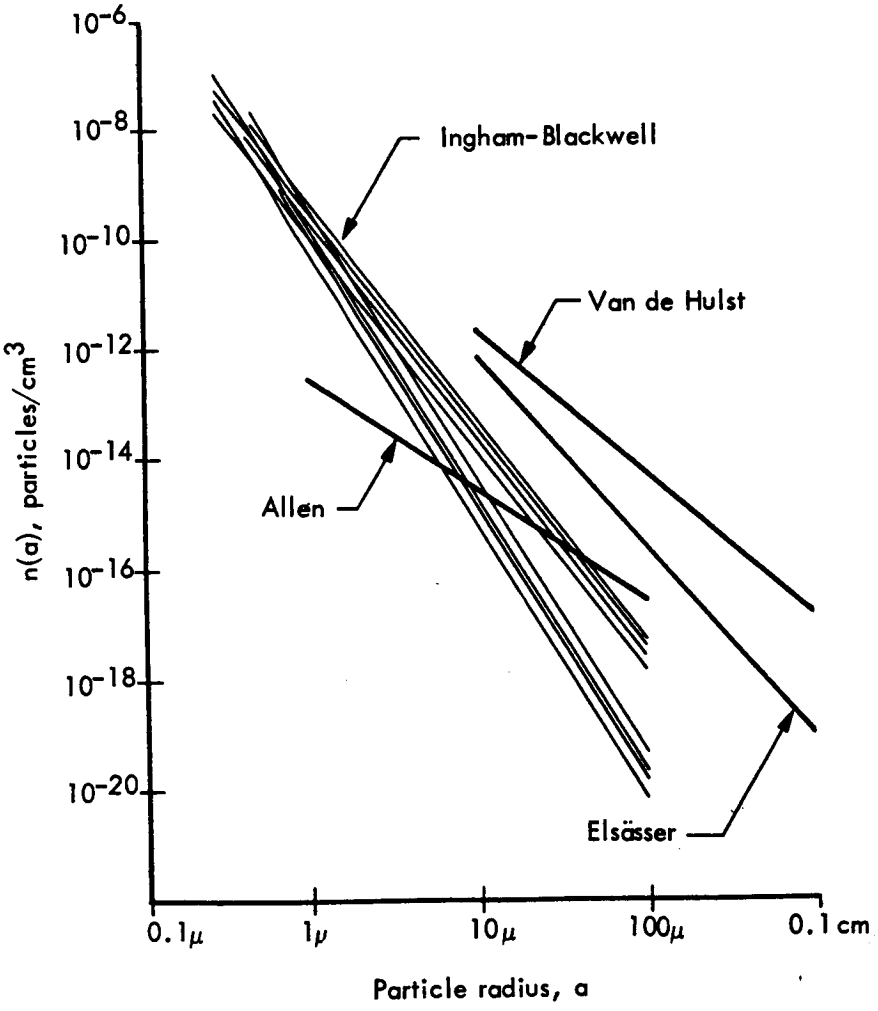

Figure 13.—Incremental size distributions of interplanetary dust.

Beard (refs. 7 and 83) evaluated equation (39) using 2×10^{-20} for C_a, 1.5 for α and values greater than 2.5 for p, to obtain a number density near Earth of 10^{-15} particles/cm^3 for all particles with radii greater than 10^{-3} centimeter. The 10^{-3} centimeter radius represents Beard's adopted value for minimum sized particle allowable in the solar system due to the effects of solar radiation pressure. In 1963, Ingham (ref. 84) reports near Earth number densities ranging from 17×10^{-15} to 130×10^{-15} particles/cm^3 for all particles with radii greater than 0.3μ; the 0.3μ radius represents Ingham's value for minimum sized particle allowable in the solar system under the influence of radiation pressure.

On the strength of an approximate analysis of the variation in dust concentration with height above Earth's surface, Beard derived a value of 10^{-12} particles/cm^3 at a distance of 100 Earth radii, indicating a concentration around Earth 10^3 times greater than free space (ref. 7). On the justifiable assumption that the particles concentrated around Earth have a velocity of approximately 10^6 cm/sec (10 km/sec) Beard computed an influx of $10^{-12} \times 10^6 = 10^{-6}$ particles/cm^2 sec, in good agreement with the direct measurements by satellites of the influx of particles with masses greater than 10^{-10} gram (see figure 10). In the same reference, Beard concludes that the dust concentration along the ecliptic plane is inversely proportional to the 1.5 power of distance from the Sun.

Many investigators report results of light scattering studies in terms of total mass per unit volume of space, ρ_s, (spatial density) which may be determined for a given incremental size distribution from:

$$\rho_s = \int_{a_1}^{a_2} m(a)\ n(a)\ da \quad (\mathrm{g/cm^3}) \tag{40}$$

when $m(a)$ is the mass distribution and $n(a)$ the number density (particles/cm^3) obtained from equation (39). Table XI (refs. 55 and 84), summarizes spatial density and number density results of various investigators.

The different values listed in the table under Blackwell and Ingham (1961) are due to various combinations of values these authors used for radius of minimum sized particles allowable in the solar system, and for p and α as defined in equation (39). Ingham derived his 1963 values from the distribution relation:

$$n(a,r)\,da = Da \exp\,(a^2/a_o^2)\ da \tag{41}$$

where a_o and D are constants (ref. 84). The different values reported in the table for this author in 1963 result from various combinations of values used for a_o, D and radius of minimum sized particles allowable in the solar system.

The values for integrated spatial density (g/cm^3) listed in table XI were derived by Dubin and McCracken (ref. 55) from:

$$\rho_A = \int_{a_1}^{a_2} \pi a^2\, n(a)\ da \ (\mathrm{cm^2/cm^3}) \tag{42}$$

TABLE XI.—*Partial Summary of Results from Studies of Zodiacal Light and Solar F-Corona in the Plane of the Ecliptic at 1 A.U.*

Investigator	Integrated spatial density, ρ_s, g/cm^3	Number density, particles/cm^3	Geometrical area per unit volume, ρ_A, cm^2/cm^3
Van de Hulst (1947)[a]	5×10^{-21}	.....	7.1×10^{-20}
Allen (1946)[a]	5×10^{-23}	.....	9.4×10^{-23}
Elsässer (1954)[a]	1.7×10^{-23}	.....	1.0×10^{-21}
Blackwell & Ingham (1961)[b]	5.1×10^{-24}	500×10^{-15}	4.1×10^{-21}
	8.2×10^{-25}	600×10^{-15}	3.5×10^{-21}
	5.3×10^{-24}	300×10^{-15}	4.9×10^{-21}
	9.0×10^{-25}	400×10^{-15}	4.2×10^{-21}
	2.0×10^{-24}	190×10^{-15}	1.7×10^{-21}
	3.3×10^{-25}	240×10^{-15}	1.4×10^{-21}
	2.1×10^{-24}	130×10^{-15}	2.0×10^{-21}
	3.3×10^{-25}	140×10^{-15}	1.6×10^{-21}
Ingham (1963)[c]	2.3×10^{-24}	130×10^{-15}	
	4.8×10^{-24}	40×10^{-15}	
	7.1×10^{-25}	40×10^{-15}	
	2.2×10^{-24}	17×10^{-15}	

[a] Reference 55.
[b] References 55 and 84.
[c] Reference 84.

where ρ_A represents the total geometrical scattering area per unit volume of space. For comparison, Dubin and McCracken (ref. 55) derived from satellite and rocket data approximate values of 3×10^{-17} and 10^{-20} for ρ_A and ρ_s, respectively. The corresponding values of Ingham, if taken as representative of light scattering studies, give the following approximate comparison (ref. 55):

	ρ_A	ρ_s
Light scattering =	$\sim 4 \times 10^{-21}$	$\sim 5 \times 10^{-24}$
Direct measurements =	$\sim 3 \times 10^{-17}$	$\sim 1 \times 10^{-20}$

The discrepancy between the results of satellites and light scattering studies indicates that the spatial and number density of dust particles within approximately 10^5 kilometers of Earth is 10^3 to 10^4 times greater than that in interplanetary space. This is in good agreement with the results of Beard (ref. 7).

The results obtained by Van de Hulst apply to particles much larger than those detected by the direct measurement technique, so comparison of the two sets of data is of little value. The values of ρ_A and ρ_s derived from the size distribution of Van de Hulst could be brought into better agreement with those derived from the distributions of Allen, Elsässer, and Ingham if a low mass density were used for the particles falling in the meteoroidal size range (that is, for particles with radii greater than approximately 10^{-2} centimeter) (ref. 55).

Accretion rates of interplanetary dust to Earth, size distribution and spatial density estimates also are made by analyzing particles gathered from ocean depths and antarctic ice caps or collected on mountain tops or in the atmosphere at high altitudes. Analyses of such collections are helpful in correlating the results of direct measurements by satellites and rockets and of light scattering studies. The literature is replete with studies on this subject (see refs. 85 to 90) but the reader is particularly referred to references 91 and 92.

Wright and Hodge (ref. 91) gathered spherules of probable and of known extraterrestrial origin, for the purpose of comparison, from a number of sources, including the stratosphere, 750-year-old Greenland ice, 55-year-old antarctic ice, the antarctic atmosphere, a New Mexico mountain top, glacial ice caves and the place of fall of the Siberian Sikhote-Alin meteorite shower. From these collections, Wright and Hodge computed the accretion rate of interplanetary dust to Earth to be 2×10^5 tons per year for particles with diameters greater than 5μ. A comparison of the results of Wright and Hodge with those of other investigators is shown in table XII (ref. 91).

TABLE XII.—*Annual Accretion Rates to Earth of Interplanetary Debris*

Type of particle	Method	Diam.	Rate of deposit, tons/yr	Investigator
Meteorites	Observed falls	> 5 cm	10^2	Watson (1956)
Meteors	Visual counts	> 5 mm	10^3	Millman (1954)
Spherules	Deep sea	>25 μ	10^2	Laevastu & Mellis (1955)
Spherules	Antarctic ice	>15 μ	1.8×10^5	Thiel & Schmidt (1961)
Spherules	Greenland ice	> 5 μ	2×10^5	Wright & Hodge (1963)
Spherules	New Mexico air	> 5 μ	1.6×10^5	Crozier (1962)
Spherules	Arctic air	> 3 μ	5×10^5	Hodge & Wildt (1958)
Spherules	Stratosphere	> 3 μ	2×10^5	Wright & Hodge (1962)
All dust	(see text)	> 5 μ	10^6	Wright & Hodge (1963)
All dust	Ni in deep sea	All	10^6	Pettersson & Rotschi (1952)
All dust	Zodiacal cloud	All	10^6	Van de Hulst (1947)
All dust	Satellite 1958α	All	10^6	Dubin (1958)

Alexander, *et al.* (ref. 50), based on data from direct measurements, computed a value of 365×10^4 tons/year for the annual accretion rate of particles with masses less than about 10^{-6} gram. Whipple (ref. 37) considers this to be an overestimate because of evidence that the small particles detected by space vehicles are mostly in orbits about Earth and, thus, would not contribute to the accretion rate. Whipple further reports that integration of equation (32) down to a mass of 10^{-6} gram contributes only 4.7×10^4 tons/year to Earth, while at smaller masses, Van de Hulst's results add only 1.6×10^{-4} tons/year (ref. 37). Even if the value reported by Alexander, *et al.* (ref. 50) is not an overestimate, the sum of their value, Whipple's and Van de Hulst's does not account for the high accretion rates estimated from

the spherule studies. Since equation (32) is extrapolated for particles with masses less than 10^{-3} gram and since direct measurements have been restricted to particles with masses less than about 10^{-7} gram, Whipple (ref. 37) suggests that an unobserved large flux of extraterrestrial material in the mass range 10^{-3} to 10^{-7} gram may be present.

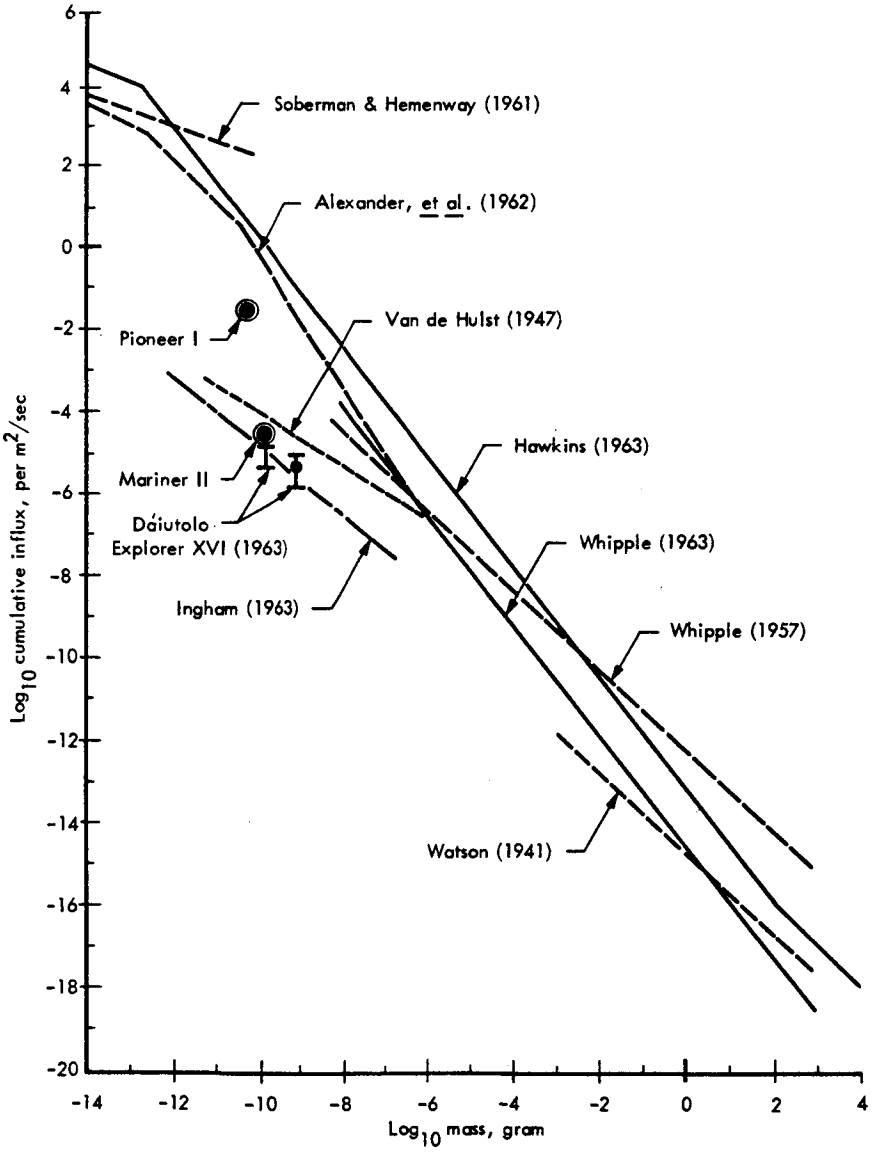

Figure 14.—Composite cumulative influx vs. particle mass.

Figure 14 combines, on one graph, the results of terrestrial observations by Watson (1941), Whipple (1957 and 1963) and Hawkins (1963); the results of direct measurements by Alexander, *et al.* (1962) and Soberman and Hemenway (1962); the results of light scattering studies by Van de Hulst (1947) and Ingham (1963); Dáiutolo's Explorer XVI results; and the data point indicated by the Mariner II spacecraft. The graph plots log cumulative influx in particles/m^2 sec. vs. log particle mass in grams and is as taken from reference 58 except for the curve representing the results of Hawkins (ref. 31) which was added for comparative purposes.

THE DUST CLOUD

Comparison of solar F–corona and zodiacal light concentration results with those obtained by direct measurements clearly indicate that the spatial density of dust within approximately 10^5 kilometers of Earth is 10^3 to 10^4 times greater than in interplanetary space. More evidence of a near Earth concentration comes from Newkirk and Eddy who observed the influx into the upper atmosphere at a height of 80 000 ft; Alexander (ref. 54) reports that these investigators determined the influx to be less than that measured by satellites and rockets, indicating, of course, that many particles detected by the satellites and rockets were in direct orbits around Earth. The strongest additional evidence of a concentration near Earth was provided by Mariner II spacecraft which measured interplanetary dust particle fluxes 10^{-4} times those measured by Earth orbiting vehicles.

Considerable literature is available which depicts possible theoretical mechanisms for creating such a cloud; the reader is referred to references 12 and 93 to 98..

Hypervelocity Impact Phenomena

An assessment of the effects of meteoroids on spacecraft requires an understanding of the phenomena attendant to the impact of an individual particle against the surface of the vehicle. The meteoroid velocity range is fairly well defined, as reported in a foregoing section of this report. Essentially all meteoroids are expected to have velocities relative to Earth between 11 and 72 km/sec and the mean velocity is estimated to be near 30 km/sec (a commonly accepted value from among the several current estimates). It must be recognized that these velocities apply only to particles in the vicinity of earth. Impact velocities will be greater or smaller depending upon the velocity of the vehicle target and so may range from near zero to greater than 80 km/sec.

Terminal ballistics has been a subject of formal study since the early 1800's when the incentive was largely related to warfare and the development of projectiles and armor. Following the earliest investigations, predicated on the treatment of the colliding objects as rigid bodies, there developed an awareness of the importance of the deformation of the impinging bodies which involves both wave propagation and local contact phenomena. The character of these effects was found to depend on the physical properties and shapes of the colliding bodies, the collision geometry and the relative impact velocity. In recent years the physical phenomena associated with the impact process at very high velocity have received a large amount of attention. These phenomena such as perforation, cratering and spalling are now at least qualitatively understood. Extensive data gathered from experimental work have led to empirical formulas which fit these phenomena over the range of conditions studied. The theory relating to impact processes too has received significant attention. However, the several approaches applied to describe quantitatively the very complex relationships between the parameters of the impact and subsequent alterations to target and projectile have given rise to points of controversy and left unresolved several major questions relating to the fundamental aspects of crater formation (ref. 99). The lack of definitive correlations in spite of the large amounts of effort, both theoretical and experimental, is reasoned by Eichelberger to arise from insufficiency of precision and difficulty of interpretation in both areas of work, coupled with too little coordination between theoretical and experimental efforts. "Specifically, the current treatments of theory lack: (1) proper equations of state for the lower pressure regime; (2) precision in the finite differencing methods; and (3)

certainty as to the influence of the mechanics of the program coding in the machine computations. The experiments lack: (1) perspicacity in the design of the experiments; (2) capability of projection at sufficiently high velocities; (3) sufficient precision and assured accuracy for detailed analysis of transient conditions."

Extensive surveys of hypervelocity impact information have been prepared by Herrmann, Jones, and Polhemus (refs. 100 to 102) which bring together data from many individual investigations and include correlation analyses of many of the various theoretical and empirical impact equations and experimental data. The present discussion of impact phenomena follows largely from these compilations, published reviews (refs. 5, 8, 36, 42 and 103 to 110) and several volumes of proceedings from recent Symposia on Hypervelocity Impact (refs. 111 to 115).

Charters, Summers, and Davidson and Sandorff (refs. 8, 103, and 110) among others have classified thick target impact into several categories which depend primarily on impact velocity. These regions are described as:

1. Low velocity impact in which the projectile is not deformed since the dynamic pressure of impact is less than the strength of the projectile. Penetration produces a deep and narrow cavity with depth varying at the 4/3 power of velocity. The in-plane stresses set up in the target are sufficiently low so that only elastic deformations occur in the plane of the plate surface and if perforation occurs a plug is sheared out of the plate.

2. As velocity increases, a critical value is reached, depending on the strengths of projectile and target, at which the projectile no longer withstands the forces of impact and begins to deform or, if brittle, to fracture. This is the beginning of the transition region of impact. As velocity is increased above this value, ductile projectiles tend to mushroom and the rate that penetration increases with velocity, begins to fall off. Brittle projectiles fragment into smaller and smaller pieces as velocity increases in this range; penetration increases slightly, then decreases before beginning again to increase with increasing velocity. As velocity increases above the critical value an increasing portion of the projectile's kinetic energy is applied to widening the crater which begins to approach hemispherical shape. The frontal area of the shattered or mushroomed projectile is much larger than that of the undeformed projectile. Consequently, a higher velocity is required to perforate a given thickness of target. As velocity increases further, the stress waves may become so intense that on first reflection of the wave system from the rear face of the target, fracture under tensile stress will occur and portions of the rear surface will be carried away by spalling. The effective thickness of the plate as a penetration barrier may thus be largely reduced.

3. When impact occurs at much higher velocities the induced stress waves will be very much greater than the mechanical strength of either projectile or target at least during the initial period of impact. The materials then behave as though they had virtually no strength. This is the region of fluid

impact behavior. At extreme velocities there may be melting and vaporization in projectile and target materials. Penetration will likely occur in the time of only one reverberation of the stress waves through the target plate, the projectile and target material being ejected both backward and forward as a spray of small particles. In the case of relatively thick targets the fluid impact phase will comprise only the initial part of the cratering process. The stress waves will rapidly attenuate to the level where target material strength properties again become significant. The discussion of the meteoroid environment contained in the foregoing section of this report shows that only particles of very small sizes and masses will be encountered with any significant frequency. Consequently, Eichelberger and Gehring (ref. 116) have stated that the impact problem concerning space vehicle structural materials corresponds more to hypervelocity crater formation in thick targets than to perforation of thin plates.

PHYSICAL MODEL OF CRATER FORMATION

A physical model of crater formation developed from transient observations has been described by Eichelberger and Gehring (ref. 117). According to this model the projectile impinges on the target at an initial velocity considerably in excess of wave propagation velocity in either material. Immediately after contact, a transient state develops in which the pressure at the interface is that pertaining to a plane impact without flow, i.e., of the order of 1 to 100 megabars. Shock waves propagate a short distance from the interface into both projectile and target, and at the same time, release of pressure at the boundary of the projectile initiates lateral flow of both materials. Consequently, in a very small fraction of a microsecond, an equilibrium condition is established in which the two shock waves become stationary with respect to the projectile-target interface. This is the fluid impact regime which, according to the model, persists for only a fraction of a microsecond, and during this interval the projectile is progressively "used up." It is characteristic of truly hypersonic impact that the rate of crater expansion during this stage is greater than the wave propagation velocities in the target material; consequently, the region of compressed material is confined to a thin shell adjacent to the crater surface, and the energy density is very high. After the projectile has been eliminated as a causative force, the shock wave, and with it the crater, continue to expand. The shock intensity and velocity decrease but the velocity of the crater surface undergoes a more rapid decrease so that the shock wave detaches and the thickness of the compressed material region increases. This process continues until the energy density behind the shock wave becomes too small to overcome the target materials' mechanical strength. From this point the shock wave expands as a low intensity plastic or an elastic wave; plastic and elastic recovery may subsequently cause some shrinkage of the crater. The expansion of the crater under low pressure conditions in the later stage of impact is a cavitation process, the duration of which

depends substantially upon the physical characteristics of the target material. In very plastic or ductile target materials, the expansion of the crater continues for very long times, apparently due to a decrease in resistance to deformation at very high strain rates. In brittle or frangible material targets, the crater expansion terminates in a shorter time and is followed by extensive crushing, fracturing and spalling. In extreme cases the fracture and spall may obscure the form of the original crater.

THICK AND QUASI-INFINITE TARGETS: THEORY AND EXPERIMENT

The qualitative aspects of the above described model have been rather widely accepted by both experimentalists and theoreticians engaged in the study of hypervelocity impact. There are large differences of opinion, however, concerning the quantitative relationships between crater formation parameters and the impact parameters (ref. 99). Parameters generally conceded to be of some importance in predicting crater dimensions, wave propagation effects, bulk deformations and fracture of projectile and target include impact velocity; mass and shape of the projectile; density; compressibility; strength; brittleness and at sufficiently high velocities the molecular energy properties of projectile and target. There is practically no agreement among independent investigators as to the precise bounds within which these various factors will predominate (ref. 107).

Theory.—The conceptual aspects and historical development of modern theories of impact and penetration are well documented and the differences in the impact models involved have been reviewed, as mentioned earlier. For the reader unfamiliar with this background the following references are strongly recommended as a minimal introduction: Herrmann and Jones, reference 100, Section III. This presentation is summarized in part by Davidson and Sandorff in reference 8; Goldsmith in reference 107; Rolsten, Hunt, and Wellnitz in reference 109, appendix A; and in reference 113.

Most present day theoretical work centers about either the hydrodynamic theory, which treats deformation in the dominant high pressure phase of hypervelocity impact as the flow of a compressible inviscid fluid, or the blast-wave theory, which was developed over the years to describe various high energy gas flows.

The general approach in applying the hydrodynamic theory is that pioneered and described by Bjork in 1958 and more recently summarized by him and compared with other approaches in a paper presented at the Sixth Symposium on Hypervelocity Impact in 1963 (ref. 118). Bjork's computations resulted in a prediction of penetration by a projectile into thick targets (quasi-infinite, or thickness of the order of 10 times the crater depth) following the approximate relation:

$$p/d \propto v^{1/3} \tag{43}$$

where p is the crater depth, d is the projectile characteristic dimension, and v is the impact velocity. The shape of the craters was found to be nearly

hemispherical for cases involving projectile and target of the same material and projectiles of square-cylinder geometry (length equal to diameter). Bjork, in the later reference cited above, has refined the expression for penetration into 1100–F aluminum targets to:

$$p/d = 11.02 \exp - 2.457/v^{0.295} \tag{44}$$

where v, the impact velocity is in km/sec. The equation is for a curve chosen to produce a smooth change of curvature on a log-log plot of p/d vs. v and which is shown to fit well in both magnitude and slope to selected experimental data (maximum velocity approximately 8 km/sec). For a given velocity, possible error in p/d should be taken to be 10 percent. It is Bjork's opinion that, for thick targets of 1100–F aluminum, the equation will be accurate to within the limits of error prescribed over the velocity range of 5.5 to 20 km/sec. At lower velocities he indicates that penetration would be overestimated because of material strength effects which the hydrodynamic model does not consider; at higher velocities, penetration would be underestimated due to increasing effects of melting and vaporization in the target. Penetrations 40 percent greater than predicted by the equations are anticipated for impact velocities near 72 km/sec. In this same reference (ref. 118) a scaling law due to A.E. Olshaker and R.L. Bjork to account for projectile material influence on the process is presented in the form:

$$(\pi_{B\text{-}A}v/\pi_{A\text{-}A}v) = F_{BA}v \tag{45}$$

where π is the normalized penetration, p/d, and the subscript B–A denotes a projectile of material B striking a target of material A, and $F_{BA}v$ is the normalized penetration ratio. It is shown that by simple extension of this law:

$$(\pi_{B\text{-}A}v/\pi_{C\text{-}A}v) = (F_{BA}v/F_{CA}v) \tag{46}$$

If the penetration of any projectile material B into target material A is known at any impact velocity, then penetration by any other projectile material C into target material A at the same velocity may be predicted.

An alternative scaling procedure which is somewhat rougher but more convenient is also given. Bjork states that, using his theoretical predictions for aluminum-on-aluminum and iron-on-iron impact, and by means of the scaling law deriving the penetrations of other projectile materials in these targets, an accurate estimate may be obtained of any projectile penetration into these materials at impact velocities to 20 km/sec.

The effects of projectile and target densities was studied by Olshaker and Bjork and their hypothesis of correlation with the cratering process reported in 1962 (ref. 119) is viewed as being substantiated by additional experimental data cited in Bjork's presentation at the Sixth Symposium on Hypervelocity Impact (reference 118; see also Zernow, reference 120).

Walsh and Tillotson (ref. 121), applying the hydrodynamic theory and using procedures generally comparable to those of Bjork, have introduced an "equivalance" principle to account for the later stages of the crater formation phenomena when pressure has fallen to approximately one megabar (ref. 99). The work described in this reference, as in Bjork's work, employed nu-

merical techniques to treat the hydrodynamic phase of axisymmetrical impact. A series of calculations for iron-on-iron impacts (thick targets) were studied in which projectile velocity and target thickness are each varied over a wide range. An equation of state correlation and dimensional analysis lead to a general description of impacts with projectiles and targets of the same metals. These investigators report that for impact velocities between approximately 5 and 250 km/sec crater dimensions vary as velocity to the 0.62 power, or:

$$p/d = K(v_0)^{0.62}/C_0 \qquad (47)$$

where p and d are standard symbols for crater and projectile dimensions, respectively. C_0, speed of sound, is defined by $C_0^2 = (\delta P/\delta\rho)_s$ (where $\delta P/\delta\rho$ is partial derivative of pressure with respect to density) evaluated at $P = 0$. From the equation of state formulations, v_0 is impact velocity, and dimensionless parameter K can be determined from a single experiment. It is pointed out that the exponent is independent of the metal under consideration; however, K depends on strength properties and thus must be determined separately for each material. Collisions of unlike materials were not considered in this work, nor were the effects of projectile shape.

Of particular interest are the exponents relating cratering to velocity resulting from these two studies. Bjork's exponent reputedly represents a dependence on momentum (velocity to the first power) while the value obtained by Walsh and Tillotson corresponds somewhat with the "two-thirds law" or volume-energy relation arrived at by many experimentalists in deriving a curve to fit their data. A controversy has developed between proponents of the two hypotheses which has become sharply focused with some experimental results now reputedly in agreement with the momentum relationship (refs. 36,99,118 and 120).

As in the case of the hydrodynamic theory the blast-wave theory approach to hypervelocity impact has been demonstrated to successfully predict shock trajectories (refs. 107,122 to 127).

The crater size formula deduced by Rae and Kirchner (ref. 124), which follows a lengthy derivation, gives for an assumed hemispherical crater:

$$Rc/d = [\tfrac{1}{12}(\gamma + 1)I_1(\gamma)]^{1/3}\,[\rho_p v^2/P]^{1/3} \qquad (48)$$

Where Rc is the crater radius, d is the diameter of the projectile (for nonspherical projectiles, d should be taken as the diameter of a sphere of equal mass), ρ_p is the density of the projectile material, v is the impact speed; P denotes the intrinsic shear strength of the target, $G/2\pi$ (G is dynamic shear modulus as measured, for example, by an ultrasonic technique); and $I_1(\gamma)$ is a function representing the influence of the equation of state. The symbol γ denotes a constant which approximates $1 + \Gamma(\rho)$ (where $\Gamma(\rho)$ is the Grüneisen Factor) and characterizes the state equation of the target. The quantity γ is actually the adiabatic index of a perfect gas whose equation of state matches that of the target in the vicinity of the impact point. The Rae and Kirchner report (ref. 124) sets forth a step-by-step procedure for

determining γ, $I_1(\gamma)$, and thus R_c. This crater-size formula implies that the kinetic energy of the impacting particle is a controlling parameter and that the dynamic strength of the target is the factor most effective in limiting penetration. These authors point out the similarity between their expression for crater size and that by Eichelberger and Gehring (ref. 116) which shows the crater volume to vary directly with the kinetic energy of the projectile, E, and inversely with the Brinell hardness, B, of the target:

$$\frac{2}{3}\pi R_c^3 = 4 \times 10^{-9} \frac{E}{B} \tag{49}$$

Yuan and Bloom (ref. 128) approach the analysis of hypersonic impact by assuming that the energy released is sufficient to melt or vaporize both the projectile and a small volume of the target during a very short interval of time. The motion of the fluid which represents the shock front is assumed to be governed by the basic equations of one-dimensional flow of a viscous compressible fluid. The Hugoniot equation of state for metallic elements, determined by other investigators through shock-wave velocity and free-surface velocity measurements to 2 megabars, was introduced into the one-dimensional equations for fluid flow and a solution obtained. Experimental data for hypervelocity like metal penetrations in copper, lead, and tin were then employed, and by an iteration technique the constants of the theoretical solution relating to the physical properties of the materials at the extreme conditions of the fluid impact regime were evaluated. The result of the work is the penetration formula:

$$p/d = 0.58 \ln \left[1 + \frac{(E/\rho) \times 10^{-4}}{\{1.0 + 1.398 \times 10^{-8} (E/\rho)^{1/2}\}^2} \frac{v^2}{E/\rho} \right] \tag{50}$$

where p is the penetration depth, d is the linear cross-sectional length of the projectile, v is the impact velocity, and $(E/\rho)^{1/2}$ is the sonic velocity of the materials in solid state at standard conditions.

The results obtained with these fluid-mechanical models can be correlated for various cases (ref. 129). However, the prediction of crater size does not derive directly from these models even though they do cover a very significant portion of the total time of the penetration process. For this reason the several investigators have had to adopt auxiliary criteria in order to apply additional analyses.

Of particular significance is the selection of a point in the shock trajectory from which to project the crater radius. There has been large variety in the criteria applied (refs. 122 and 129), and thus significant differences in predicted crater sizes. Restated, this reflects that there are large differences of opinion as to applicable scaling laws and no generally accepted theoretical means of predicting size. To make an unequivocal determination of crater size an accounting must be made of the processes, external or otherwise to the fluid regime, where material strength and strain-rate effects are important. Recent work by Riney (refs. 130 to 133) provides for inclusion of viscoelastic and/or elastic-plastic models to augment the hydrodynamic equations

of state in current use. On the basis of recently reported calculations (ref. 131) describing cratering by a cylindrical projectile (radius equal to length, L) impacting a thick target of like metal, Riney concludes that: momentum scaling is not justified; energy scaling for geometrically similar impact situations is accurately predicted by taking into account the different rates of shock propagation in the early stages of cratering; penetration depth is related to impact velocity according to:

$$p_c/L = K_e\, v_o^{2/3} \tag{51}$$

for $v_o \geqq v_o^*$ (threshold velocity for energy scaling or 2/3 law; $v_o < 0.76$ cm/μ sec for lead and aluminum, except for aluminum alloys in which strain-rate and strength effects persist for pressures up to 0.2 mb) and with K_e, the corresponding experimental constant, and L, the length of projectile.

Rolsten and Hunt, in recent reports on their work with nylon, glass, and aluminum projectiles impacting aluminum targets (refs. 134 and 135), conclude that crater damage can be related to tensile strength by using equations for uniformly accelerated rectilinear motion when the measured crater dimensions are corrected for relaxation after the pressure release. These investigators judge that future correlations of impact damage with material properties may be more productive and that better concordance may be obtained between theoretical and empirical results when cognizance is afforded the afterflow or springback in the target material, e.g., the compressive properties.

Quasi-theoretical solutions.—Several investigators have approached the quantitative description of impact phenomena from analyses of experimental data, after which they have formulated models and developed quasi-theoretical techniques for predicting penetration depth. Recent contributions of this type by Kinslow, Heyda, Engel and Moore, MacCormack and Gault appear in references 113 and 114. Most of the data available for such work has derived from rather low impact velocities relative to the range of major concern in considering the meteoroid environment. The validity of extrapolation to higher velocities appears hazardous in most cases in view of the nature of the derived models and of the assumptions required in these techniques. Bohn and Fuchs developed a quantitative relationship for describing penetration depth and time which has been restated by Fuchs (ref. 106). According to the fundamental concept adopted, the resistive forces $R(v)$ between the mass of the projectile and the target material are the combined result of three components, each of which are functions of the instantaneous velocity v so that:

$$R(v) = f_1(v^0) + f_2(v^1) + f_3(v^2) \tag{52}$$

which by virtue of Newton's second law of motion also equates to $-m(dv/dt)$. This approach leads to an expression for maximum penetration depth χ^* in a semi-infinite target:

$$x^*\ (v_o) = \frac{m}{\beta}\left[\ln\ \{1 + (\beta/\alpha)^{1/2} v_o\} - \frac{\beta^{1/2}\ v_o}{\alpha^{1/2} + \beta^{1/2}\ v_o}\right] \tag{53}$$

where m is the projectile mass, v_o is the initial velocity, α is substituted for $f_1(v^o)$, and β is substituted for $f_3(v^2)/v^2$. The functions of instantaneous velocity, f_1 and f_3 reflect dependence upon: cross-section of the projectile; a difficult-to-define stress factor which may be approximated by Brinell Hardness; a shape factor for the projectile; and density of target material. Function f_2 is accounted for by adopting a substitution of $2\ \alpha^{1/2}\ \beta^{1/2}\ v^1$.

J. K. Wall in a more recent article (ref. 136) derives an expression for penetration into massive targets by integrating an equation for projectile motion. In his model, the projectile is significantly deformed immediately after impact by the initial shock wave and subsequent expansion waves; the projectile is assumed to be retarded by a pressure on its face resulting from weak waves. The results indicate: (1) penetration should increase with projectile impact momentum per unit frontal area, as suggested by Collins and Kinard in NASA TN D–238 (1960), and inversely with the acoustic impedance of the target; (2) penetration is only weakly dependent on target strength *per se*, but is strongly dependent on the plastic wave speed of the target material which is closely related to strength properties; and (3) as impact speed increases, the diameter of the projectile and high temperature properties of the target have an increasingly important effect on penetration. Reasonable agreement is reported with experimental data for spherical and squat-cylindrical projectiles at impact velocities to 10 km/sec.

Experimental results and empirical correlation.—A large amount of experimental work has been done concerning impact into quasi-infinite and thick targets. These two classifications of target thickness are generally defined in a manner comparable to that of Jones, Polhemus and Herrmann (ref. 102) which states: "Quasi-infinite targets are . . . so thick that the rear surface of the target does not influence cratering. Thick targets . . . include targets in which the presence of the rear surface affects the crater-size, and in which the rear surface may be damaged, and includes targets which are just sufficiently thin to be perforated (ballistic limit)." The previously mentioned surveys by these authors (refs. 100 to 102) contain summaries of a large amount of the resulting data and include, as feasible, comparisons of the results from different laboratories, and the empirical expressions developed to fit particular groups of data. The latter expressions are also compared with theoretical results. The latest of these surveys (ref. 102) has shown that recent experimental work has essentially confirmed the earlier empirical expressions. Kineke and Richards (ref. 137) report on experiments in which aluminum projectiles were impacted at 9.7 km/sec and beryllium projectiles at 15.5 km/sec into 1100 aluminum and 2014 aluminum alloy targets. Their results indicate that the influence of the mechanical strength of the target in determining final crater dimensions, extends unimpaired for impact velocities up to 15.5 km/sec. These data have also been applied to demonstrate that crater volume is proportional to the projectile energy. The correlation equation (logarithmic law) developed

by Herrmann and Jones (refs. 100, 102, and 112) and since used to a considerable extent in applied work and estimates of meteoroid damage (refs. 20, 37, and 138) is:

$$p/d = K_1 \ln [1 + (\rho_t v^2/K_2 H_t)] \qquad (54)$$

where p is penetration depth, d is the projectile dimension, ρ_t is the target material density, H_t is the target hardness (Brinell), v is the impact velocity, and the K_1 and K_2 constants have values related to the material combination (see ref. 100, table V and ref. 102, tables 2.1 and 2.2 for available constants for like-metal impacts). This relation is considered applicable only over the velocity range in which the data from which it derives was obtained (up to ~10 km/sec). Justification does not exist for extrapolating present experimental results to much higher impact velocities. The accuracy of some of the early data is considered suspect; however, the preponderance of the information available on quasi-infinite targets provides useful comparisons with theoretical predictions in this configuration with the simplest boundary conditions (ref. 102). The reader is reminded, however, of the observations of Eichelberger (ref. 99) cited earlier, regarding the lack of definitive correlations.

It has been demonstrated by data plots (ref. 102), that the scaling law due to Bjork and Olshaker, discussed previously, is reasonable in quasi-infinite targets. This type of scaling is very useful. It is only necessary to construct empirical fits to data for each target material impacted by a similar projectile material, results for all other projectile materials being deduced by the scaling law. It is surmised that similar scaling applies to ballistic limits and spall thresholds in thick targets. This, however, awaits experimental verification.

Ballistic limits have previously been calculated and broadly adopted; these were based on the assumption that a target of thickness 1.5 times the penetration in a quasi-infinite target is just perforated (refs. 8, 36, and 102). Recent results reported by Maiden (ref. 20) show this supposition is in error. The factor apparently increases with velocity and evidently values higher than 1.5 are possible even at relatively low impact velocities. Experimental work is urgently needed in this area in view of the importance of the ballistic limit and threshold for spall in practical applications.

Although recent techniques have extended the capacities of ballistic ranges to velocities in excess of 10 km/sec, it appears that attainment of velocities exceeding 15 to 20 km/sec in controlled experiments is needed to provide additional understanding and insight into hypervelocity impact phenomena.

THIN TARGETS

The result of impact on thin targets is perforation. The parameters of primary concern in this damage process are: the size of the hole; and the damage potential of the spall or spray projected from the rear of the target. Theoretical treatments by Bull (ref. 139), Maiden (refs. 20, 140), Sandorff (ref. 141), and Krause (ref. 142) have developed several of the concepts and techniques mentioned in the foregoing discussion of theory to the more com-

plicated configurations involving thin plates by adding a boundary condition accounting for the rear surface of the target.

Riney (ref. 131) reports additional results from his work described earlier, arising from calculations involving aluminum and iron plate targets of thickness equal to the radius of the impacting like-metal projectile. Projectile radius in these calculations was equal to projectile length. In these cases, the pressure pulse due to impact velocities of 7.6 and 20 km/sec is relieved by spallation in the opposite free surface before much of the energy can be transmitted radially into the target. The pressure in the central part of the configuration rapidly falls to zero and an expanding spallation bubble is formed. The material in the bubble is completely shattered and remains at a high temperature. The total forward momentum of the configuration after impact exceeds the original axial momentum. If the thickness of the plate is less than the projectile radius, the leading central portion of the spallation bubble travels at the velocity of the projectile at impact.

Bjork (ref. 118) gives pressure contours and particle velocities at various times after impact for cases in which 10 centimeter long, 10 centimeter diameter aluminum projectiles impact at 20 km/sec against two thicknesses of aluminum targets, 1 and 2 centimeter. The effect of target thickness is clearly shown in the results for these targets. The rarefaction from the rear of the thin target more quickly weakens the shock than in the case of the thicker target so that for corresponding times the shock in the thicker target is seen to be the stronger. In the case of the thinner target, the lower pressures from this source lead to less lateral expansion; thus more mass is carried in the forward direction and the dispersion angle projected from the rear of the target is smaller. For the same reason the strength of the shock reaching the rear surface of the projectile is also smaller. Finally a smaller hole will result in the thinner target, since less impulse per unit lateral area is applied, and the pressure in the thinner plate is more rapidly relieved by rarefaction waves. Hole radii estimated from calculations in this study are 9 and 12 centimeters for the thin and thicker targets, respectively.

Recent years have witnessed an increase in the experimental work devoted to determining the effects of hypervelocity impacts on thin targets. Determination of hole sizes is relatively straightforward; however, assessment of the damage potential of the material projected beyond the rear face of the target is much more difficult. Jones, Polhemus and Herrmann (ref. 102) relate that many experiments have employed a quasi-infinite plate (witness plate) spaced at various distances behind the thin target, to obtain information on depth of penetration and extent of the impacted area resulting from the fragments issued by perforation and spall mechanisms. Other experimenters have used a thin witness plate, and following impact, tested to determine changes of its structural integrity (ref. 143). It has been found that although a quasi-infinite witness plate provides a useful indication of spall damage potential attendant to low velocity impacts, it is not suitable for

this purpose at high velocities. In such cases the spray due to thin plate perforation may be finely divided and results in very little damage to the witness plate although the impulse delivered by the spray may be sufficient to cause spalling, bulging, or tearing and petaling in a thin second target without significant penetration. Efforts have also been applied to measure the size, mass, and velocity distribution of the spall or spray issuing from the rear of a thin target. This becomes a major undertaking in high velocity impacts where a very large number of particles constitute the spray.

Recent experiments have provided for a more detailed physical description of thin plate perforation which includes important phenomena which do not pertain to the general description of impact into thick targets presented earlier in this review. The shock impinging on the rear surface of a thin target is reflected as a release wave and travels back into the target at the material's sonic speed. The result is that the shock pressure is reduced and particle velocity is increased. Upon reaching the projectile-target interface the release wave is refracted and a rarefaction wave travels into the projectile (this interface interaction does not occur in target-projectile combinations of the same material). If the rarefaction wave interacts with the shock wave in the projectile, the shock pressure there is reduced and particle velocity is increased. At impact velocities somewhat above the critical velocity for extreme projectile deformation, the projectile is extensively fragmented and upon perforation of the target, that portion not ejected as spray from the forming crater is projected together with some of the target material as a fine spray from rear surface of the target. If the target thickness is such that the rarefaction wave quickly overtakes and greatly reduces the intensity of the shock wave traveling into the projectile, the rear end of the projectile will not "see" the impact and thus will continue to travel intact at the impact velocity. The intact portion of the projectile represents significant damage potential to a second target in such a case. The spray issuing from the back face of a perforated target appears in the form of an expanding bubble, the fastest particles traveling along axial direction. Observations have revealed that the maximum number of fragments is obtained from the thinnest target and the number decreases as target thickness increases. Spray from the thinner targets is more concentrated about the normal through the point of impact and the maximum dispersion angle is smaller. This is due to the rarefaction waves arriving more quickly to interact with and weaken the pressure pulse which expands laterally in the target. For this same reason the diameter of the perforation also depends upon target thickness. This weakening of the pressure pulse by rarefaction waves also causes a lower intensity shock to impinge on the rear surface of thicker targets resulting in a spray of large particles issued at a lower velocity. When target thickness is just sufficient so that perforation does not occur, rear surface damage is of the form of a spall or bulge. At very high impact velocities, melting will occur in thin targets. Damage to a second target or witness plate will then

result from a pressure pulse due to the metallic vapor impinging upon it. It is expected that pitting of the second plate would be minimal and damage would arise from spall or petaling.

If hydrodynamic theory applies to hypervelocity impact perforation of thin targets, direct geometrical scaling should exist between projectile size and damage to the thin plate, provided that plate thickness is also scaled and the impact velocity of concern is constant. The experimental work of Watson, Becker and Gibson (refs. 144 and 148) suggests that such is the case. Their work involved aluminum 2024–T3 sheet targets impacted by steel projectiles at a velocity of 3.2 km/sec. The ratio of target thickness to projectile length, t/d, was varied and the characteristics of the spray ejected from the back of the target plate were studied. Their results show that the mass of the target spall increased as the cube of the projectile size. Since plate thickness was scaled, it is indicated that perforation area is directly scalable. The total mass, as well as the total number of projectile spray particles increased as the cube of projectile size. However, the number of target spall particles increased as the square of projectile size, possibly due, according to these investigators, to the fact that the number of particles per unit of spall surface is determined by the peak pressure at the rear surface of the target (according to hydrodynamic theory, this peak pressure remains the same with the scaling of the target thickness). Therefore, with the area of the spall surface increasing as the square of the projectile size, the number of particles should increase in the same manner.

It was illustrated by Herrmann and Jones (ref. 100) that the projectile strength did not affect penetration in quasi-infinite targets above the transition region. It might therefore be surmised that the same holds for thin plate damage. Studies by Halperson and Porter, summarized by Jones, *et al.* (ref. 102) involving the perforation of aluminum 2024–T3 plates by steel spheres of varying hardness in the velocity range from 0.5 to 5.5 km/sec, indicate that within the experimental scatter, no significant differences in hole area are observed for Rockwell "C" hardnesses of 10, 20–30, and 60–65.

The effect of projectile density is also difficult to determine, as the majority of the experiments measuring single plate damage employ steel projectiles. The only available comparison is the work by Olshaker (ref. 145) involving spherical lead and steel projectiles impacting lead plates. These tests were conducted at a velocity of 2.56 km/sec over a t/d range of 0.089 to 1.88. It is observed that there is no difference in hole size produced by the two projectiles up to a t/d of 0.7. However, as the thickness is increased further, the hole areas made by the two types of projectiles diverge, and approach their respective crater area values in quasi-infinite targets.

The experimenters who have investigated the effect of various parameters on single sheet damage have presented their data in various ways (ref. 102). Watson (ref. 112) measured the entry and exit diameters, while Olshaker (ref. 145) working with lead under conditions which resulted in a perfora-

tion such as that described for ductile materials measured the diameter at the midplane of the plate.

Watson's results indicate that the entry area in a finite target approaches the crater area in a quasi-infinite target as the thickness of the plate is increased. The tests, involving 0.159 centimeter by 0.159 centimeter cylindrical steel projectiles impacting various thicknesses (t/d ranging from 1 to 5) of aluminum, magnesium, and lead targets at an impact velocity of 3.17 km/sec, were repeated at least five times for each set of experimental conditions. In the graphical data presented, only the entry areas are indicated; however, it is noted that the mean exit areas are essentially the same up to $t/d = 3.0$. For $t/d > 3$, the exit area is less than the entrance area; thus, the perforation in the plate attains a maximum area roughly equivalent to the crater area in a quasi-infinite target. This value is attained, however, at different thicknesses for the various materials. Maximum hole areas occurred in lead and 2S–0 aluminum at a t/d of 3.0 and in 17S–0 and 2024–T3 aluminum at a t/d of about 2.0. In the case of magnesium, the hole attains quasi-infiinite crater size at a t/d of slightly less than one, but continues to increase until a t/d of three is reached, where it exceeds the quasi-infinite value. This may be attributed to excessive surface spallation.

With diminishing sheet thickness, a decrease in hole area is observed. Olshaker's results clearly illustrate the thickness effect at the lower t/d values. The perforation area for both the steel and the lead projectiles increased linearly with t/d up to a ratio value of about 0.7. The reason for a decrease in hole area with diminishing sheet thickness is suggested by the physical model of thin plate perforation, which indicates a quicker reduction of shock strength caused by the weakening effect of the rarefaction from the rear of the target which in turn leads to a smaller impulse per unit of lateral area.

The foregoing discussion indicated that single plate hole size approaches a maximum comparable to the quasi-infinite crater size as target thickness is increased. A dependence of crater size upon target material in quasi-infinite targets was indicated by Herrmann and Jones (ref. 100) and other investigators as discussed previously. Therefore, target material should be a factor in determining the hole area in a plate; however, Jones, *et al.* (ref. 102) have found no available data to corroborate this.

Watson (ref. 112) has observed a definite correlation between hole size and the strength of the target material in his experiments with steel projectiles impacting 2S–0, 17S–0, and 2024–T3 aluminum alloy plates at a velocity of 3.17 km/sec; results show that perforation area increases as target strength decreases. Maiden (ref. 20) investigated the effects of variation of plate strength on damage to a secondary target (or witness plate) positioned 5.48 centimeter behind the initial plate, using aluminum spheres as projectiles, 2024–T3 aluminum as the shielded witness plate, and 2S–0, 2024–T3, and 7075–T6 aluminum alloys as the shields. At an impact velocity of 6.1 km/sec

and a t/d of 0.17 (the ratio applies to the shield or initial plate impacted), Maiden observed no significant dependence of shielded target (witness plate) damage upon the shield strength. There was, however, a difference in the results in that the higher strength material did a better job of breaking up the projectile, as evidenced by smaller individual craters in the witness plate (ref. 102).

In the low velocity regime (below the critical velocity for projectile fragmentation) the hole area in perforated thin targets is approximately the same as the effective projectile cross-section indicating the shearing or punching mechanism. Penetration into a witness plate may exceed that which occurs in an unshielded target since it is apparently easier to penetrate the shield than to penetrate an equal distance in the witness plate because, as described before, the rarefaction from the rear surface of the shield tends to increase the particle velocity. As velocity increases into the transition region and beyond, the shield begins to more and more effectively fragment the projectile thus causing penetration in the witness plate to be less than in unshielded, quasi-infinite targets. The hole area in perforated thin targets impacted in this velocity regime increases as an approximately linear function of the impact velocity (ref. 102).

The distribution of the spall following perforation of a thin plate has been treated in the majority of experiments in terms of the semi-vertex angle of the spray ejected. This angle has been observed experimentally as a function of impact velocity, target thickness and material combination. Theoretical estimates are available from the work of Bull (ref. 139) and Lull (included in detail in the summary by Herrmann and Jones, reference 100).

Bull's theory (also treated in reference 102, appendix B) yields, for like projectile and target materials, a constant value of 45° for varying impact velocity and plate thickness. Olshaker (ref. 145) has investigated the relationship between plate thickness and spray angle for the case of lead projectiles and targets at an impact velocity of 2.56 km/sec. His results indicate an asymptotic approach to the 45° value of Bull and are in approximate agreement with the values of Lull up to a t/d of 0.27, after which they diverge, with the theory predicting angles larger than those observed.

Watson, Gibson and Becker (ref. 144) have investigated extensively the spatial, mass, and velocity distributions of the fragments produced in the perforation process, Jones, *et al.* (ref. 102) summarize the results of this work involving steel projectiles impacting 2024–T3 aluminum plates at t/d values of 1, 2 and 3 at an impact velocity of 4.0 km/sec. The results indicate that, for all thicknesses, population density is maximun directly beneath the impact point and decreases monotonically with increasing angle of dispersion. However, the population density, and therefore the total number of spall fragments, is seen to decrease with increasing plate thickness. As in the case of population density, the mass per unit of solid angle is maximum on the center line, and decreases with increasing angles of dis-

persion for all thicknesses tested. The mass densities, however, increase with increasing plate thickness.

The average mass of a spall particle must increase with plate thickness since the population density decreases and the mass density increases with increasing plate thickness. The dependency of the average individual particle mass upon plate thickness at velocities of 3.17 and 4.0 km/sec is illustrated in the results obtained by Watson, *et al.* The average mass of spall particle issuing from the plate is observed to increase by approximately an order of magnitude for a t/d range of one to three.

The maximum fragment velocity has been shown by Humes (ref. 146) to be always less than, and to increase linearly with, impact velocity for the case of 2024–T4 aluminum projectiles impacting 2024–T3 aluminum plates (t/d of 0.568) at velocities ranging from approximately 1 to 4 km/sec. For an impact velocity of 4.08 km/sec, the maximum fragment velocity varied from about 2.49 to 1.21 km/sec over dispersion angles from 0° to 45°.

In summary, the perforation area in a thin plate remains constant with increasing impact velocity until the projectile breaks up. Above this velocity, the area increases with about the first power of the impact velocity. In this region, the target strength becomes effective in reducing the hole size, the hole being smaller for plates made of stronger alloys.

For very thin plates, the hole area is approximately the same as the projectile cross-section area. In thicker targets, the hole size increases. It has been ascertained that the hole size in a ductile plate attains a maximum area roughly equivalent to the crater area in a quasi-infinite target. On the other hand, the hole size in a brittle plate attains a maximum area somewhat greater than quasi-infinite crater size due to excessive surface spallation.

Direct geometrical scaling between the perforation area and the projectile size exists, provided that plate thickness is also scaled and the impact velocity remains constant. Scaling of the subsequent damage to a shielded target, however, is not possible as the number of resulting spall particles does not remain constant with varying projectile size, while the mass does increase as the cube of the projectile size (ref. 102).

EFFECT OF OBLIQUE IMPACT

All of the foregoing discussion of the impact phenomena was derived from studies of normal impacts (projectile path perpendicular to target surface). When considering the effects of the meteoroid environment, it is evident that many impacts will involve particles approaching targets at oblique angles of incidence.

The volume and shape of craters produced in lead by the impact of steel pellets at 3 km/sec have been studied as functions of the angle of incidence for angles up to 70° from the normal by Bryan and Pugh (ref. 147). Their results show that at normal incidence the crater is not quite hemispherical, since penetration depth is greater than the crater radius. Careful measure-

ments of the craters show that elongation begins to occur as soon as the incidence angle deviates from zero. They conclude that at any angle of incidence, the volume is proportional to the incident kinetic energy, and the proportionality constant is a linear function of the cosine of the angle of incidence.

Eichelberger and Gehring noted the above described work and observed that the effect is great enough to be of considerable importance in estimating damage to a space vehicle (ref. 116). They took this effect into consideration by stating that, in sufficiently thick skins, a meteoroid having kinetic energy E (in a coordinate system fixed with respect to the space vehicle) will produce a hemispherical crater of volume τ, given by:

$$\tau = 4 \times 10^{-9} (E/B) \cos \alpha \text{ (cgs units)} \qquad (55)$$

where B is the Brinell hardness number of the skin material, and α is the angle of incidence.

Watson, Becker, and Gibson have reported (ref. 148) experimental results associated with the distributions of numbers of spall particles resulting from oblique impacts on thin targets. They point out that the oblique impact data do not permit as simple an interpretation as data from normal impacts. The added complexities are understandable inasmuch as the center of spall impact on the witness plate does not lie on a line perpendicularly beneath the perforation in the target nor along the original line of flight of the projectile; it is found to lie between these two extremes. Hence, the distribution of particles, in terms of the target-witness plate geometry used for normal impacts, is not independent of the azimuthal coordinate ϕ, (departure from the projection of projectile path on the witness plate). Results reflecting the dependence of spall particle numbers upon the coordinate ϕ, reveal several significant features: (1) the center of spall impact on the witness plate is displaced radially outward along $\phi = 0$ (in the azimuthal direction corresponding to the line of flight of the projectile); (2) the density of spall particles is maximum along $\phi = 0$ and diminishes progressively and symmetrically in both the positive and negative angular directions away from $\phi = 0$; (3) the percentage of the total number of spall particles found in any given element of spall impact area is independent of target thickness and projectile velocity.

Plotted data representing the displacements of the centers of spall impact on the witness target, as a function of both impact angle and plate thickness, show that: (1) the displacement angle increases with the impact angle up to impact angle values of between 50° and 60° after which a decrease in displacement angle is noted for further increases in impact angle [With respect to the decrease for impact angles greater than about 60°, it is believed that the axis for the envelope of the spray (projectile remains and associated target particles) flowing through the perforation in the plate is different from the axis of target spall produced shock interactions. The interplay of two such distinct distributions could conceivably cause displacement angle to be a double-valued fuction of impact angle]; (2) displacement angle is always

less than impact angle; (3) there is a tendency for the 10 percentile group of spray particles of highest penetration capability to have lower displacement angles; however, the difference is small and for practical purposes they are interpreted to be the same as those for the aggregate group.

Mortensen, *et al.* (ref. 149) have found that when a projectile strikes a target at oblique incidence, the impact area is larger than on a normal target by $1/\sin\theta$, where θ is the angle between the projectile path and the target plate surface. If the effective projectile area were the only consideration in determining hole area, a given projectile would be expected to produce a larger hole at oblique incidence. In impacts against 0.1 in. aluminum alloy targets at 90°, 50° and 20° incidence, these investigators did not find any such area relationship to hold.

The 20° data, although containing excessive scatter, clearly show that the damage caused by projectiles to targets at 20° obliquity is significantly less than damage to targets at 90° and at 50° (damage in these two cases is quite similar).

Target hole vs. projectile mass data for the 50° and 20° data show hole sizes formed at 20° are only slightly smaller than those formed by equivalent masses at 50°. The data on target hole area vs. projectile area plots progressively become more scattered as the obliquity goes from 90° to 50° to 20°; however, the hole area vs. projectile mass plots progressively become less scattered and reach a fairly smooth relationship at 20° obliquity. For impact under such severe conditions of obliquity, projectile mass is clearly more important than area in determining target hole area, even for relatively thin plates.

IONIZATION ASSOCIATED WITH HYPERVELOCITY IMPACT

Another phenomenon associated with hypervelocity impact is that of ionization manifested by electrically charged particles emitted from the site of the impact. Presumably, the large energy release associated with the impact is sufficient to produce ionization and the ions or electrons can be extracted by means of electrical collector systems. Friichtenicht and Slattery (refs. 150 and 151) have reported on the quantity of charge emitted from semi-infinite targets as a function of target material, projectile material, and particle velocity and mass. The experiments were conducted with micron-size iron and carbon black (graphite) particles impacting at velocities up to 16 km/sec. All of the data fits the empirical relationship:

$$Q_c = K E_p \frac{v}{A} \tag{56}$$

where Q_c is the charge collected, K a constant, E_p the particle energy, A the atomic weight of the particle material, and v the particle velocity. The quantity K contains target material parameters and has not yet been evaluated.

Design Considerations

Specific spacecraft components receiving considerable design attention from the standpoint of damage by interplanetary debris include optical and/or heat transfer surfaces, liquid filled containers (radiators and fuel tanks), expandable structures, and vehicle hulls. In addition, designers are concerned with the probability of penetration of a given thickness of material and possible weight saving concepts. These subjects as they relate to the environment and impact theory will be discussed in the remaining portion of this report.

DAMAGING EFFECTS OF MICROMETEOROIDS

The effects of meteoroid impact can be divided into those resulting from the small dust particles (micrometeoroids) and those resulting from the more massive bodies (meteoroids). Momentum and/or energy considerations, which usually dominate hypervelocity impact problems, are essentially irrelevant when considering damage by micrometeoroids because the momentum imparted per unit impacted area is far too small to initiate a shock wave or to produce in any significant degree the damage mechanisms described in the hypervelocity impact section of the present report (ref. 152). At escape velocities, it is most probable that evaporation processes obscure all other energy dissipative mechanisms for impacting particles of this size (ref. 83). Evaporation dissipates energy at a rate of 10^{34} ev/cm^2 sec so that long before any heat is conducted or radiated, the molecules and atoms of the micrometeoroid and of the local surface impacted vaporize and dissociate, dissipating all the energy. The result is a shallow crater on the surface having the same area as the micrometeoroid and a depth dependent on micrometeoroid density of 5 to 50 percent of its width; that is, the crater is a hemispherical section: micrometeoroids with densities large enough to create hemispherical pits are unlikely (ref. 83).

Micrometeoroid erosion has been one of the most difficult problems to estimate, for few laboratory experiments have been conducted with particles of this size impacting at velocities greater than escape. Therefore, many theories exist predicting negligible to complete erosion. In addition, it has been reasoned that due to the relatively low crushing strength of such particles, impacts would produce a coating or covering of a surface with meteoroidal substance rather than pitting (refs. 83 and 153). In the event of either erosion or material deposition, surface properties, particularly emissivity, could be appreciably altered. In view of the fact that the environment section of

this report shows that the vast majority of particles to be encountered in space will be of micrometeoroid size, their damage potential to the optical properties of exposed lenses, mirrors, windows and temperature control surfaces should not be ignored. Documented evidence of damage by such particles follows.

Surfaces.—Jaffe and Rittenhouse (ref. 154), using Bjork's hydrodynamic theory of impact penetration, have determined that the surface of an aluminum plate located in space will be eroded at a rate of 1 angstrom per year; close to Earth (within the confines of the dust cloud), this increases to about 200 angstroms per year. The erosion will be in the form of small hemispherical craters having diameters generally less than 10^{-3} centimeter if impacting particles have the density of solid stone. The number of craters for solid stone particles will increase from one per few cm^2/yr far from Earth to over 10^4 per cm^2/yr at low altitudes. For porous dust particles, the number of craters will be about 10^{-3} per cm^2/yr far from Earth and 10 per cm^2/yr at low altitudes. In brittle materials, such as glass and plastic, each crater will be surrounded by an area of cracks, or very shallow spall, several times the crater diameter. It has also been reported that for a 2200 angstrom thick aluminum skin on a 100 foot sphere the time for complete surface erosion by micrometeoroids would be about 4.7 years (ref. 155). A check on the above estimate results from isotope analyses of meteorites picked up on Earth's surface which have indicated that iron meteoroids of asteroidal origin are eroded by smaller particulate matter (dust and protons) in space at a rate of less than 30 angstroms per year (ref. 154).

Since the optical or thermal radiation characteristics of most spacecraft surfaces are controlled by a thin layer of material (ref. 156), it is quite likely that these surfaces will succumb to the continual bombardment of micrometeoroids and in time (1 to 10 years) fail in their function. This is more obvious when one considers that altering optical properties requires surface erosion only to a depth of $\lambda/2$ (where λ is the radiation wavelength of interest, approximately 4000 angstroms), or less than 0.1μ (ref. 152).

The relative merit of typical metals used as optical surfaces has been investigated by Leigh (ref. 157). This author reports on reflectivity/emissivity changes produced by simulated micrometeoroid impacts on gold, aluminum, stainless steel (types 304 and 316), chromium plate on brass substrate, tungsten and silver. Micrometeoroids were simulated with spherical zirconium alloy particles 100μ in diameter, accelerated to a velocity in excess of 5000 ft/sec (1.4 km/sec). The order of metals in increasing area damaged per impact was stainless steel type 304, tungsten, aluminum, chromium plate, silver, stainless steel type 316, and gold. This sequence appears to follow that of metal hardness, since chromium would probably lie above aluminum if it had not been a thin plating on a brass substrate. The conclusion drawn was that softer metals tend to sputter away more readily and to give a larger crater at these velocities. The order of metals in percent change

in reflectivity per unit area damaged was stainless type 304, tungsten, silver, chromium plate, gold, aluminum and stainless type 316. A final sequence was established representing the percent change in reflectivity per number of impacts: in decreasing order of percent change this was silver, gold, stainless type 316, tungsten, stainless type 304, chromium plate and aluminum. It was concluded that metals with higher reflectance show the greatest percentage decreases in reflectivity as a result of particle impact.

Another report of significance is that by Whitnah, *et al.* (ref. 158) who investigated the effects of pitting by micrometeoroids and other foreign matter on the heat transfer rates of reentry body surfaces in air, helium and nitrogen atmospheres at temperatures to 1000° C; smooth and roughened copper heat transfer models were utilized. The most important results of this study were:

1. The convective heat transfer coefficient for spherically shaped models was strongly influenced by the presence of pits. The mean convective coefficients increased by factors of 3 to 4 for the maximum roughness studies. A small number of surface pits was extremely effective in increasing the heat transfer to a body; with 15.5 pit/cm^2, the mean heat transfer coefficient was approximately twice that obtained for a smooth model.

2. With turbulent flow conditions over the roughened models, local heat transfer coefficient was maximum in the range of $\theta = 20°$ to 40°, where θ is the angle between the stagnation point and the point where the coefficient is measured; maximum value varied with stagnation pressure and degree of roughness. A peak value of approximately 4.5 times the stagnation point coefficient was measured on a model with 314 pits/cm^2 at $\theta = 25°$ for a stagnation pressure of 3.9 atmospheres.

3. Heat transfer in the laminar flow regions near the stagnation point was independent of surface roughness for the cases studied. However, the transition point moved forward with increased roughness.

4. Design of heat sink reentry bodies, with the assumption of turbulent heat transfer rates for a smooth surface, will not provide adequate protection if the surface is pitted to a sufficient degree.

5. The ablation process, observed in experiments with naphthalene models, was affected by surface irregularities in somewhat the same manner as heat transfer to permanent (non-ablating) surfaces.

6. Self-healing of pits during the ablation process was insignificant in the naphthalene models tested; however, a small amount of material was removed from the bottom of the pits.

7. Surface roughness and pitting can also result from alloying of surface material with small quantities of the foreign matter.

8. In a theoretical investigation of alloy formation with foreign bodies it was found that the rate of formation was controlled by the rate of diffusion of the material involved, and was highly sensitive to temperature. This process should be of greater interest to long-duration hypersonic glide vehicles rather than to ballistic missiles.

Erosion by dust particles of exposed man-suit systems has been considered only slightly in the literature (see references 159 and 160); however, the possibility exists of altering surface optical properties which regulate the heat balance of the suit. It appears that this is not a significant area of concern and that suit structural design could easily cope with the problem of complete penetration by dust erosion (ref. 160).

Though in actuality little can be done to prevent micrometeoroid damage to optical surfaces (ref. 33), high velocity impact testing of materials, such as low density oxides and coated non-metallic sandwich panels, would determine their actual behavior and reliable estimates of lifetimes could be made (ref. 161). The greatest single obstacle to achieving hypervelocities for experimental studies with larger, more massive particles has been that of projectile shattering prior to impact. The cohesive forces of a particle too often cannot withstand the extremely high acceleration rates required to obtain the hypervelocity within a reasonable distance. However, in surface erosion studies, such shattering could be turned into an advantage if, with the utilization of modern high-speed photography, the craters produced on the impacted surface can be associated with a particular shattered fragment (ref. 34).

Attitude and noise.—Attitude changes and noise are incidental effects resulting from bombardment by micrometeoroids and only a brief mention of each will be given. White (ref. 162), using generally accepted estimates of the momentum of micrometeoroids, derived a general expression relating angular disturbance to system parameters and probability of impact. The expression was applied to a 24-hour communications satellite and results indicated an angular disturbance for this vehicle with an exposure time of one year to be on the order of 10^{-3} deg/sec. The probability of this disturbance was computed to be 0.368; thus, one vehicle out of three could be expected to incur a disturbance of this magnitude. Noise levels produced by micrometeoroids continually striking a spacecraft are not considered to be of sufficient intensity to have a detrimental effect on an astronaut. Estimates of the noise produced, however, are unreliable because of the lack of a theoretical model (ref. 152).

DAMAGING EFFECTS OF METEOROIDS

Impacts by the more massive meteoroids will be less frequent than those by micrometeoroids, but the larger bodies are capable of producing catastrophic damage due to their high kinetic energy; a typical 0.5 gram particle traveling at a speed of 30 km/sec possesses a kinetic energy of about 10^5 joules. The phenomena of impact by a particle of this size have been considered in some detail in the foregoing section of the present report. The most damaging effects include cratering, penetration, perforation (puncture) and spallation. Spall fragments from the inside surface of a vehicle hull may be ejected inward at a velocity sufficiently high to cause serious damage to

components or personnel inside. Diameters of spall fragments are usually several times the thickness of the impacted plate; thickness of spalled fragments may be from about 0.1 to 0.5 times the impacted plate thickness (ref. 33). In addition, impact of these more massive bodies on the surfaces of a vehicle may include vibrations in the skin and/or other parts of the structure. The vibration amplitude may be sufficiently large to cause ceramic coatings to spall or flake off or even to crack welded joints in the structure (ref. 35).

Liquid filled containers.—When a meteoroid impacts liquid filled tanks, there is more to be concerned with than penetration; the high speed impact results in generation of shock waves in the liquid sufficiently large to effect catastrophic damage. Esgar (ref. 163) reports that firing an aluminum pellet at about 7000 ft/sec (2.12 km/sec) into a small pressurized tank containing water generated pressures well in excess of 100 000 psi. The pressure pulse, of short duration, was localized and resulted initially in local failure.

Zero-gravity studies have indicated that liquid contained in an unbaffled tank will be in contact with the walls and that any gas present will tend to form a pocket in the center of the tank. As a consequence, pressure rise will be generated in the contained liquid for all impacts occurring in space regardless of point of incidence (ref. 164). In addition, fluid temperature is most important because of its effects on material properties of the tank wall. Cryogenic propellants would make the tank walls more susceptible to brittle fracture; liquid oxygen, because of lower compressibility, may present more of a problem than liquid hydrogen (ref. 163). It has been reported that impacting tanks of aluminum or stainless steel containing liquid oxygen with projectiles at velocities up to 7500 ft/sec (2.28 km/sec) resulted in rupture with no burning of tank material due to the presence of the oxygen. When the tank wall was made of titanium alloy (5 Al–2.5Sn) there was a violent reaction. After impact, a series of detonations occurred, and the subsequent burning completely consumed the titanium wall. Therefore, even though titanium may have weight advantages, its use in oxidant tanks is questionable because of its high reactivity (ref. 163).

R. J. Brun, *et al.* (ref. 165) from an analysis of the meteoroid protection needed for various propellant tank configurations, reports that beryllium offers a greater resistance to penetration per unit weight than either aluminum or steel. This conclusion was based on the weight required for a probability of no failure of 0.92 and tank weight required by design for a working pressure of 60 lb/in^2 absolute. High values of specific heat, melting point, and heat of fusion make beryllium preferable over aluminum and steel for protection against meteoroid penetration.

Stepka and Morse (ref. 164) have reported on results of a preliminary investigation directed at obtaining an understanding of the factors affecting catastrophic propellant-tank failure resulting from high-velocity impact. Tank walls, 1/32-inch and 1/16-inch thick, made of 7075–T6 aluminum and

60 percent cold-reduced AISI–301 stainless steel were impacted by spheres of nylon, aluminum, steel, or tungsten carbide ranging from 1/16 to 7/32 inch in diameter; impact velocities ranged from 1650 to 7500 ft/sec (0.5 to 2.28 km/sec). The contained fluids of this experiment were water, glycerin and liquid nitrogen. A summary of the results included:

1. Catastrophic fracturing of specimens rather than simple puncturing occurred when the impact velocity exceeded a critical value, which was dependent on particle size, particle and material density, specimen material and thickness, initial static stress level in the specimen before impact and liquid contained in the tank.

2. Impacts into tanks where the liquid level was only slightly above the impact point resulted in failures similar to those obtained in completely filled tanks.

3. Catastrophic fracturing of gas-pressurized tanks resulted from impacts by low velocity deformable projectiles (nylon spheres) through bending and tearing, rather than from smooth puncturing of tank walls. High velocity impacts by these projectiles into gas-pressurized tanks resulted in smoothly punctured holes and no fracturing.

4. Tank walls of AISI–301 stainless steel, initially stressed to the yield point by contained water, were more resistant to fracture from the additional stresses induced by the impacting particle than walls of 2014–T6 and 7075–T6 aluminum of the same thickness. No fracture of the walls made of the stainless steel were obtained within the range of test variables employed.

5. Effects of compressibility of the contained liquid on fracturing of specimens were found to be small. Only slightly higher impact velocities were required to fracture projectiles on tanks containing glycerine (about one-half as compressible as water) than on tanks filled with water.

6. The combined effects of lower temperature and greater compressibility of liquid on impact velocity required to fracture 7075–T6 aluminum tanks containing nitrogen were small. The resulting fractures, however, were more severe than those obtained on water filled tanks.

7. Pressure pulses generated in the water filled tanks by the impacting particles were large but decayed rapidly and approached ambient pressures within about 5 inches from the point of impact. Pressures in excess of 100 000 psi were generated at approximately 0.6 inch from the impact point.

8. The shock front generated in the water filled tank traveled only a few inches from the point of impact before fracture of the wall occurred. Fractures occurred between 27 and 40 μsec after impact. For the thicknesses of materials investigated, the pressure pulse generated in water and the resulting forces contributing to the initial fracture of tank walls were local phenomena and were independent of tank size of radius greater than a few inches. For further verification, impacts were made into two sizes of water filled tanks whose volumes differed by a ratio of 25; there was no significant effect of tank size.

In a similar investigation, Carter (ref. 166) found that ignition and explosive destruction of simulated 1/32-inch-thick steel-case rocket motors could result from impacts by 3/32-inch-diameter steel spheres traveling at a velocity of approximately 10 900 ft/sec (3.3 km/sec). These tests were performed at an ambient pressure of 0.12 inch Hg.

Perhaps the most vulnerable component of a spacecraft containing a power system which must rid itself of waste heat is the radiator. In the near vacuum of space, convective heat transfer is not possible, and therefore, a large radiator is required to remove the heat. One beneficial characteristic of a space radiator is that it lends itself to being segmented in such a manner that a penetrated segment can be isolated from the rest of the system without disastrous effects. However, preliminary analysis indicates that this component may require shielding involving a greater weight penalty than any other component of the spacecraft.

Lieblein, *et al.* (ref. 167) have reported results of an experimental investigation of hypervelocity impact into typical radiator metals to explore effects of tube material and its temperature, angle of impact, liner thickness and tube size. Spherical glass projectiles were used to impact tubes of niobium-one percent zirconium and cast aluminum with and without HS–25 inner liners at a velocity of approximately 25 000 ft/sec (7.6 km/sec). Spalling and dimpling of tube inner surface in thicknesses substantially greater than that required to prevent perforation occurred; both effects therefore should be considered in tube armor design. Significant differences were observed between impacts into tubes and plates. In general, decreasing the tube size below an outside diameter of about 1.5 inches tended to reduce depth of penetration and spalling, indicating an advantage in using small diameter tubes. Presence of the thin HS-25 liner on the inside of the cast aluminum armor tended to suppress spalling and permit a greater depth of penetration without puncture; considerable dimpling did occur. Other significant results to be considered in radiator design include: (1) variation in depth of penetration appeared to correlate well with the normal component of the impact velocity; (2) increasing depth of penetration with increasing target temperature up to 700° F appeared to correlate well with the variation of modulus of elasticity or Brinell hardness of target material; and (3) depth of penetration in aluminum was in essential agreement with the predictions of two commonly used empirical relations (Loeffler, *et al.*—1962, and Charters and Summers—1958). The depth of penetration in niobium-one percent zirconium, however, appeared to be substantially lower than predicted by these relations.

Various radiator design concepts for maximum protection from meteoroids have been reported in the literature. The interested reader is referred to references 168 to 171.

Hulls.—Spacecraft hulls present a problem to the designer from the standpoint that a complete penetration could, as in the case of a radiator, be disastrous, particularly, in the case of a manned vehicle. For instance, if the

hull of a vehicle were completely penetrated, both explosive decompression and penetrated fragments could cause serious damage to the contents of the vehicle. Also, the detachment of a spall from the inside of the hull, even without complete penetration, constitutes a hazard. Obviously, the structural requirements to protect against such catastrophic impacts to spacecraft hulls should be considered in detail. To insure a high probability of survival for a spacecraft of long duration, this area would demand an untolerable weight based on single plate theory.

Weight savings can be achieved by utilizing the fact that the meteoroid flux is not isotropic in space. In the environment section of this report it has been shown that most meteoroids travel in orbits near the plane of the ecliptic. Also, it appears that the majority of the meteoroids are catching up to Earth (see figure 1). These distributions suggest that the best orientation for a critical portion of a hull is parallel to the plane of the ecliptic with the major axis parallel to the apex of Earth's way (ref. 20). Obviously, it is not possible to orient all vulnerable components in this manner; thus, additional weight saving concepts are mandatory.

Two significant approaches in reducing the weight requirements of vulnerable areas are shields and/or self-sealing devices. The application of both techniques is complex as indicated by the many reports that have been published on this subject. In the application of such weight saving concepts a probability of so many impacts should be computed for each component, since some may be punctured several times before initiating catastrophic failure (ref. 20).

PROTECTIVE CONCEPTS

Shields.—The importance of the shield (or bumper) concept and its attendant weight saving feature is attested by the voluminous publications appearing on the subject in recent years. (For example, see references 20, 36, 79, 102, 109, 115, 131, 145, 146, and 172 to 185.) The underlying concept of the shield is to provide a sacrificial element which would expend the energy associated with an impacting projectile. As has been discussed in the foregoing section of this report, when a plate is penetrated by a hypervelocity projectile an expanding bubble of fragments is produced. Not only are the fragments spread over a large area, but also, the velocity component, normal to the plate, of the many fragments is significantly reduced below the impact velocity of the original projectile. Both of these factors would reduce the effect of a projectile on a target (witness plate) placed behind such a plate since less momentum and energy per unit area would be applied than if the target were not shielded (ref. 20).

Various parameters such as shield material and thickness and distance from the target have been investigated to determine optimum conditions. Results have shown that considerable weight savings can be obtained without sacrificing safety; for the same probability of penetration, weight reductions

of over 50 percent may be expected. The latter statement is, of course, predicated on the assumption that meteoroids can be shattered by shields to the same degree that simulated projectiles have been in the laboratory.

Wallace, *et al.* (refs. 172, 173) investigated shielding of 2024–T4 aluminum (1 inch thick) with stainless type 302, 1100–H4 aluminum and AZ31B–H24 magnesium against normally impacting right circular cylinder projectiles (0.125 and 0.25 inch in both diameter and length) of steel, aluminum and titanium. Velocities ranged from 11 000 to 20 000 ft/sec (3.34 to 6.1 km/sec), shield spacings from 0.25 to 1.0 inch and shield thicknesses from 0.005 to 0.063 inch. With extremely thin shields, low velocity (3.34 km/sec) projectiles did not fragment; penetration increased as shield thickness increased for the thinnest shields. For greater shield thicknesses, projectiles shattered. This effect was not discernible in the higher velocity range so apparently the thinnest shields used shattered the projectiles. The optimum value of $\rho_s h_s / \rho_w h_o$) where ρ_s is shield material density; h_s, depth of shield penetration; ρ_w, wall material density; and h_o, penetration depth by an equivalent impact into an unshielded specimen) decreased with increasing velocity, approaching zero at ultrahigh velocities. The best shield thickness for minimum total penetration (shield plus target) was in the range 0.063 to 0.125 inch; optimum spacing was approximately 0.75 inch; it was suspected that even thinner shields may be optimum for higher impact velocities. Either modulus of elasticity or density was the controlling factor in shield material optimization; among the materials tested, steel appeared to be the best. If modulus of elasticity is the controlling factor, beryllium should be effective for meteoroid shields because of its high modulus and low density (ref. 173). Shield spacing did have an effect on spray angle of the penetrated fragments: crater mouth or pockmarked area on the target tended to remain constant or sometimes increase as shield spacing decreased. This was attributed to the possibility of air trapped beneath the spray and, therefore, should not be expected in vacuum (ref. 173). Many of the thin shields were damaged more than would be expected from the initial impact. A considerable portion of this damage was probably due to particles ejected from the shielded target by impacting fragments which penetrated the shield.

Funkhouser (ref. 184) has reported results from preliminary investigations involving 0.062-inch-diameter copper spheres impacting target-shield systems (both components of 2024–T4 aluminum alloy) at velocities to 12 500 ft/sec (3.8 km/sec). With the shield thickness and spacing held constant at 0.031 and 1.0 inch, respectively, the copper projectiles fragmented on impact with the shield at a velocity between 8000 and 9000 ft/sec (2.43 and 2.73 km/sec), reducing total penetration. With projectile velocity held constant at about 11 500 ft/sec (3.5 km/sec) and shield spacing held constant at 1 inch, a bumper thickness between 0.01 and 0.02 inch gave the best protection against penetration. Increasing the spacing of the 0.031

inch thick shields beyond a distance of 2 inches had little effect on total penetration at an average projectile velocity of 12 200 ft/sec (3.7 km/sec).

The preliminary results of Funkhouser were subsequently verified by Humes (ref. 146) who investigated the shielding effect of a single bumper of 2024—T3 or 2024—T4 aluminum alloy shielding a quasi-infinite wall of 2024—T4 aluminum alloy. In this investigation, shield thickness was varied from 0.010 to 0.250 inch and shield spacing from 0 to 6 inches. The projectiles were 0.062-inch-diameter spheres made of electrolytic tough pitch copper and 0.220-inch-diameter spheres of 2024—T4 aluminum alloy; velocities ranged to 15 000 ft/sec (4.56 km/sec). Results reported by Humes showed that at impact velocities greater than 8000 ft/sec (2.42 km/sec), the projectiles were shattered by the shields into many small fragments, each of which possessed only a small fraction of the initial kinetic energy of the original projectile. In some systems, penetration into the shielded plate increased as impact velocity increased until a maximum total (bumper plus target) penetration was reached at approximately 10 000 ft/sec (3.03 km/sec). The total penetration decreased with further increases in impact velocity. At velocities too low to cause fragmentation of the projectile, the total penetration was independent of shield spacing. At velocities great enough to cause projectile fragmentation (2.42 km/sec), the total penetration decreased with increased shield spacing, up to a point, beyond which further increases had no effect. A shield spacing of greater than eight projectile diameters was required to cause the total penetration to decrease with increasing impact velocities from 9000 ft/sec (2.73 km/sec) to 14 000 ft/sec (4.25 km/sec). A shield thickness of 0.5 times the projectile diameter produced the lowest maximum total penetration and therefore was considered the most effective of those investigated.

Olshaker (ref. 145) reported experimental results from impacting lead and steel projectiles 0.125 inch in diameter into corroding lead (99.9 percent pure) targets shielded by the same material; a velocity of 2.5 km/sec was used. Results of these investigations showed that a shield of thickness slightly less than half the projectile diameter and at a separation distance of about five projectile diameters reduced penetration of shield plus target to approximately one-third the penetration depth in unshielded targets. Only insignificant differences resulted by varying the impacting projectile from steel to lead. This investigation also showed that a shield does not become more effective when divided into two half-thicknesses and placed at the same over-all distance from the primary target.

In reference 20, Maiden summarizes the research performed at General Motors Defense Research Laboratories on shielding by metallic plates. Using 4.8 millimeter spherical projectiles of aluminum, results were obtained on systems consisting of 2024—T3 aluminum shields (0.076 to 3.17 millimeters thick) spaced at 5.48 centimeters from targets of 6.4-millimeter-thick 2024—T3 aluminum sheets; projectile velocity was 6.1 km/sec. With the thinnest

shields (0.076 and 0.204 millimeter), the targets were completely penetrated; with medium thickness shields (0.408 and 0.816 millimeter) a spall was detached, while with the thickest shields (1.632 and 3.170 millimeter), damage resulted only to the front of the targets. A plot of total depth of penetration, including shield thickness but excluding spall effects, shows that there is an optimum shield thickness for minimum damage. For the impact conditions employed by Maiden, this optimum was such that the ratio of shield to projectile weight per unit area was in the approximate range of 0.25 to 0.5. Note that this optimum excludes the effects of spalling. Maiden also reported that providing the impact velocity is above 3 km/sec, the optimum shield thickness is relatively independent of velocity. If this result is generally true, it means that, for a given projectile and target material, the best shield as selected from laboratory tests will be optimum even at extreme meteoroid velocities. Maiden considers this point important enough to warrant further experimental examination.

Maiden (ref. 20) also reported results of tests conducted on shields of magnesium, aluminum, titanium, copper and gold (24 carat) having weights per unit area of 0.113, 0.226 and 0.452 g/cm^2. The projectile, velocity, target, and spacing were the same as in the preceding tests. Results indicated that, for a shield weight of 0.113 g/cm^2, the materials were almost equally effective. However, for the other shield weights, the increasing order of material effectiveness was: magnesium, aluminum, titanium, copper, gold. The peak impact pressure experienced by the shielded target increased with the following order of equal weight shield material: magnesium, aluminum, titanium, copper and gold. Also, for each impact the rarefaction (tension) wave, formed by reflection of the shock from the back of the shield, overtook the shock in the projectile and reduced shield strength. This occurred more quickly as one progressed from equal weight shields of magnesium to gold. Maiden concluded that the best shield material, based on a fixed weight basis, would depend on which of the two effects predominates. The experimental results indicated that for shields of weight 0.113 g/cm^2, the two effects were compensating; however, for greater ratios of shield to projectile weight per unit area, the maximum pressure effect predominated. A plot of the ratio of total depth of penetration to projectile diameter vs. the ratio of shield thickness to projectile diameter indicates that the optimum shield of those tested at General Motors was the 0.15-millimeter-thick gold sheet. This corresponds to a shield to projectile weight per unit area of 0.35. It was noted, that although the two heavier sets of shields became more effective as one progressed from magnesium to gold, the increase was not great.

Maiden (ref. 20) also reported on the effect of velocity on penetration depth from results of tests using the aluminum spherical projectiles impacting 2024–T3 aluminum targets, unprotected and shielded with 0.79 millimeter thick 2024–T3 aluminum plates. At impact velocities up to about 2.5 km/sec, the depth of penetration into the shielded target was slightly more than

penetration into an unprotected target. Apparently, at these velocities, it is easier to perforate the shield than to penetrate an equal distance into the main target. As the velocity was increased from 2.5 km/sec to the maximum, 6.1 km/sec, the shield became more effective.

For impact velocities of 6.1 km/sec, the spread of penetrated fragments decreased and there was less variation in velocity normal to the shield among the fragments for successively thinner shields. As a result, the shields became increasingly ineffective. Riney (ref. 131) also has reported that if the thickness of a shield is less than the radius of the high velocity projectile, the leading central portion of the spallation bubble or penetrating fragments will travel with the velocity of the projectile at impact. This indicates that the use of very thin plates as shields could result in greater damage to the structure being shielded if the spacing between shield and structure is not great enough.

In summary, Maiden states that at impact velocities of 6 km/sec and greater, penetration of a target can be reduced by a factor of about 5 with an optimum shield. Spalling can still occur from the inside wall of the target, however, and this must be accounted for by multiplying the total penetration depth, including bumper thickness, by some factor. Maiden assumed this factor to be 2 and computed that the weight of protective material necessary for typical Lunar or Martian vehicles could be reduced by a factor of 5 through use of an optimum bumper. He suggested that spalling could possibly be reduced by increasing the distance between the bumper and shielded target to allow more space for the penetrating fragments to spread out, since the total depth of penetration remains substantially constant after certain spacing has been obtained. The greater spread of fragments would reduce the momentum and energy per unit area applied to the shielded target, and hence reduce the tendency to spall.

Suggested extensions of the bumper concept of spacecraft protection range from shields with multisheets to combinations of polymeric materials and composites with metallic structures in multiple-wall configurations. The emphasis presently being given polymers results from the successful application of materials such as epoxy resin filament-wound Fiberglas composites in high-performance pressure containers (ref. 181). Single-wall configurations of such composites would still incur severe weight penalities; however, inasmuch as multidirectional orientations of the filaments would minimize crack propagation initiated by meteoroid impact, this characteristic combines with other advantages of filament-wound plastic composites to make them potentially the most promising material for an inner wall of a multiple-wall structure (ref. 181).

The multisheet concept has been investigated by the Nysmith and Summers (ref. 79) using multiple layers of thin 2024–T3 aluminum alclad sheet. Projectiles of small Pyrex glass spheres, representative of stony meteoroids, were fired into the structures at velocities to 11 000 ft/sec (3.34 km/sec). Results

indicated that increasing the number of sheets in a structure while keeping the total thickness constant and increasing the spacing between sheets tended to increase the penetration resistance of a structure of constant weight per unit area. The suggestion by Wallace (ref. 180) that foamed metals placed between shield and target should be beneficial was somewhat verified by Nysmith and Summers who used glass-wool between layers of the thin multisheet structures. The filler was found to increase penetration resistance substantially with a small increase in weight. This effect of filler on relatively low velocity impacts is important in light of the results reported by Wallace, *et al.* (refs. 172 and 173) on the shielding effectiveness of thin sheets impacted with projectiles traveling at the same velocity (3.34 km/sec). As mentioned earlier, they found that a 3.34 km/sec projectile did not fragment on penetration of 0.005-inch thick shields and that this resulted in more damage to the shielded plate than the plate would have received had it not been protected. It appears, then, that the use of a lightweight filler would maintain the weight-saving feature of thin shields which are capable of shattering particles at higher velocities.

Pipitone and Reynolds (ref. 182) have investigated several meteoroid protection systems utilizing combinations of both homogeneous and heterogeneous materials. These investigators considered single, double and triple wall configurations, with and without polymeric foam spacers. The specimens were impacted with spherical projectiles of Pyrex (0.063-inch diameter) and steel (0.042-inch diameter) traveling at velocities of approximately 16.5 to 21.9 km/sec. For the double wall configuration, the outer wall served as a bumper to fragment the penetrating projectile, the spacer positioned the outer wall and served to arrest and absorb the shattered, impacting fragments; the inner wall served as the gas retaining structural wall of a spacecraft. For the triple wall configuration, a spacer was included between each wall. Results of the tests showed that, without a bumper, the penetration resistance of polyurethane foam spacers (density 1.2 lb/ft^3) to Pyrex projectiles with velocities of 21 900 ft/sec (6.7 km/sec) was comparable to, or better than, the resistance of equal weight aluminum structures. The foam spacer exhibited an efficiency by weight of 15.7 times that of a single aluminum wall. Both rigid and flexible foam spacers tended to absorb and arrest impacting fragments through vaporization. When foam spacers were not used, aluminum structural walls sustained greater damage than equivalent walls of Dacron-Neoprene fabric when impacted with Pyrex projectiles traveling at 20 000 ft/sec (6.1 km/sec). Both aluminum sheet and a Fiberglas-silicone composite bumper were superior to an equal-weight panel of crushed aluminum honeycomb against 20 000 ft/sec (6.1 km/sec) Pyrex projectiles. Failures observed about impact holes for some materials indicated that bumpers should be made of homogeneous materials or of high temperature composites.

Another advantage associated with the use of polymeric materials in pro-

tective concepts is their applicability to foldable or expandable structures. Samples of a composite for such applications have been constructed of a butyl rubber elastomer and Dacron cords. A 0.1 inch thick specimen of this composite with approximately 65 percent elastomer was reported to have a miximum tensile strength of 1800 lb/in.^{2} and to be easily foldable (ref. 176). Such composites are particularly applicable in shielding inflatable structures from micrometeoroids.

Results of specific investigations of hypervelocity impact damage to nonmetallic materials is meager; however, some insight can be gained from those reported by Kinard and Collins (ref. 175). These investigators impacted Bakelite (phenolic) laminate, graphite, nylon and 2024–T4 aluminum targets with projectiles of copper, lead, steel and nylon traveling at velocities from 500 to 20 000 ft/sec (0.15 to 6.1 km/sec). The projectiles were right circular cylinders, cone cylinders, and spheres. Results indicated that the same projectile and target properties govern penetration in both metallic and nonmetallic materials throughout the velocity range investigated. The physical appearance of craters was found to be very different in metallic and nonmetallic target materials. Craters formed in nonmetallic targets were slender, partially filled cavities while those formed in the aluminum targets were the usual open hemispherical cavities.

Self-sealing structures.—The application of self-sealing structures to reduce the hazards of meteoroid perforation is a relatively new approach, but considerable effort has been expended toward its realization. Design concepts may, in general, be classified as mechanical or chemical, depending on the mode of activating the sealing process. A variety of configurations, primarily variations of sandwich-honeycomb core structures, applying the concepts have been successfully tested in the laboratory (refs. 186, 187, 188, and 190).

A highly effective mechanical approach has been to prestress the elastomeric sealant in compression. This technique, which utilizes the recovery of sealant material to achieve the closure, has been very successful for extremely localized damage. Materials for this application should have appropriate thermal and vacuum properties and low shear strength characteristics under dynamic conditions when simply confined (ref. 20). Another prestressing technique uses an elastomer and foaming reagent which causes an unconfined volume expansion of 200 to 300 percent upon curing. The sandwich-honeycomb core panel is filled with the uncured sealant compound to a volume fraction which would produce the desired prestress level; the sealant is then cured at the required temperature. Bonding of panel face plate should be accomplished with a material whose softening point is above the cure temperatures of the sealant. This latter technique has shown successful sealing characteristics with a high degree of reliability. It is possible that under certain environmental conditions and with massive face sheet and sealant damage or tearout, macromotion of sealant into the perforated zone will be required. For this reason, the elastomeric sphere concept was initiated. In this approach, the

conventional sealant is replaced by discrete elastomeric spheres to a predetermined packing density. Upon penetration, the pressure differential between the inside cabin and the vacuum of space forces the spheres toward the entrant hole and effects the sealing. Sphere size, packing density, and material will control the mobility of the spheres and the sealability. This concept has exhibited residual leakage rates comparable with the mechanical system employing sealant recovery as the mechanism of sealing (ref. 188).

Chemical concepts rely on the dynamic action of the penetrating particle to initiate a reaction which closes the hole. In one concept, an uncured polymer is separated from the catalyst by a thin, nonreactive membrane. Upon complete perforation, the pressure differential across the sandwich panel forces a mixture of polymer and catalyst through the hole. Extremely fast curing mixtures have been used with complete and repeatable sealing action. In another technique, small bags of catalyst are interspersed in the sealant void to localize curing action to the area of penetration; catalyst bag size is an important factor in this method. For uniform distribution of the catalyst in the uncured elastomer, microencapsulation techniques could be adopted. In all chemical concepts where the sealant materials are initially fluid, careful attention must be given to the rheological or flow properties of the polymer. The viscosity of the material must be such as to permit an initial gradual flow through the hole without excessive loss. Cure rate must obviously be rapid enough to "set up" the material in the hole. Environmental stability must be carefully considered against mission time, as degradation can severely alter flow rates and, hence, sealability (ref. 188).

Typical self-sealing configurations being investigated consist of metallic or polymeric composite facings separated from an elastomer-reinforced back-up plate by a honeycomb core of polymeric and/or metallic material or various sections as necessary to combine multiple concepts. For example, a section of foamed elastomer could be used with a section containing elastomeric spheres or encapsulating bags (refs. 186, 188, and 190). The function of the honeycomb core is to contain the sealant and provide damage confinement through the addition of bonding surfaces in the sealant volume. Tuckerman, *et al.* (ref. 186) have reported: the sealing material should be elastomeric and have cohesive strength high enough to resist tearing but low enough for collapse into the puncture under the pressure differential; the confining structure for the sealant should have a cell form with a low shear modulus but a high tear strength; unoriented fabric-reinforced elastomers seem best for the back-up sheets; and elastomeric adhesives appear best for bonding the sealing structure to the vehicle structure. Optimization in materials selection has not been reached, however.

Piechocki (ref. 20) reported that impacting 0.125-inch diameter steel spheres at a velocity of 20 000 ft/sec (6.1 km/sec) into specimens with aluminum honeycomb cores resulted in massive damage. Radial collapse of cell walls as much as 12 times the projectile diameter, with attendant sealant

damage, was observed. The use of phenolic Fiberglas core, with attention to maintaining good core-to-sealant bonding, greatly alleviated the damage. Subsequent firings resulted in little or no core damage and localized puncturing was achieved. Control of reflected rear face shock wave was reported by D'Anna, *et al.* (ref. 190) to be essential to obtain effective sealing, particularly in the chemically activated self-sealing panel configurations. In a study of techniques to achieve this, Piechocki (ref. 188) substituted Neoprene for the metallic back plate of a panel and received immediate improvement marked by decreased deformation of back-up sheet and adjacent sealant. The resiliency of the Neoprene permitted recovery from radial deformations due to the passage of the particle and enhanced hole closure. On the same subject, Gatzek and Isenberg (ref. 181) have reported that a honeycomb confining structure of low modulus but high tear strength (for example, phenolic-Fiberglas) for the sealant appears most effective in confining the shock wave.

Average leakage rates of configurations investigated by Piechocki (ref. 188) were reported to be on the order of 1 to 2 lb/day for a pressure differential of 14.7 psi; however, zero leakage was obtained for some designs. In many instances, specimens with a detectable leak across a 14.7 psi pressure differential exhibited almost complete sealing at a 4 to 5 psi differential. The above rates were obtained after the specimens were punctured with 0.125-inch diameter steel spheres traveling at a speed of 10 000 to 20 000 ft/sec (3.04 to 6.1 km/sec).

PROBABILITY OF PERFORATION

Essentially the only calculations of the probability for perforation of space vehicles based on the 1963 estimates of the environments have been presented by Whipple (ref. 37). The penetration law applied in the analysis was that of Herrmann and Jones (ref. 112) in the form:

$$p/d = 0.6\, K_o^{2/3} \ln (1 + K_o^{2/3}\, B/4) \text{ (cgs units)} \qquad (57)$$

where p is penetration depth; d, projectile dimension; K_o, ratio of meteoroid density to target density (ρ/ρ_t); and B, the "Best Number," is $\rho_t v^2/H$ (where v is impact velocity and H is Brinell hardness). Whipple modified the above equation to express penetration in terms of mass with an assumed meteoroid density, so that for spherical particles:

$$p = 0.6\, [6m\rho/\pi\rho_t^2]^{1/3}\, [\ln \{1 + (K_o^{2/3}\, B/4)\}] \text{ (cgs units)} \qquad (58)$$

The analysis was demonstrated for a near Earth vehicle with an aluminum skin 0.1-centimeter thick. Meteoroid velocity was assumed to be 22 km/sec, and meteoroid density was assumed to be 0.44 g/cm^3. A limiting mass of 1.4×10^{-4} gram was computed from equation (58) and a corresponding cumulative influx rate of 5×10^{-10} particles/m^2-sec was determined with equation (32). The average time to perforation of a 3 meter diameter sphere was found to be 2.3 years. For an influx rate according to equation (33), the corresponding average time to perforation was 8.7 years. To obtain probabilities Whipple used the commonly applied relation $P/p = 1.5$, where

P is the perforation thickness (ballistic limit), and p is penetration depth (see the discussion of ballistic limits which indicates that this ratio may have values considerably greater than 1.5).

In summary of the analysis based on equations (32) and (58), Whipple presents a "best estimate" of the number of meteoroids, N, (per m^2/sec) moving randomly in space and just able to perforate a thin aluminum skin of thickness P, to be:

$$\log_{10} N = -4.02 \log_{10} P - 13.33 \quad \text{"best estimate"} \qquad (59)$$

To determine a "pessimistic estimate," the perforation thickness was increased by a factor of 2 over that from equation (58) and combined with the rate of influx from equation (32) to give:

$$\log_{10} N = -402 \log_{10} P - 12.12 \quad \text{"pessimistic estimate"} \qquad (60)$$

An "optimistic estimate" for smaller thicknesses was obtained from equation (58) and the influx rate from equation (33):

$$\log_{10} N = -3 \log_{10} P - 12.94 \quad \text{"optimistic estimate"} \qquad (61)$$

Since his adopted influx rate, equation (32), extrapolates so well to the data obtained by Alexander, *et al.* (ref. 50) from space vehicles near Earth (see figure 7), Whipple continued his "best estimate" without change for micrometeoroids near Earth. Whipple concedes that, since the smaller particles are probably in orbit about Earth, his adopted velocity of encounter (22 km/sec) is too high and that this continuation is undoubtedly rather pessi-

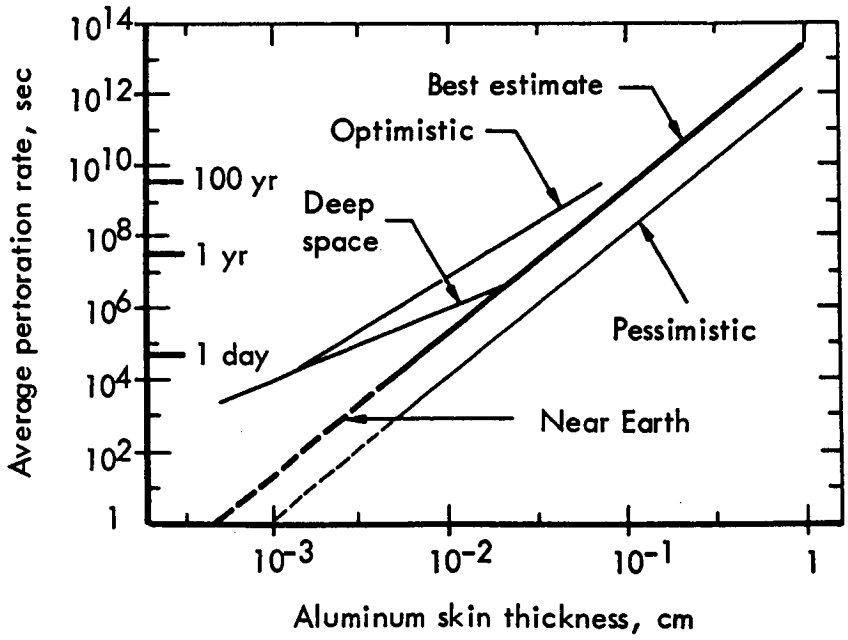

Figure 15.—Meteoroid perforation of aluminum skin in space.

mistic. For a body in deep space, perhaps more than 5×10^4 to 2×10^5 kilometers from Earth, Whipple combined Van de Hulst's influx equation ($\log_{10} N = -0.65 \log_{10} m - 10.44$) with equation (58) to obtain the following "deep space estimate":

$$\log_{10} N = -1.94 \log_{10} P - 9.88 \quad \text{"deep space estimate"} \qquad (62)$$

Figure 15 (ref. 37), presents the results of calculations of skin perforation in space for 2024 aluminum according to equations (59), (60), (61) and (62). The figure plots average time to perforation in seconds vs. thickness of aluminum. (Whipple stated that the equivalent times for steel should be increased by about a factor of 10.) It can be seen that the "optimistic" curve meets the "best estimate" curve at a relatively large skin thickness and, beyond the dust belt, meets the "deep space" curve at a relatively small skin thickness. Uncertainties of the curves were considered to be possibly an order of magnitude, particularly for the smaller masses. Whipple compared his results with those obtained from Explorer XVI (refs. 58 and 60) and obtained agreement within an order of magnitude.

The error introduced by the uncertainty in meteoroid density, ρ, affects both influx, N, and the mass as a function of perforation, P. From equations (32) and (58) and the adopted value of P/p, neglecting the logarithmic term in equation (58), Whipple obtained the proportionality:

$$N \propto P^{-4.02} (.044/\rho)^{1.34} \qquad (63)$$

from which it can be seen that the number of particles perforating a thin skin decreases only as $\rho^{1.34}$ when ρ is increased with respect to the adopted value of 0.44 g/cm^3. Equations (59) and (60) can be corrected readily by equation (63) for a different value of meteoroid density.

Concluding Remarks

A summary of information on meteoroid environment has considered in detail the properties and distribution of space debris as determined from: terrestrial observation of meteors; direct measurements by space vehicles; zodiacal light studies; and analyses of terrestrially accreted dust. Reported items of particular significance include: establishment by Hawkins and Upton of a cumulative influx law for photographic meteors inversely dependent on meteor mass to the 1.34 power; and adoption of a density of 0.44 g/cm^3 by Whipple for a zero magnitude meteor with a velocity of 30 km/sec.

The recent literature concerning hypervelocity impact phenomena, cratering, perforation and spalling, was summarized. A brief account was also included of the ionization phenomena attendant to hypervelocity impact. Realistic evaluation of the applicability of the work reviewed in this report to the meteoroid hazard problem is seriously hampered by present limitations of velocity, instrumentation, and control in experimental studies. Extrapolations of data, particularly into much higher velocity ranges, give results of questionable validity and several investigators have repeatedly warned against such practice. However, it is seen that, due to the lack of more appropriate data, extrapolations are employed in attempts to demonstrate applicability of various theories and to estimate the damage which may occur to surfaces and structures exposed in the space environment.

The review of protective design considerations included weight reduction techniques, particularly the shield or bumper concept and self-sealing structures, and probabilities of perforation. Thin metallic shields have been consistently demonstrated to dissipate the energy associated with the impacting projectiles in the laboratory; however, the question remains as to whether meteoroids will react with such structures in the same manner. Weight savings exceeding those provided by metallic shields have been obtained through use of polymeric composites; however, a considerable weight penalty remains. Self-sealing structures have been proven in their capabilities, but optimization of material selection and design configuration for space vehicles has not been obtained. Recent revisions to estimates of the meteoroid environment and penetration due to hypervelocity impact have caused a considerable reduction in the calculated probabilities for perforation.

References

1. Whipple, Fred L.; and Hawkins, Gerald S.: Meteors. Handbuch der Physik, Bd. LII, Astrophysik III; Das Sonnensystem (S. Flügge, ed.), Springer (Berlin), 1959, pp. 519–564.
2. McKinley, David: Meteor Science and Engineering. McGraw-Hill Co. Inc., 1961.
3. Eiwen, Charles J.; and Winer, David E.: Criteria for Environmental Analysis of Weapon Systems. (American Machine & Foundry Co., New York, N.Y.). U.S. Wright Air Development Division. WADD Tech. Rep. 60–627, Aug. 1960.
4. Winer, David E.: A Review of Extraterrestrial Matter Proc. Inst. Environmental Sciences, Apr. 1961. pp. 455–464.
5. Davison, Elmer H.; and Winslow, Paul C., Jr.: Space Debris Hazard Evaluation. NASA TN D–1105, 1961.
6. Shaw, J. H.: Natural Environment of Interplanetary Space. (Ohio State University Research Foundation). WADD Phase TN 4; Contract AF–33(616)–5914; ASTIA Doc. AD–25023, Jan. 1960.
7. Beard, David B.; Comets and Cometary Debris in the Solar System. Revs. Geophysics vol. 1, May 1963, pp. 211–219.
8. Davidson, John R.; and Sandorff, Paul E.: Environmental Problems of Space Flight Structures. II. Meteoroid Hazard. NASA TN D–1493, 1963.
9. Dauvillier, A.: Cosmic Dust. George Newnes (London), 1963.
10. Hopkins, Alan K. Because a Marble-size Meteroid Will Wreck A Spacecraft . . . You Don't Worry About the Big Ones. Machine Design, vol. 34, no. 23, Sept. 1962, pp. 142–145.
11. Gehrels, T.: Observations of Asteroids. *In* Proceedings of Lunar and Planetary Exploration Colloquium. North American Aviation, Inc., Space & Information Systems Division, Downey, California, vol. 2, no. 4, Nov. 1961.
12. Whipple, Fred L.: Dust and Meteorites. (Smithsonian Institution, Astrophysical Observatory, Cambridge, Mass.) Astronautics, vol. 7, no. 8, Aug. 1962, pp. 40–42.
13. Volkoff, John J.: Protection Requirements for the Resistance of Meteoroid Penetration Damage of Interplanetary Spacecraft Systems. California Institute of Technology, Paiadena Jet Propulsion Laboratory, Tech. Rept. no. 32–410, July 1964.
14. Briggs, Robert E.: Steady-State Space Distribution of Meteoric Particles Under the Operation of the Poynting-Robertson Effect. (Smithsonian Astrophysical Observatory, Cambridge, Mass.) Astronomical J., vol. 67, no. 10, Dec. 1962, pp. 710–723.
15. McMinn, William O.: Dynamical Effects of Solar Electromagnetic Radiation on Interplanetary Matter. (American Machine & Foundry Co., New York, N. Y.). Inst. Environmental Sciences, Proc., Apr. 1961, pp. 451–454.
16. Whipple, Fred L.: The Meteoritic Risk to Space Vehicles. Vistas in Astronautics, vol. I. Pergamon (New York), 1958, pp. 115–124.
17. Black, Sydney D.: Space-Debris Hazards of Interplanetary Exploration. J. Spacecraft and Rockets, vol. 1, May-June 1964, pp. 317–332.
18. Best, G. T.: The Acoretion of Meteoritic Material by the Earth. (Queen's University, Belfast, Ireland). Space Research. First International Space Science Symposium, Proc., (Hilde Kallmann Bijl, ed.) 1960, pp. 1023–1032.

19. CAMPEN, C. F., JR., ET AL.: Handbook of Geophysics for Air Force Designers. First Ed. Geophysics Research Directorate, Air Force Cambridge Research Center, Air Research and Development Command. 1957.

20. MAIDEN, C. J.: Meteoroid Impact. Defense Research Laboratories, Santa Barbara, Calif. TM–63–203; DDC Doc. AD–406169. Apr. 1963.

21. MCCRACKEN, CURTIS W.: Acoustic Detection of Meteoric Particles, vol. II, appendix B. An Analysis of Rocket and Earth Satellite Measurements of Micrometeoric Influx. (Oklahoma State University, Stillwater). U.S. Air Force Cambridge Research Center, Geophysics Research Directorate, AF Report AFCRC–TR–60–272; ASTIA Doc. AD–240260.

22. ÖPIK, E. J.: The Masses and Structures of Meteors. Meteors (A Symposium on Meteor Physics, T. R. Kaiser, ed), Pergamon (London) 1955, pp. 33–35.

23. GOETTELMAN, R. C.; SOFTKY, S. D.; ARNOLD, J. S.; AND FARRAND, W. B.: The Meteoroid and Cosmic-Ray Environment of Space Vehicles and Techniques for Measuring Parameters Affecting Them. (Stanford Research Institute, Menlo Park, Calif.) U.S. Wright Air Development Division, WADD Tech. Rept. 60–46; ASTIA Doc. AD–262013, Feb. 1961.

24. HAWKINS, GERALD S.; AND UPTON, EDWARD K. L.: The Influx Rate of Meteors in the Earth's Atmosphere. Astrophysics J., vol. 128, Nov. 1958, 727–735.

25. EVANS, S.; AND HALL, J. E.: Meteor Ionizing and Luminous Efficiencies. Meteors (A Symposium on Meteor Physics, T. R. Kaiser, ed.), Pergamon (London), 1955. pp. 18–22.

26. KAISER, T. R.: The Interpretation of Radio Echoes from Meteor Trails. Meteors (A Symposium on Meteor Physics, T. R. Kaiser, ed.), Pergamon (London), 1955, pp. 55–64.

27. HAWKINS, GERALD S.; AND SOUTHWORTH, RICHARD B.: The Physical Characteristics of Meteors. NASA CR–51366, July 1963.

28. HAWKINS, GERALD S.; AND SOUTHWORTH, RICHARD B.: The Statistics of Meteors in the Earth's Atmosphere. Smithsonian Contrib. Astrophys., vol. 2, no. 11, 1958, pp. 349–364.

29. KALLMANN, H. K.: Relationship Between Masses and Visual Magnitudes of Meteors. Meteors (A Symposium on Meteor Physics, T. R. Kaiser, ed.), Pergamon (London), 1955, pp. 43–54.

30. MCCOY, T. M.: Hyperenvironment Simulation. Part I. Definition and Effects of Space Vehicle Environment Natural and Induced. (Northrop Corp., Hawthorne, Calif., Norair Div.). U.S. Wright Air Development Division, WADD Tech. Rept. 60–785, Jan. 1961.

31. HAWKINS, GERALD S.: The Meteor Population. NASA CR–51365, Aug. 1963.

32. DAVISON, ELMER H.; AND WINSLOW, PAUL C., JR.: Direct Evaluation of Meteoroid Hazard. Aerospace Eng., vol. 21, no. 2, Feb. 1962, pp. 24–33.

33. JAFFE, L. D.; AND RITTENHOUSE, J. B.: Behavior of Materials in Space Environments. California Institute of Technology, Pasadena, Jet Propulsion Laboratory. JPL Tech. Rept. 32–150; ASTIA Doc. AD–266548, Nov. 1961.

34. HOPKINS, ALAN K.: Meteoretics and Hypervelocity Studies. Aeronautical Systems Division, Wright-Patterson Air Force Base, Ohio, ASD Tech. Rept. 61–322, July 1961, pp. 152–170.

35. HOPKINS, ALAN K.: The Meteoroid Hazard and Its Simulation. Symposium on Effects of Space Environment on Materials. (National Symposium, Soc. of Aerospace Material & Process Engineers, St. Louis, May 7–9, 1962).

36. KORNHAUSER, M.: Structural Effects of Impact. Spartan Books, Baltimore. 1964.

37. WHIPPLE, FRED L.: On Meteoroids and Penetration. (Smithsonian Astrophysical Observatory, Cambridge, Mass.). J. Geophys. Res., vol. 68, Sept. 1963, pp. 4929–4939.

38. Hawkins, Gerald S.; Lindblad, Bertil-Anders; and Southworth, Richard B The Velocity of Faint Meteors. NASA CR–51346, June 1963.

39. Whipple, Fred L.: On the Velocities and Orbits of Meteors, Fireballs, and Meteorites. Meteors (A Symposium on Meteor Physics, T. R. Kaiser, ed.), Pergamon (London), 1955, pp. 149–156.

40. Millman, Peter M.: Survey of Observations of Meteor Trails. (National Research Council, Canada. Radio & Electrical Engineering Division). AIAA J., vol. 1, May 1963, pp. 1028–1033.

41. Livingston, W. A., Jr.: Outer-Space Environment Models for Use With Space Vehicle Simulators. (Cornell Aeronautical Lab., Inc., Buffalo, N. Y.). Aerospace Medical Research Labs., Wright-Patterson Air Force Base, Ohio. AF Tech. Doc. Rept. 62–40, May 1962.

42. Dalton, Charles C.: Estimation of Tolerance Limits for Meteoroid Hazard to Space Vehicles 100–500 Kilometers Above the Surface of the Earth. NASA TN D–1996, 1964.

43. Halliday, Ian: The Spectrum of an Asteroidal Meteor Fragment, Canada, Dominion Observatory, Ottawa. Astrophys. J., vol. 132, Sept. 1960, pp. 482–485.

44. O'Keefe, J. A.: The Origin of Tektites NASA TN D–490, 1960.

45. Verniani, Franco:On Meteor Ablation in the Atmosphere. (Centro di Studio per la Fisica Delle Microonde, Firenze. Consiglio Nazionale Dele Ricerche). Contract AF–61 (052)–227, Tech. Note N. 4; ASTIA Doc. AD–243569, Mar. 1960.

46. Whipple, Fred L.: On Meteoroids and Penetration (Smithsonian Astrophysical Observatory, Cambridge, Mass.). J. Astron. Sci., vol. 10, 1963, pp. 92–94.

47. Kaiser, T. R.: Meteors and the Abundance of Interplanetary Matter. Space Sci. Revs., vol. 1, Mar. 1963, pp. 554–575.

48. Weiss, A. A.: The Distribution of Meteor Masses for Sporadic Meteors and Three Showers. (Australia. Commonwealth Scientific & Industrial Research Organization, Div. of Radiophysics, Chippendale). Australian J. Phys. 14:102–119, Mar. 1961.

49. Alexander, W. M.; McCracken, C. W.; Secretan, L.; and Berg, O. E.: Rocket Satellite, and Space-Probe Measurements of Interplanetary Dust. (Presented at the Third International Space Science Symposium of the Committee on Space Research (COSPAR), Washington, D. C., May 1962). IGY Bulletin No. 61:7–16, July 1962.

50. Alexander, W. M., et al.: Review of Direct Measurements of Interplanetary Dust from Satellites and Probes. (Goddard Space Flight Center, NASA). (Paper presented at the COSPAR Meeting, May 1962). NASA Preprint X–613–62–25.

51. McCracken, C. W.; Alexander, W. M.; and Dubin, M.: Direct Measurements of Dust Particles in the Vicinity of Earth. NASA TN D–1174, 1961.

52. LaGow, H. E.; and Alexander, W. M.: Recent Direct Measurements by Satellites of Cosmic Dust in the Vicinity of the Earth. NASA TN D–488, 1960.

53. Alexander, W. M.; McCracken, C. W.; and Secretan, L.: Micrometeoroid Impact Damage. (Goddard Space Flight Center, NASA). Bulletin 30. Shock, Vibration & Associated Environments, part V, May 1962, pp. 92–96.

54. Alexander, W. M.: Interplanetary Dust. (Goddard Space Flight Center, NASA). Am. Geophys. Union, Trans. 44:464–469, June 1963. (U.S. National Report 1960–1963, Thirteenth General Assembly, International Union of Geodesy & Geophysics.)

55. Dubin, Maurice; and McCracken, Curtis W.: Measurements of Distributions of Interplanetary Dust. Astronomical J., vol. 67, no. 5, June 1962, pp. 248–256. (Presented at the Symposium on Small Meteoric Particles in the Earth's Neighborhood, 110th Meeting of the American Astronomical Society, Cambridge, Mass., Apr. 2, 1962.)

56. McCracken, C. W.; Alexander, W. M.; and Dubin, M.: Direct Measurement of Interplanetary Dust Particles in the Vicinity of Earth. Nature, vol. 192, Nov. 1961, pp. 441–442.

57. U.S. Air Force Cambridge Research Laboratories, Geophysics Research Directorate: Proceedings of the Symposium on the Astronomy and Physics of Meteors. Geophysical Research Papers No. 75, Research Rept. 62–497. (Held at Smithsonian Astrophysical Observatory, Cambridge, Mass., 28 Aug.–1 Sept. 1961.)

58. D'Aiutolo, Charles T.: First Meteoroid-Penetration Data for Snap Designers. Nucleonics, vol. 21, no. 11, Nov. 1963, pp. 51–55.

59. First Results From the Explorer XVI Micrometeoroid Satellite. IG Bulletin No. 7, Apr. 1963, pp. 648–652.

60. Hastings, Earl C., Jr.: The Explorer XVI Micrometeoroid Satellite Description and Preliminary Results for the Period December 16, 1962, through January 13, 1963. NASA TM X–810, Feb. 1963.

61. Dubin, Maurice: IGY Micrometeorite Measurements. U.S. Air Force Cambridge Research Center. Space Research. First International Space Science Symposium, Proc., (Hilde Kallman Bijl, ed.), 1960, pp. 1042–1058.

62. Dubin, Maurice: Meteoritic Dust Measured from Explorer I. Planetary & Space Sci., vol. 2, 1960, pp. 121–129.

63. Dubin, M.; Alexander, W. M.; and Berg, O. E.: Cosmic Dust Showers by Direct Measurements. *In* Proceedings of the Symposium on the Astronomy and Physics of Meteors, pp. 109–114. (Held at Smithsonian Astrophysical Observatory, Cambridge, Mass. 28 Aug.–1 Sept. 1961.)

64. Alexander, W. M.; and Berg, O. E.: Microparticle Hypervelocity Impacts From Ranger I. *In* Fifth Symposium on Hypervelocity Impact, Proc., vol. 1, part 2, Apr. 1962, pp. 645–651.

65. Soberman, R. K.; and Della Lucca, L.: Micrometeorite Measurements from the Midas II Satellite (1960 ζ 1). U.S. Air Force Cambridge Research Labs. Geophysics Research Directorate AF Report AFCRL–1053; GRD Research Notes 72, Nov. 1961.

66. McCracken, C. W.; and Alexander, W. M.: The Distribution of Small Interplanetary Dust Particles in the Vicinity of Earth. *In* Proceedings of the Symposium on the Astronomy and Physics of Meteors, pp. 71–83. (Held at Smithsonian Astrophysical Observatory, Cambridge, Mass., 28 Aug.–1 Sept., 1961.)

67. Buck, Richard F.: Acoustic Detection of Meteoric Particles. U.S. Air Force Cambridge Research Center. Geophysics Research Directorate. AF Report AFCRC–TR–60–272; ASTIA Doc. AD–240259, Apr. 1960.

68. Nazarova, T. N.: The Results of Studies of Meteoric Dust by Means of Sputnik III and Space Rockets. Space Research. First International Space Science Symposium, Proc., (Hilde Kallmann Bijl, ed.), 1960, pp. 1059–1062.

69. Nazarova, T. N.: Investigations of Meteoric Dust by Means of Rockets and Artifical Earth Satellites (in Russian.) Iskusstvennyye Sputniki Zemli, no. 12, 1962, pp. 141–144.

70. Brayshaw, J. M.: Mars Atmosphere Entry Parametric Study. California Institute of Technology, Jet Propulsion Laboratory. Tech. Rept. 32–458, Sept. 1963.

71. Nazarova, T. N.: Results of Investigation of the Meteoric Matter by Means of Instruments Installed on Cosmic Rockets. ARS J. vol. 31, May 1961, pp. 713–714.

72. Krassovsky, V. I.: Some Geophysical and Astronomical Aspects of Soviet Space Research Academy of Science of the USSR. Institute of Atmospheric Physics. Endeavour, vol. 21, Apr. 1962, pp. 65–72.

73. Aleksandrov, S. G.; and Federov, R. Ye.: Soviet Satellites and Space Ships (Selected Articles). U.S. Wright-Patterson Air Force Base, Ohio. Foreign Technology Division. AF Translation FTD–TT–62–121/1+2; ASTIA Doc. AD–273888 (Feb. 1962). (Source: Sovetskiye Sputniki i Kosmicheskiye Korabli, 2nd ed., Moscow 1961, Akademiya Nauk SSSR, pp. 24–82, 117–124, 144–147, 182–184, 217–242, 256–394, 427–456.)

74. New, J. C.: Scientific Satellites and the Space Environment. (U.S. Office of the Secretary of Defense. Research and Engineering. Bulletin 30, pp. 75–91). May 1962. *In* Shock, Vibration and Associated Environments, part V.

75. Friichtenicht, J. F.: Two-Million-Volt Electrostatic Accelerator for Hypervelocity Research. (Space Technology Lab., Inc., Canoga Park, Calif.). Rev. Sci. Instruments, vol. 33, Feb. 1962, pp. 209–212.

76. Soberman, R. K., et. al.: Micrometeorite Collection From A Recoverable Sounding Rocket. U.S. Air Force Cambridge Research Labs. Geophysics Research Directorate. AF Report AFCRL–1049; GRD Research Notes 71, Nov. 1961.

77. Juno II Summary Project Report. Volume I. Explorer VII Satellite. NASA TN D–608. 1961.

78. LaGow, H. E.; and Secretan, L.: Results of Micrometeoroite Penetration Experiment on the Explorer VII Satellite (1959 IOTA). NASA TN D–1722, 1963.

79. Nysmith, C. Robert; and Summers, James L.: Preliminary Investigation of Impact on Multiple-Sheet Structures and An Evaluation of the Meteoroid Hazard To Space Vehicles. NASA TN D–1039, 1961.

80. Anon.: Explorer XVI, the Micrometeoroid Satellite. NASA Facts (A–1–63). 1963.

81. Alexander, W. M.; McCracken, C. W.; and LaGow, H. E.: Interplanetary Dust Particles of Micro-Size Probably Associated With the Leonid Meteor Stream. (Goddard Space Flight Center, NASA) J. Geophys. Res., vol. 66, Nov. 1961, pp. 3970–3973.

82. Dubin, M.; Alexander, W. M.; and Berg, O. E.: Direct Measurements of Cosmic Dust Showers. NASA TN D–1544. Jan. 1963.

83. Beard, David B.: Interplanetary Dust Distribution and Erosion Effects, *In* First Symposium: Surface Effects on Spacecraft Materials. John Wiley & Sons, Inc., 1960. pp. 378–390.

84. Ingham, M. F.: Interplanetary Matter. Space Sci. Revs., vol. 1, Mar. 1963, pp. 576–588.

85. Laevastu, Taivo; and Mellis, Otto: Size and Mass Distribution of Cosmic Dust. J. Geophys. Res., vol. 66, Aug. 1961, pp. 2507–2508.

86. Crozier, W. D.: Micrometeorite Measurements-Satellite and Ground-Level Data Compared. J. Geophys. Res., vol. 66, Sept. 1961, pp. 2793–2795.

87. Hodge, Paul W.: Sampling Dust from the Stratosphere. Smithsonian Institution, Astrophysical Observatory, Cambridge, Mass., Smithsonian Contributions to Astrophysics, vol. 5, no. 10, 1961.

88. Parkin, D. W.; Hunter, W.; and Brownlow, A. E.: Metallic Cosmic Dust With Amorphous Attachments. Nature, vol. 193, Feb. 1962, pp. 639–642.

89. Wright, F. W.; and Hodge, P. W.: Space Density of Dust in the Stratosphere. Smithsonian Astrophysical Observatory, Cambridge, Mass. Nature, vol. 195, July 1962, p. 269.

90. Wasson, John T.: Radioactivity in Interplanetary Dust. U.S. Air Force Cambridge Research Labs. Icarus, vol. 2, June 1963, pp. 54–87.

91. Wright, Frances W.; Hodge, Paul W., and Chester C. Longway, Jr.: Studies of Particles for Extraterrestrial Origin. 1. Chemical Analyses of 118 Particles. J. Geophys. Res, vol. 68, Oct. 1963, pp. 5575–5587.

92. Schmidt, Richard A.: A Survey of Data on Microscopic Extraterrestrial Particles. University of Wisconsin, Geophysical & Polar Research Center. Research Report Series No. 63–2, Jan. 1963.

93. Fremlin, J. H.; Beard, David B.; and Whipple, Fred L.: The Dust Cloud About the Earth. Nature, vol. 191, July 1961, pp. 31–34.

94. Moroz, V. L.: On A "Dust Envelope" of the Earth (In Russian.) Iskusstvennyye Sputniki Zemli, no. 12, 1962, pp. 151–158.

95. Dole, S. H.: The Gravitational Concentration of Particles in Space Near the Earth. Planetary & Space Sci., vol. 9, Sept. 1962, pp. 541–553.

96. Ruskol, Ye. L.: The Origin of the Concentration of Interplanetary Dust About the Earth. Planetary & Space Sci., vol. 11, Mar. 1963, pp. 311–316. (Translated from: Iskusstvennyye Sputniki Zemli, vol. 12, 1962, p. 145.)

97. Idlis, G. M.: Origin and Size Distribution of Dust Particles in Layers of the Earth's Atmosphere. Akademiya Nauk Kazakhskoy SSR, Alma Ata Astrofizicheskiy Institut (In Russian), Izvestiya, vol. 12, 1961, pp. 99–103.

98. Dole, S. H.: Meteoroid Concentration by the Earth's Gravitational Field. Also issued as DDC document AD–429108.

99. Eichelberger, Robert J.: Summary: Theoretical and Experimental Studies of Crater Formation. *In* Proceedings of the Sixth Symposium on Hypervelocity Impact, vol. II, part 2, Aug. 1963, pp. 683–705.

100. Herrmann, Walter; and Jones, Arfon H.: Survey of Hypervelocity Impact Information. Massachusetts Institute of Technology, Cambridge, Mass. Aeroelastic & Structure Research Lab. MIT Report 99–1; ASTIA Doc. AD–267289, Sept. 1961.

101. Herrmann, Walter; and Jones, Arfon H.: Survey of Hypervelocity Impact Information; Addendum. Massachusetts Institute of Technology, Cambridge, Mass., Aeroelastic & Structure Research Lab. MIT Report 99–1; ASTIA Doc. AD–267209, Oct. 1961.

102. Jones, Arfon H.; Polhemus, J. F.; and Herrmann, W.: Survey of Hypervelocity Impact Information II. Massachusetts Institute of Technology, Cambridge, Mass., Aeroelastic & Structures Research Lab. MIT Report no. 99–2; ASTIA Doc. AD–432815, Dec. 1963.

103. Charters, A. C.: High-Speed Impact. Scientific American, vol. 203, no. 4, Oct. 1960, pp. 128–131, 135–140.

104. Rodriguez, David: Meteoroid Shielding for Space Vehicles. (Ford Motor Co., Aeronutronic Div., Newport Beach, California). Aerospace Eng., vol. 19(12), Dec. 1960, pp. 20–23, 55, 58, 60, 62, 64, and 65–66.

105. Bjork, R. L.: Meteoroids vs Space Vehicles. (Rand Corp. Santa Monica, California). ARS J., vol. 31, June 1961, pp. 803–807.

106. Fuchs, Otto P.: Impact Phenomena. (Temple University, Philadelphia, Pa.). AIAA J., vol. 1, Sept. 1963, pp. 2124–2126.

107. Goldsmith, Werner: Impact: The Collision of Solids. (California University, Berkeley). Applied Mechanics Revs., vol. 16, Nov. 1963, pp. 855–866.

108. Dubin, Maurice: Meteoroid Effects on Space Exploration. NASA TN D–1839, 1963.

109. Rolsten, R. F.; Hunt, H. H.; and Wellnitz, J. N.: Study of Principles of Meteoroid Protection. General Dynamics. Astronautics. San Diego, Calif. Report no. AE–62–0413, Apr. 1962.

110. Summers, James L.: Investigations of High-Speed Impact: Regions of Impact and Impact at Oblique Angles. NASA TN D–94, Oct. 1959.

111. Proceedings of the Fifth Symposium on Hypervelocity Impact. vol. I, part 1, Apr. 1962, pp. 1–330. (Sponsored by U.S. Navy, U.S. Army, and U.S. Air Force. Denver, Colo., Oct. 30–Nov. 1, 1961.)

112. Proceedings of the Fifth Symposium on Hypervelocity Impact. vol. I, part 2, Apr. 1962, pp. 331–663. (Sponsored by U.S. Navy, U.S. Army, and U.S. Air Force. Denver, Colo., Oct. 30–Nov. 1, 1961.)

113. Proceedings of the Sixth Symposium on Hypervelocity Impact. vol. II, part 1, Aug. 1963, pp. 1–336. (Sponsored by U.S. Navy, U.S. Army, and U.S. Air Force. Cleveland, Ohio, Apr. 30–May 2, 1963.)

114. Proceedings of the Sixth Symposium on Hypervelocity Impact. vol. II, part 2. Aug. 1963, pp. 337–709. (Sponsored by U.S. Navy, U.S. Army, and U.S. Air Force. Cleveland, Ohio, Apr. 30–May 2, 1963.)

115. Proceedings of the Sixth Symposium on Hypervelocity Impact. vol. III, Aug. 1963, pp. 1–395. (Sponsored by U.S. Navy, U.S. Army, and U.S. Air Force. Cleveland, Ohio, Apr. 30–May 2, 1963.)

116. EICHELBERGER, R. J.; AND GEHRING, J. W.: Effects of Meteoroid Impacts on Space Vehicles. ARS J., vol. 32, Oct. 1962, pp. 1583–1591.

117. EICHELBERGER, R. J.; AND GEHRING, J. W.: Effects of Meteoroid Impacts on Space Vehicles. American Rocket Society Space Flight Report to the Nation, New York Coliseum, Oct. 9–15, 1961. ARS Paper 2030–61, 1961.

118. BJORK, ROBERT L.: Review of Physical Processes in Hypervelocity Impact and Penetration. *In* Proceedings of the Sixth Symposium on Hypervelocity Impact, vol. II, part 1, Aug. 1963, pp. 1–58.

119. OLSHAKER, A. E.; AND BJORK, R. L.: Hydrodynamics Applied to Hypervelocity Impact. *In* proceedings of the Fifth Symposium on Hypervelocity Impact, vol. I, part 1, Apr. 1962, pp. 185–239.

120. ZERNOW, L.: Introductory Paper-Experimentation. *In* Proceedings of the Sixth Symposium on Hypervelocity Impact, vol. III, Aug. 1963, pp. 1–11.

121. WALSH, J. M.; AND TILLOTSON, J. H.: Hydrodynamics of Hypervelocity Impact. In Proceedings of the Sixth Symposium on Hypervelocity Impact, vol. II, part 1, Aug. 1963, pp. 59–104.

122. RAE, WILLIAM J.; AND KIRCHNER, HENRY P.: A Blast-Wave Theory of Crater Formation in Semi-Infinite Targets. *In* Proceedings of the Sixth Symposium on Hypervelocity Impact, vol. II, part 1, Aug. 1963, pp. 163–227.

123. DAVIDS, N.; CALVIT, H. H.; AND JOHNSON, O. T.: Spherical Shock Waves and Cavity Formation in Metals. *In* Proceedings of the Sixth Symposium on Hypervelocity Impact, vol. II, part 1, Aug. 1963, pp. 229–271.

124. RAE, WILLIAM J.; AND KIRCHNER, HENRY P.: A Study of Meteoroid Impact Phenomena. Cornell Aeronautical Laboratory, Inc., Report No. RM–1655–M–4; Contractor Report CR–50171, Feb. 1963.

125. ANDRIANKIN, E. I.; AND STEPANOV, YU.S.: The Depth of Penetration Upon Impact of Meteor Particles. Planetary & Space Sci., vol. 11, Nov. 1963, pp. 1365–1373 (From Iskusstvennyye Sputniki Zemli, no. 15, 1963, p. 44).

126. HUANG, Y. K.; AND DAVIDS, NORMAN: Shock Dynamics of Hypervelocity Impact of Metals. Franklin Inst. J., vol. 276, July 1963, pp. 39–50.

127. GOLDSMITH, WERNER: Analytical Versions of Penetration Processes. (U.S. Naval Ordnance Test Station, China Lake, Calif. NOTS TP–2811; U.S. Bureau of Naval Weapons Report 7812; ASTIA Doc. AD–273718), Feb. 1962.

128. YUAN, S. W.; AND BLOOM, A. M.: Analytical Approach to Hypervelocity Impact. AIAA J., vol. 2, no. 9, Sept. 1964, pp. 1667–1669.

129. RAE, WILLIAM J.: AND HERTZBERG, A.: On the Possibility of Simulating Meteoroid Impact by the Use of Lasers. Cornell Aeronautical Lab., Inc., Report No. AI–1821–A–1; Contractor Report CR–54029, Apr. 1964.

130. RINEY, T. D.: Visco-Plastic Solution of Hypervelocity Impact Cratering Phenomenon. *In* Proceedings of the Sixth Symposium on Hypervelocity Impact, vol. II, part 1, Aug. 1963, pp. 105–140.

131. RINEY, T. D.: Theoretical Hypervelocity Impact Calculations Using the Picwick Code. (U.S. Air Force Systems Command, Air Proving Ground Center, Eglin Air Force Base, Fla.) Technical Documentary Report ATL–TDR–64–8, Mar. 1964.

132. RINEY, T. D.: Theory of High Speed Impact (Summary Report) (U.S. Air Force Systems Command, Air Proving Ground Center, Eglin Air Force Base, Fla.) AF Report APGC–TDR–62–20, Mar. 1962.

133. RINEY, T. D.: A Visco-Plastic Model for Hypervelocity Impact (First Quarterly Report). (U.S. Air Force Systems Command, Air Proving Ground Center, Eglin Air Force Base, Fla.) AF Report APGC–TN–61–16, Apr. 1961.

134. ROLSTEN, R. F.; AND HUNT, H. H.: Impact Force and Crater Surface Area. AIAA J., vol. 1, Aug. 1963, pp. 1893–1895.

135. ROLSTEN, R. F.: Impact Force Per Crater Area Related to the Tensile Strength. J. Spacecraft and Rockets, vol. 1, May–June 1964, pp. 351–352.

136. WALL, JOHN K.: Theoretical Penetration of Hypervelocity Projectiles Into Massive Targets. AIAA J., vol. 2, July 1964, pp. 1242–1246.

137. KINEKE, J. H., JR.; AND RICHARDS, L. G.: Influence of Target Strength on Hypervelocity Crater Formation in Aluminum. *In* Proceeding of the Sixth Symposium on Hypervelocity Impact, vol. II, part 2, Aug. 1963, pp. 513–524.

138. STERBENTZ, WILLIAM H.; AND LONG, LOREN L.: Meteoroid Effects on Nuclear Rocket Space Vehicle Mission Success. *In* Proceedings of the Sixth Symposium on Hypervelocity Impact, vol. III, Aug. 1963, pp. 357–385.

139. BULL, G. V.: On the Impact of Pellets With Thin Plates, Theoretical Considerations. Part 1. Arthur D. Little, Inc., ADL Report 63270–03–01, Jan. 1962.

140. MAIDEN, C. J.: Experimental and Theoretical Results Concerning the Protective Ability of a Thin Shield Against Hypervelocity Projectiles. *In* Proceedings of the Sixth Symposium on Hypervelocity Impact, vol. III, Aug. 1963, pp. 69–156.

141. SANDORFF, P. E.: A Meteoroid Bumper Design Criterion. *In* Proceedings of the Sixth Symposium on Hypervelocity Impact, vol. III, Aug. 1963, pp. 41–67.

142. KRAUS, H.: Two Dimensional Analysis of a Hypervelocity Impact Upon a Visco-Plastic Plate. *In* Proceedings of the Sixth Symposium on Hypervelocity Impact, vol. III, Aug. 1963, pp. 13–40.

143. NYSMITH, C. ROBERT; AND SUMMERS, JAMES L.: An Experimental Investigation of the Impact Resistance of Double-Sheet Structures at Velocities to 24,000 Feet Per Second. NASA TN D–1431, 1962.

144. BECKER, KARL R.; WATSON, RICHARD W.; AND GIBSON, FRANK C.: Hypervelocity Impact Phenomena. U.S. Bureau of Mines, Explosives Research Laboratory, Nov. 1961.

145. OLSHAKER, ARNOLD E.: Experimental Investigation in Lead of the Whipple "Meteor Bumper." Massachusetts Institute of Technology, Cambridge, J. Applied Phys., vol. 31, Dec. 1960, pp. 2118–2120.

146. HUMES, DONALD H.: An Experimental Investigation of the Effectiveness of Single Aluminum Meteoroid Bumpers. NASA TN D–1784, 1963.

147. BRYAN, GEORGE M.; AND PUGH, EMERSON M.: Cratering of Lead by Oblique Impacts of Hypervelocity Steel Pellets. J. Applied Phys., vol. 33, Feb. 1962, pp. 734–738.

148. WATSON, R. W.; BECKER, K. R.; AND GIBSON, F. C.: Thin Plate Perforation Studies With Projectiles in the Velocity Range from 2 to 5 km/sec. *In* Proceedings of the Sixth Symposium on Hypervelocity Impact, vol. III, Aug. 1963, pp. 207–248.

149. MORTENSEN, R. B.; FERGUSON, J. E.; JOYCE, J. P.; AND KREYENHAGEN, K. H.: Effects of 3 to 12 km/sec Impacts on Finite Targets. *In* Proceedings of Sixth Symposium on Hypervelocity Impact, vol. III, Aug. 1963, pp. 157–205.

150. FRIICHTENICHT, J. F.; AND SLATTERY, J. C.: Ionization Associated with Hypervelocity Impact. NASA TN D–2091, Aug. 1963.

151. FRIICHTENICHT, J. F.; AND SLATTERY, J. C.: Ionization Associated with Hypervelocity Impact. *In* Proceedings of the Sixth Symposium on Hypervelocity Impact, vol. II, part 2, 1963, pp. 591–612.

152. HART, EUGENE M.: Effects of Outer-Space Environment Important to Simulation of Space Vehicles. Aeronautical Systems Division, Wright-Patterson Air Force Base, ASD Technical Report 61–201, Aug. 1961.

153. BARLOW, JOSEPH: A Review of Impact and Pressure Wave Loading of Structures. Washington University, 1961. (ASTIA Document, AD–268716.)

154. JAFFE, LEONARD D.; AND RITTENHOUSE, JOHN B.: Behavior of Materials in Space Environments. ARS J., vol. 32, Mar. 1962, pp. 320–346.

155. MATTHEWS, C. O.; AND FINCH, W. L.: Report on the LMSC Spacecraft Materials Reliability Program. Symposium on Effects of Space Environment on Materials. National Symposium, Soc. of Aerospace Material & Process Engineers, St. Louis, May 7–9, 1962.

156. National Research Council, Materials Advisory Board: Materials Problems Associated With the Thermal Control of Space Vehicles. NRC Report MAB–155–M, Oct. 1959.

157. Leigh, Charles H.: Spectral Emissivity of Metals After Damage by Particle Impact. NASA Contractor Report CR–53235, Aug. 1962.

158. Whitnah, J.; Upton, J.; Griffith, R.; Morfitt, G.; Jorgenson, G.; and Rotenberg, D.: Research on the Effects of Collisions of Small Particles With Bodies Moving at Hypersonic Speed. Part III. Erosion and Heat Transfer Effects. WADC Technical Report 58–498, part III, Dec. 1960.

159. Cardarelli, Nathan F.: Space Suit Materials Testing Program. Inst. Environmental Sciences, Proc., Apr. 1962. pp. 369–376.

160. Belasco, Norman: Extra Vehicular Protection During Orbital and Lunar Explorations. IAS Paper 62–66. Presented at the IAS 30th Annual Meeting, New York, January 22–24, 1962.

161. Dukes, Wilfred H.; and Anthony, Frank M.: Thermal Protection of Lifting Reentry Vehicles. Aerospace Eng., vol. 22, no. 1, Jan. 1963, pp. 108–124.

162. Hendricks, P. L.: Structural Materials to 1800°F (Steel and Titanium). Wright-Patterson Air Force Base, ASD Technical Report 61–322, July 1961, pp. 40–54.

163. Esgar, Jack B.: Fuel Tanks for Spacecraft: The Difficulties. Mech. Eng., vol. 85, Apr. 1963, pp. 44–47.

164. Stepka, Francis S.; and Morse, C. Robert: Preliminary Investigation of Catastrophic Fracture of Liquid-filled Tanks Impacted by High-Velocity Particles. NASA TN D–1537, May 1963.

165. Brun, R. J.; Livingood, J.N.B.; Rosenberg, E. G.; and Drier, D. W.: Analysis of Liquid-Hydrogen Storage Problems for Unmanned Nuclear-Powered Mars Vehicles. NASA TN D–587, Jan. 1962.

166. Carter, David J., Jr.: A Preliminary Investigation on the Destruction of Solid-Propellant Rocket Motors by Impact From Small Particles. NASA TN D–442, Sept. 1960.

167. Lieblein, Seymour; Clough, N.; and McMillian, A. R.: Hypervelocity Impact Damage Characteristics in Armored Space Radiator Tubes. NASA TN D–2472, 1964.

168. English, Robert E.; and Guentert, Donald C.: Segmenting of Radiators for Meteoroid Protection. ARS J., vol. 31, Aug. 1961, pp. 1162–1164.

169. Weatherston, Roger C.: The Radiation Amplifier—A New Approach to Heat Rejection From Space Powerplants. Institute of the Aerospace Sciences, IAS Paper 62–73. Presented at the IAS 30th Annual Meeting, New York, Jan. 22–24, 1962.

170. Diedrich, James H.: Materials Problems Associated With the Design of Radiators for Space Powerplants. Paper prepared for the American Nuclear Society Meeting, Cincinnati, Ohio, Apr. 17–19, 1963.

171. Johnson, Alfred L.: State of the Art: Spacecraft Radiators. Space/Aeronautics, vol. 37, no. 1, Jan. 1962, pp. 76–78.

172. Wallace, R. R.; Vinson, J. R.; and Kornhauser, M.: Effects of Hypervelocity Particles on Shielded Structures. ARS J., vol. 32, Aug. 1962, pp. 1231–1237.

173. Wallace, R. R. Jr.; Vinson, J. R.; and Körnhauser, M.: Effects of Hypervelocity Particles on Shielded Structures. American Rocket Society Paper 1683–61, 1961.

174. Dynamics and Structures: Space/Aeronautics, vol. 40, no. 2, July 1963, pp. 39–50.

175. Kinard, Willam H.; and Collins, Rufus D., Jr.: An Investigation of High-velocity Impact Cratering Into Nonmetallic Targets and Correlation of Penetration Data for Metallic and Nonmetallic Targets. NASA TN D–726, 1961.

176. Osborne, Robert S.; Keffer, Clarence O.; and Look, George: Materials and Structures for Space Stations. Astronautics, vol. 7, no. 9, Sept. 1962, pp. 36–39.

177. Pezdirtz, G. F.: Polymers for Spacecraft. Modern Plastics, vol. 40, no. 12, Aug. 1963, pp. 123–134.

178. Rolsten, R. F.; and Hunt, H. H.: Bumpers and Core Materials for Meteoroid Protection Space/Aeronautics, vol. 40, no. 4, Sept. 1963, pp. 105, and 107–111.

179. BROOKS, GEORGE W.: Research Design Considerations, and Technological Problems of Structures for Spacecraft. Proc. NASA-University Conference on the Science and Technology of Space Exploration (Chicago, Ill.), Nov. 1–3, 1962. NASA SP 11, vol. 2, Dec. 1962, pp. 521–532.

180. WALLACE, R. R.: Design Applications of Foamed Metals. American Rocket Society, ARS Paper 2412–62.

181. GATZEK, LEO E.; AND ISENBERG, LIONEL: The Effect of Space Environment on Reinforced Plastics. SPE J., vol. 19, Apr. 1963, pp. 383–386.

182. PIPITONE, S. J.; AND REYNOLDS, B. W.: Effectiveness of Foam Structures for Meteoroid Protection. J. Spacecraft & Rockets, vol. 1, no. 1, Jan. 1964, pp. 37–43.

183. BELLER, WILLIAM: 'Bumper' May Cure Meteoroid Hazard. Missiles & Rockets, vol. 9, no. 19, Nov. 1961, pp. 32 and 35.

184. FUNKHOUSER, JOHN O.: A Preliminary Investigation of the Effect of Bumpers as a Means of Reducing Projectile Penetration. NASA TN D–802, Apr. 1961.

185. COOMBS, L. C.: How Much Meteoroid Shielding for Spacecraft? Space/Aeronautics, vol. 39, no. 4, Apr. 1963, pp. 101–103.

186. TUCKERMAN, A. J.; MIZUMO, V. I.; AND D'ANNA, P. J.: Self-Sealing Sandwich for Meteoroid Protection. Space/Aeronautics, vol. 35, no. 3, Mar. 1961, pp. 56–57.

187. SPAIN, R. G.; AND HOUSE, P. A.: Self-Sealants for Aerospace Vehicles. Proc. Seventh Joint Army-Navy-Air Force Conference on Elastomer Research & Development, Oct. 22–24, 1962. ONR–13, vol. 1, Oct. 1962, pp. 129–152.

188. PIECHOCKI, JAMES J.: Self-Sealing Spacecraft Structures in the Meteoroid Environment. NASA CR–50 000, Apr. 1963.

189. PIECHOCKI, JAMES J.: Self-Sealing Spacecraft Structures. J. Spacecraft and Rockets, vol. 1, May–June 1964, pp. 207–275.

190. D'ANNA, PHILIP J.; HEITZ, ROGER M.; AND PIECHOCKI, JAMES J.: Self-Sealing Structures for Control of the Meteoroid Hazard to Space Vehicles. NASA CR–120, Oct. 1964.

Additional References For General Reading

North American Aviation, Inc. Missile Division: Study of Hypervelocity Impact of Particles on Materials. (Final Summary Report) MD–59–114, Contract DA–04–495–ORD–1477, June 1960.

Sandorff, Paul E.: Structures Considerations in Design for Space Boosters. ARS J., vol. 30, 999–1008, Nov. 1960.

Ferguson, W. J.; and McKinney K. R.: The Influence of Temperature Elevation on the Penetration of Missiles Into Copper Targets. U.S. Naval Research Laboratory Rept. 5407, Nov. 1959.

Altshuler, Saul; et al.: The Scientific Objectives of the Able–5 Program. Physics Today, vol. 14, no. 1, Jan. 1961, pp. 20–27.

Dow, Norris F., ed.: Important Research Problems in Advanced Flight Structures Design, 1960. NASA TN D–518, June 1960.

Lampert, Seymour: Aerospace Structures Gap. Aircraft and Missiles, vol. 4, no. 1, Jan. 1961, pp. 58–61.

Hibbs, A. R.: The Distribution of Micrometeorites Near the Earth. J. Geophys. Res., vol. 66, Feb. 1961, pp. 371–377.

Brown, H.: The Density and Mass Distribution of Meteoritic Bodies in the Neighborhood of the Earth's Orbit. Space Research, First International Space Science Symposium, Proc. (Hilde Kallmann Bijl, ed.) 1960, pp. 1063–1070.

Geiss, Johannes; and Oeschger, Hans: The Impact of Cosmic Radiation in Meteorites. Space Research, First International Space Science Symposium, Proc. (Hilde Kallmann Bijl. ed.), 1960, pp. 1071–1079.

Abbott, K. H.: Metallurgical Observation of High Velocity Impact. U.S. Arsenal Laboratory, Technical Report WAL–TR–161.85/1, Sept. 1960.

Ungar, E. W.: Particle Impacts on the Melt Layer of an Ablating Body. ARS J., vol. 30, Sept. 1960, pp. 799–805.

Brown, Harrison: Addendum: The Density and Mass Distribution of Meteoritic Bodies in the Neighborhood of the Earth's Orbit. J. Geophys. Res., vol. 66, Apr. 1961, pp. 1316–1317.

Bjork, Robert L.: Meteoroid Hazard to Nuclear Spacecraft. Nucleonics, vol. 19, no. 4, Apr. 1961, pp. 91–92.

Hughes, D. S.; Gourley, L. E.; and Gourley, Mary F.: Shock-Wave Compression of Iron and Bismuth. J. Applied Phys., vol. 32, Apr. 1961, pp. 624–629.

Jet Propulsion Laboratory, California Institute of Technology: Scientific Experiments for Ranger 1 and 2. Technical Report 32–55, Contract NASw–6, Jan. 1961.

Gettings, Hal: S–55 to Explore Threat of Punctures From 'Space Dust'. Missiles and Rockets, vol. 8, no. 24, June 1961, pp. 14–15.

Anon: AF Probe Finds Heavy "Dust" Band. Missiles and Rockets, vol. 9, no. 1, July 1961, pp. 41.

Kinard, William H., and Collins, Rufus D.: A Technique for Obtaining Hypervelocity Impact Data by Using the Relative Velocities of Two Projectiles. NASA TN D–724, 1961.

Keay, C. S. L., and Ellyett, C.: The Latitude Dependence of Radar Meteor Shower Observations. J. Geophys. Res., vol. 66, Aug. 1961, pp. 2337–2343.

ZIPKIN, M. A.: Environmental Problems in the Design of Space Power Systems. Aerospace Eng., vol. 20, no. 8, Aug. 1961, pp. 14–15, 38–44.

BOHN, J. LLOYD, ET AL.: Research Directed Towards the Study of Transducing Meteoric Impacts. Temple Univ., Contract AF–19(604)–1894, Dec. 1960. (ASTIA Document, AD–249–949).

BERKOWITZ, HARVEY MARTIN: Longitudinal Impact of a Semi-Infinite Elastic Cylindrical Shell. Columbia University, Dept. of Civil Engineering and Engineering Mechanics, Tech. Rept. 27, CU–1–61–ONR–266(08)–CE, Jan. 1961. (ASTIA Document, AD–255–869).

FRASIER, J. T.: Hypervelocity Impact Studies in Wax. Aberdeen Proving Ground, Ballistic Research Laboratories, Rept. 1124, Feb. 1961. (ASTIA Document, AD–255–772).

HALPERSON, S. M., AND HALL, D.A.: Mechanics of Ballistic Damage (Shock Studies in Transparent Plastic by High-Speed Photographic Techniques). Report of NRL Progress, Sept. 1961, pp. 37–39.

LEYBOURNE, JAMES J.: Scientific Sensors for Space Vehicles. Astronautics, vol. 6, no. 11, Nov. 1961, pp. 36–37.

GILBERT, M. B.: Space Environment. Wright-Patterson Air Force Base, ASD Tech. Rept. 61–322, July 1961, pp. 1–7.

JAFFE, LEONARD D., AND RITTENHOUSE, JOHN B.: Behavior of Materials in Space Environments. ARS Paper 2033–61, 1961.

DOW, NORRIS: Structures and Materials. Astronautics, vol. 6, no. 12, Dec. 1961, pp. 52–53, 62, 64.

JAFFE, L. D.: Effects of Space Environment Upon Plastics and Elastomers. Jet Propulsion Laboratory, C. I. T., Tech. Rept. 32–176, Nov. 1961.

MIRTOV, B. A.: Meteoric Matter and Some Geophysical Problems of the Upper Atmosphere. ARS J., vol. 43, Jan. 1962, pp. 143–151.

BARABASHOV, N. P.; BRONSHTEN, V. A.; ET AL.: The Moon. Wright-Patterson Air Force Base, Report MCL–882/1 + 2, May 1961. (ASTIA Document, AD–261–784).

GRANNIS, PAUL: Dust Formation and Radiation Damage on the Lunar Surface. General Motors Corporation, Contract NASA NsG 119–61, Sept. 1961.

WACHOLDER, B. V.; AND FAYER, E.: Study of Instrumentation and Techniques for Monitoring Vehicle and Equipment Environments at High Altitude. Instrumentation and Monitoring Techniques. Wright Air Development Center Tech. Note 59–307, vol. III, June 1960. (ASTIA Document, AD–268–090).

BRONER, M. A.; AND LANDER, G. A.: How Bad is the Moon Environment? Space/Aeronautics, vol. 37, no. 4, Apr. 1962, pp. 92–96.

ARTHUR D. LITTLE, INC.: Liquid Propellant Losses During Space Flight. Report 63270–00–02, Contract NAS 5–664, Second Quarterly Progress Report, May 1961.

GATZEK, LEO E.; AND ISENBERG, LIONEL: The Effect of Space Environment on Reinforced Plastics. Symposium on Effects of Space Environment on Materials. National Symposium, Soc. of Aerospace Material & Process Engineers, St. Louis, May 7–9, 1962.

DENARDO, B. PAT: Measurements of Momentum Transfer From Plastic Projectiles to Massive Aluminum Targets at Speeds up to 25 600 Feet per Second. NASA TN D–1210, 1962.

WACHOLDER, B. V.; AND FAYER, E.: Effects of High-Altitude Environments on Vehicles and Equipment Study of Instrumentation and Techniques for Monitoring Vehicle and Equipment Environment at High Altitudes. Wright Air Development Center Tech. Note 59–307, vol. II, June 1960.

ANTHONY, F. M.; ET AL.: Analytical Methods and Design Studies. Investigation of Feasibility of Utilizing Available Heat Resistant Materials for Hypersonic Leading Edge Applications. vol. II. Wright Air Development Center Tech. Note 59–744, vol. II, Mar. 1961. (ASTIA Document, AD–265–083).

WEBER, RICHARD J.: Influence of Meteoroid Hazards on Selection of Spacecraft Propellants. ARS J. vol. 32, July 1962, pp. 1105–1106.

LEHR, S. N.; MARTIRE, L. J.; AND TRONOLONE, V. J.: Equipment Design Considerations for Space Environment. Space Technology Laboratories, Inc., STL/TR/9990–6032–RU000, Feb. 1962.

WIEDERHORN, NORMAN M.: The Space Environment and its Interactions With Liquid Propellants and Their Storage Systems. Arthur D. Little, Inc., Rept. C–63270–02–1. Contract NAS 5–664, Sept. 1961. (ASTIA Document, AD–226–034).

BOBROVNIKOFF, N. T.: Natural Environment of the Moon. Wright Air Development Center Phase Technical Note 3, June 1959. (ASTIA Document, AD–242–177).

HEYMANN, D.; AND FLUIT, J. M.: Sputtering by 20-Kev A_r+ Ions at Normal Incidence on Meteorites. J. Geophys. Res., vol. 67, July 1962, pp. 2921–2924.

WYCKOFF, ROBERT C.: Venus Mission in 1962. Astronautics, vol. 7, no. 7, July 1962, pp. 54–59.

EDMINSTON, R. M.: The Production of Meteoroid Hole Area in a Space Vehicle Near the Earth. Institute of the Aerospace Sciences, IAS Paper 62–29, 1962.

JAFFE, L. D., AND RITTERHOUSE, J. B.: How Materials Behave in Space. Materials in Design Eng., vol. 56, no. 3, Sept. 1962, pp. 97–104.

HOPKINS, ALAN K.: Because a Marble-Size Meteoroid Will Wreck a Spacecraft . . . You Don't Worry About the Big Ones. Machine Design, vol. 34, no. 23, Sept. 1962, pp. 142–145.

KOLSKY, H.; AND DOUCH, L. S.: Experimental Studies in Plastic Wave Propagation. J. Mech. Phys. Solids, vol. 10, July/Sept. 1962, pp. 195–223.

GARDNER, ANNESTA R.: What You Can Learn From High-Speed Testing. Product Eng., vol. 33, no. 22, Oct. 1962, pp. 41–49.

STEPHENSON, W. B.: Investigation of High-Speed Impact: a Technique. Aerospace Eng., vol. 21, no. 11, Nov. 1962, pp. 10–16.

CROSS, BRUCE; AND RALSTON, MARGARET: Creating Space in the Lab., Hypervelocity Guns. Product Eng., vol. 33, no. 23, Nov. 1962, pp. 116–117.

CZARNECKI, EDWIN G.: State of the Art—1962. Structures and Materials. Astronautics, vol. 7, no. 11, Nov. 1962, pp. 132–133, 135.

FINKELMAN, E. M.: Optimized Protection Against Environmental Hazards in Space. Aerospace Eng., vol. 21, no. 12, Dec. 1962, pp. 41–48..

CHIOU, CHING-GWEI; GROW, R. W.; AND PALMER, E. P.: Precision Measurement of Lead-to-Lead Impact. Utah Univ., Tech. Rept. 23, Contract AF–49 (638)–462, Oct. 1961. (ASTIA Document, AD–270–009).

JENSEN, JAMES R.; AND PALMER, E. P.: A Laboratory Investigation of Meteor Physics. Utah Univ., Tech. Rept. 22, Contract AF–49(638)–462, Oct. 1961. (ASTIA Document, AD–270–181).

FUGELSO, L. E.; ARENTZ, A. A., JR.; AND POCZATEK, J. J.: Mechanics of Penetration. I. Metallic Plates, Theory and Applications. American Machine and Foundry Company, MR 1127, Contract DA–19–129–QM–1542, Oct. 1961. (ASTIA Document, AD–272–947).

ANON: High-Velocity Impact Studies, Utah Univ., Tech. Rept. OSR–24, Contract AF–49(638)–462, Oct. 1961. (ASTIA Document, AD–271–470).

LAIDLAW, W. R.; AND WYKES, JOHN H.: Potential Aerothermoelastic Problems Associated With Advanced Vehicle Design. Wright-Patterson Air Force Base, ASD Tech. Rept. 61–645, Feb. 1962, pp. 120–160.

DUVALL, GEORGE E.: Shock Waves in the Study of Solids. Applied Mechanics Revs., vol. 15, Nov. 1962, pp. 849–854.

KELLER, DONALD V.; AND TRULIO, JOHN G.: Mechanism of Spall in Lucite. J. Applied Phys., vol. 34, Jan. 1963, pp. 172–175.

MILLER, BARRY: NASA Studies Hazards of Lunar Impact Particles. Aviation Week, vol. 78, no. 2, Jan. 1963, pp. 54–55, 59.

NEW, JOHN C.: The Dynamic Environment of Space. Lecture 1. Environmental Technology Lecture Series. Sponsored Jointly by Institute of Environmental Sciences and the George Washington University, 1962.

FRANKEL, HENRY E.: Properties of Materials. Lecture 10. Environmental Technology Lecture Series, Sponsored Jointly by Institute of Environmental Sciences and the George Washington University, 1962.

MAR, J.: Meteoroid Impact on the Topside Sounder Satellite. Can. Aeronautics & Space J., vol. 8, Nov. 1962, pp. 237–240.

BALCHAN, A. S.: A Radiographic Study of Shock-Loaded Iron. J. Applied Phys., vol. 34, Feb. 1963, pp. 241–245.

CORCORAN, J. W.; AND KELLY, J. M.: Phenomena of Penetration in Light Weight Rigid Personnel Armor Materials. Beckman & Whitley, Inc., RD–63, Contract DA–19–129–QM–1574, Dec. 1961. (ASTIA Document, AD–273–060).

ADAMS, HARRY E.: Instrumentation for Use in the Study of Extraterrestrial Particles. U.S. Air Force Cambridge Research Laboratories. Rept. 1079, Nov. 1961. (ASTIA Document, AD–269–316).

BECKER, KARL R.: ET AL.: Hypervelocity Impact Phenomena. U.S. Bureau of Mines, Nov. 1961. (ASTIA Document, AD–270–930).

SCHERRER, VICTOR E.; AND MCMATH, ROBERT R.: Hypervelocity Particle Effects on Material. Technical Operations, Inc., Contract AF–33(616)–8423, Dec. 1961. (ASTIA Document, AD–272–669).

BOWEN, E. F.: A Lunar Effect on the Incoming Meteor Rate. J. Geophys. Res., vol. 68, Mar. 1963, pp. 1401–1403.

HALPERSON, S. M.; FULLER, R. H.; AND SCHLEMMER, H. V.: NRL Hypervelocity Accelerator (Three-Inch Light-Gas Gun). NRL Progress, Aug. 1962, pp. 12–16.

KEYES, R. T.: Investigation of High Velocity Impact and Some High Explosive Phenomena. Utah Univ. Contract AF–18(603)–100, Dec. 1961. (ASTIA Document, AD–269–769).

BOUQUET, FRANK L., JR.: The Radiation Hazard of Space. Space/Aeronautics, vol. 39, no. 5, May 1963, pp. 72–77.

WUNSCH, D. C.; SOAPES, T. D.; AND GUENTHER, A. H.: Acceleration of Thin Plates by Exploding Foil Techniques. Kirtland Air Force Base, Rept. AFSWC–TDR–61–75, Jan. 1962. (ASTIA Document, AD–272–078).

ANON: Phenomena in the Upper Atmosphere. Review of Soviet Literature. U.S. Library of Congress, Aerospace Information Division, Report 62–31, Feb. 1962. (ASTIA Document, AD–275–188).

SCHERRER, VICTOR E.; AND MCMATH, ROBERT R.: Hypervelocity Particle Effects on Material. Technical Operations, Inc., Rept. TO–B 62–12, Contract AF–33 (616)–8423, March 1962. (ASTIA Document. AD–273–493).

RINEY, T. D.: Difference Scheme for Axisymmetric Impact Problem. General Electric Co. Contract Rept. APGC–TDR–62–19, Mar. 1962. (ASTIA Document, AD–273–992).

BENA, RONALD A., Compiler: Geophysical Exploration in Aerospace During 1961. U.S. Air Force Cambridge Research Laboratories, Mar. 1962. (ASTIA Document, AD–273–758).

SOUTHWORTH, R. B.: On S. H. Dole's Paper, "The Gravitational Concentration of Particles in Space Near the Earth." Planetary & Space Sci., vol. 11, May 1963, pp. 499–503.

KARACHENTSEV, I. D.: The Effect of Micrometeoric Particles on Optical Surfaces of Telescopes Beyond the Earth's Atmosphere. (Title in Russian.) Iskusstvennye Sputniki Zemli, no. 15, pp. 57–65, 1963.

ANDRIANKIN, E. I.; AND SEPANOV, YU. S: On the Depth of Perforation due to the Impacts of Meteoric Particles. (Title in Russian). Iskusstvennye Sputniki Zemli, no. 15, pp. 44–52, 1963.

JONES, G. H. S.: Some Comments on Cratering. Defense Research Board of Canada. Suffield Special Publication 22, Apr. 1962. (ASTIA Document AD–276–943).

BOURDEAU, R. E.; DONLEY, J. L.; AND WHIPPLE, E. C. JR.: Instrumentation of the Ionosphere Direct Measurement Satellite (Explorer VIII). NASA TN D–414, Apr. 1962. (ASTIA Document, AD–274–563).

DOLÆ, S. H.: The Gravitational Concentration of Particulate Matter in the Space Near the Earth. Rand Corporation, Memorandum RM–2879–PR, Contract AF–49 (638)–700. Apr. 1962. (ASTIA Document, AD–274–594.)

DURBERG, JOHN A.: Space Vehicle Environment and Some NASA Facilities for Their Simulation. U.S. Office of the Secretary of Defense, Bulletin 31, pp. 12–20; Shock, Vibration and Associated Environments, Part II, Mar. 1963.

SHAPIRO, IRWIN I.: New Method for Investigating Micrometeroid Fluxes. J. Geophys. Res., vol. 68, Aug. 1963, pp. 4697–4705.

CURRAN, DONALD R.: Nonhydrodynamic Attenuation of Shock Waves in Aluminum. J. Applied Phys., vol. 34, Sept. 1963, pp. 2677–2685.

MILLARE, HUGH T., JR.: The Rate of Arrival of Meteorites at the Surface of the Earth. J. Geophys. Res., Vol. 68, July 1963, pp. 4297–4303.

MILLARD, HUGH T., JR.; AND BROWN, HARRISON: Meteoritic Time-of-Fall Patterns. Icarus, vol. 2, 1963, pp. 137–151.

VEDDER, JAMES F.: Charging and Acceleration of Microparticles. Rev. Sci. Instruments, vol. 34, Nov. 1963, pp. 1175–1183.

ROLSTEN, R. F., AND SCHMITT, R. A.: Hypervelocity Impact of Radioactive Projectiles into Stainless Steel and Aluminum. J. Applied Phys., vol. 34, Oct. 1963, pp. 3010–3012.

GAULT, DONALD E.; SHOEMAKER, EUGENE M.; AND MOORE, HENRY J.: Spray Ejected From the Lunar Surface. NASA TN D–1767, Apr. 1963.

ANON: Study of Target Penetration Prediction by High-Speed and Ultra-High Speed Ballistic Impact. U. S. Air Force Systems Command. Tech. Doc. Rept. APGC TDR–62–35, May 1962. (ASTIA Document, AD–276–426).

RECHT, R. F.; AND IPSON, T. W.: Ballistic Perforation Dynamics, ASME Trans., J. Applied Mech., vol 30E, no. 3, Sept. 1963, pp. 384–390.

ANON: Research Directed Toward the Design, Construction and Analysis of Experiments for Determining Influx Rate of Meteoritic Particles in the Earth's Atmosphere. U.S. Air Force Cambridge Research Laboratories, Rept. AFCRL–63–663, June 1963.

EPSTEIN, A.; AND HAMILTON, A. F.: Exit, Space and Re-entry Structural Design Criteria. Republic Aviation Corp., Wright-Patterson Air Force Base, Tech. Doc. Rept. 62–641, Dec. 1962. (ASTIA Document, AD–295–902).

JOHNSON, FRANCIS S.; AND WEBB, WILLIS L.: The Atmosphere and Near Space. Astronautics & Aerospace Eng., 1(10), Nov. 1963, pp. 81–85, 87.

FIELDER, GILBERT: Erosion and Deposition on the Moon. Planetary & Space Sci., vol. 11, Nov. 1963, pp. 1335–1340.

D'ANNA, PHILIP J.; HEITZ, ROGER M.; PIECHOCKI, JAMES J.; AND HUNTER, RICHARD W.: Self-Sealing Structures for Control of the Meteoroid Hazard to Space Vehicles. Northrop Corp. Rept. NSL 62–132–3, Contract NASr–102, Jan. 1963.

YOUNGER, D. G.; EDMISTON, R. M.; AND CRUM, R. G.: Nonrigid and Semirigid Structures for Expandable Spacecraft. Ford Motor Co. Wright-Patterson Air Force Base, Tech. Doc. Rept. 62–568, Nov. 1962. (ASTIA Document, AD–292–736).

HOLMS, ARTHUR G.: The Design of Micrometeroid Penetration Experiments as Single-Sampling Life-Test Sampling Plans. NASA TN D–1989, Mar. 1964.

NYSMITH, C. ROBERT; SUMMERS, JAMES L.; AND DENARDO, B. PAT: Investigation of the Impact of Copper Filaments Into Aluminum Targets at Velocities to 16 000 Feet per Second. NASA TN D–1981, Feb. 1964.

RALSTEIN, R. F.; HUNT, H. H.; AND WELLINITZ, J. N.: Study of Principles of Meteoroid Protection. General Dynamics Astronautics, Rept. AE–62–0092, Contract NAS–8–875, Jan. 1962.

ÖPIK, E. J.: Meteor Excitation, Ionization, and Atomic Luminous Efficiency. Meters (A Symposium on Meteor Physics), (T. R. Kaiser, ed.) Pergamon Press, 1955, pp. 29–32.

ROBERTS, D. L.: The Scientific Objectives of Deep Space Investigations: Interplanetary Space Beyond 1 AU. IIT Research Institute, Rept. P–5, Contract NASr–65 (06), Feb. 1964.

SCHALL, R.; AND THOMER, G.: Flash Radiographic Measurement of the Shock Compressibility of Magnesium Alloy, Lucite, and Polyethylene. Air Force Special Weapons Center, Kirtland Air Force Base, Tech. Doc. Rept. AFSWC/TDR–62–134, Oct. 1962. (ASTIA Document, AD–291–568).

ENTRES, S. L.: The Meteorite Environment of Earth Satellites. Royal Aircraft Esablishment, (British). Tech. Memo Space 9, Nov. 1962. (ASTIA Document, AD–292–049).

KREYENHAGEN, K. N.; FERGUSON, J. E.; AND RANDALL, R. R.: Impact and Penetration of 0.100-Inch Aluminum Plates by Aluminum Projectiles at 29 000–33 000 Feet per Second. Aerojet-General Corp., Eglin Air Force Base, APGC Tech. Doc. Rept. APGC–TDR–62–40, July 1962. (ASTIA Document, AD–278–537).

HOOPER, A. F.: Compilation of Materials Research Data. General Dynamics/Astronautics, Rept. AE–62–0942, Contract AF 33 (616)7984, Dec. 1962. (ASTIA Document, AD–292–669).

CHOU, PEI CH:; KARPP, ROBERT R.; AND ZAJAC, LAWRENCE J.: Decay of Strong Plane Shocks in an Ideal Gas. NASA CR–107, Sept. 1964.

CLAPP, SAMUAL S.; AND BUCK, RICHARD F.: Design, Development, and Construction of Micrometeorite Detection Systems. Appendix: A Transistorized Digital Computer With Both Real and Stored Time Analog Readoutt of Information—for Use in Deep Space Investigations of Micrometeor Phenomena, by Dave C. Mueller. Oklahoma State University. U.S. Air Force Cambridge Research Laboratories, Rept. AFCRL–64–98, Dec. 1963.

KARPOV, B. G.: Transient Response of Wax Targets to Pellet Impact at 4 km/sec. U.S. Aberdeen Proving Ground, Ballistic Research Laboratories, Rept. 1226, Oct. 1963. (ASTIA Document, AD–428–221).

ANON: Structures for Space Operations. NASA SP–28, Dec. 1962.

HAWKINS, GERALD S.: Variation in the Occurrence Rate of Meteors. Harvard Reprint Series II, no. 90, 1956.

JACCHIA, LUIGI G.: A Comparative Analysis of Atmospheric Densities From Meteor Decelerations Observed in Massachusetts and New Mexico. Havard University. Cambridge Tech. Rept. 10, Contract DA–19–020–ORD–1093, 1952.

MILLMAN, PETER M.; AND MCINTOSH, BRUCE A.: Meteor Radar Statistics. I. Can. J. Phys., vol. 42, Sept. 1964, pp. 1730–1742.

ANON: Proceedings of Symposium on Structural Dynamics Under High Impulse Loading. Wright-Patterson Air Force Base, Tech. Doc. Rept. ASD–TDR–63–140, May 1963. (ASTIA Document, AD–408–777).

MARK, HERMAN; GOLDBERG, GARY; AND MIRTICH, MICHAEL J.: Determination of Cratering Energy Densities for Metal Targets by Means of Reflectivity Measurements. AIAA J., vol. 2, May 1964, pp. 965–966.

ANON: Proceeding of the Sixth Symposium on Hypervelocity Impact, vol. I. Contract DA–31–124–ARO(D)–16. Sponsored by: U.S. Army, U.S. Air Force, and U.S. Navy, Apr. 30, 1963.

ROLSTEN, R. F.; HUNT, H. H.; AND MEYER, K. H.: Deformation and Wave Structure Produced by High-Velocity Impact. J. Applied Phys., vol. 35, May 1964, pp. 1655–1656.

Selected Bibliographies

HODGE, PAUL W.; WRIGHT, FRANCES, W.; AND HOFFLEIT, DORRIT: An Annotated Bibliography on Interplanetary Dust. Smithsonian Contribution to Astrophysics, vol. 5, no. 8, Smithsonian Astrophysical Observatory, 1961.

GOLDMANN, J. B.; AND HOLLISTER, W. L.: Effects of Micrometeorites on Space Vehicles: An Annotated Bibliography. Lockheed Aircraft Corp., Missiles and Space Division. Special Bibliography SB–61–37, July 1961. (ASTIA Document, AD–263821).

COTNER, J. R.; AND WEERTMAN, J.: Bibliography on High Speed Deformation of Materials (1950–1961). Special Weapons Center, Kirtland Air Force Base, May 15, 1961. (ASTIA Document, AD–261376).

EVANS, GEORGE R.: Antenna and Radome Materials and Properties for Space and Satellite Use: An Annotated Bibliography. Lockheed Aircraft Corp., Missiles and Space Division, Special Bibliography SB–61–45, Oct. 1961. (ASTIA Document, AD–269554).

HOLLISTER, WILLIAM L.: Shielding: An Annotated Bibliography. Lockheed Aircraft Corp., Missiles and Space Division, Special Bibliography SB–62–2, Feb. 1962. (ASTIA Document, AD–274015).

HERCULES, WENDELL L.: Shock and Vibration Environment. A Report Bibliography by Armed Services Technical Information Agency. Aug. 1962. (ASTIA Document, AD–277392).

SALISBURY, JOHN W.; VAN TASSEL, ROGER A.; AND ADLER, JOEL E. M.: Bibliography of Lunar and Planetary Research, 1961. U.S. Air Force Cambridge Research Laboratories, L.G. Hanscom Field, July 1962.

GRAZIANO, EUGENE E.; AND MCCORMICK, HELEN B.: The Meteoroid Hazard to Space Vehicles; An Annotated Bibliography. Lockheed Aircraft Corp., Missiles and Space Division, Special Bibliography SB–63–58, Aug. 1963. (ASTIA Document, AD–431973).

MSFC METEOROID DAMAGE WORKING GROUP: A Bibliography Concerning Aspects of the Meteoroid Hazard. George C. Marshall Space Flight Center, NASA, MDWG–63–2, Apr. 1, 1963. (ASTIA Document, AD–407350).

MAGNOLIA, L. R.: Interplanetary Matter: A Bibliography. Space Technology Laboratories, Inc., Research Bibliography no. 42, June 1962. (ASTIA Document, AD–276064).

☆ U. S. GOVERNMENT PRINTING OFFICE: 1965—779-741

"The aeronautical and space activities of the United States shall be conducted so as to contribute . . . to the expansion of human knowledge of phenomena in the atmosphere and space. The Administration shall provide for the widest practicable and appropriate dissemination of information concerning its activities and the results thereof."

—NATIONAL AERONAUTICS AND SPACE ACT OF 1958

NASA SCIENTIFIC AND TECHNICAL PUBLICATIONS

TECHNICAL REPORTS: Scientific and technical information considered important, complete, and a lasting contribution to existing knowledge.

TECHNICAL NOTES: Information less broad in scope but nevertheless of importance as a contribution to existing knowledge.

TECHNICAL MEMORANDUMS: Information receiving limited distribution because of preliminary data, security classification, or other reasons.

CONTRACTOR REPORTS: Technical information generated in connection with a NASA contract or grant and released under NASA auspices.

TECHNICAL TRANSLATIONS: Information published in a foreign language considered to merit NASA distribution in English.

SPECIAL PUBLICATIONS: Information derived from or of value to NASA activities. Publications include conference proceedings, monographs, data compilations, handbooks, sourcebooks, and special bibliographies.

TECHNOLOGY UTILIZATION PUBLICATIONS: Information on technology used by NASA that may be of particular interest in commercial and other nonaerospace applications. Publications include Tech Briefs; Technology Utilization Reports and Notes; and Technology Surveys.

Details on the availability of these publications may be obtained from:

SCIENTIFIC AND TECHNICAL INFORMATION DIVISION

NATIONAL AERONAUTICS AND SPACE ADMINISTRATION

Washington, D.C. 20546

1302